A Computational Investigation of the Biosynthesis of Lanosterol

---

A thesis submitted in partial fulfilment of the

requirements for the degree of

Doctor of Philosophy in Chemistry

in the

University of Canterbury

by

Michael A. E. Townsend

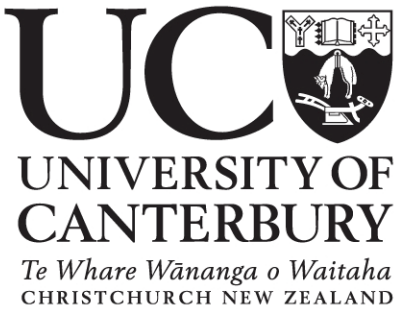

University of Canterbury

2006

Contents

Abbreviations

E	Electronic energy
G	Gibbs free energy
HF	Hartree–Fock ab initio method
MP2	Second order Møller–Plesset perturbation theory method
B3LYP	Becke-3-parameter Lee–Yang–Parr density functional method
TS	Transition state
IRC	Intrinsic reaction coordinate
ZPE, ZPC	Zero-point energy, Zero-point correction
PES	Potential energy surface
SWE	Schrödinger wave equation

Conversion and Scaling Factors[*]

1 hartree = 627.5095 kcal mol^{-1}

1 hartree = 27.2116 eV

1 kcal mol^{-1} = 4.184 kJ mol^{-1}

Method	ZPE scaling factor
HF/3-21G	0.9409
HF/6-31G(d)	0.9135
MP2(Full)	0.9646
B3LYP/6-31G(d)	0.9804

[*] From reference [21].

Abstract

The biosynthesis of the steroid precursor molecule lanosterol is a remarkable process in which the enzyme-bound substrate 2,3-*S*-oxidosqualene forms four new carbocyclic rings by a cascade of cation–alkene addition reactions, followed by a series of 1,2-methyl and hydride shifts. The work presented in this thesis is a computational study of the reactions of compounds designed to model the oxidosqualene–lanosterol cyclisation in order to establish details of the mechanism of this amazing cyclisation.

The initiation of oxidosqualene cyclisation has been modelled by the intermolecular reaction of protonated oxirane and methylpropene. The S_N2-like ring opening of the protonated epoxide is strongly exothermic with a low barrier to reaction; the geometry of the gas phase reaction has been found to be significantly affected by hyperconjugative stabilisations and low energy steric interactions. The energy profile and geometry of this reaction can now be compared to analogous intramolecular reactions such as the formation of the lanosterol A-ring.

The competing five- and six-membered cyclisations of a series of substituted A-ring model compounds was investigated. It has been found that the facile cleavage of the protonated epoxide causes the reaction to behave more as an electrophilic addition than as a nucleophilic ring-opening substitution. This behaviour accounts for the general preference of protonated epoxides to react at the more substituted carbon atom, while epoxides in neutral or basic media react at the least sterically hindered carbon. With consideration for Baldwin's rules for ring closure, it is seen that the series of model compounds generally favours six-membered ring formation *endo* at the epoxide.

The formation of the lanosterol B-ring was studied using a bicyclic model system. Previous computational studies had predicted the B-ring to close with readily with an activation energy of less than 1 kcal mol^{-1}, however the present study has found a significant barrier to cyclisation of ca. 5–7 kcal mol^{-1} in this gas-phase model at the HF/6-31G(d) level of theory. This barrier is thought to arise from the closure of the B-ring in a sterically hindered twist-boat conformation.

Chapter 1: Introduction

The biosynthesis of steroids and related polycyclic triterpene compounds occurs, in animals and fungi, via the tetracyclic precursor molecule lanosterol (**1.3**). Lanosterol is formed by cyclisation of 2,3-(*S*)-oxidosqualene (**1.1**), and subsequent rearrangement, in a remarkable process that forms four carbocyclic rings and seven new stereocentres and is catalysed by the single enzyme oxidosqualene cyclase (Figure 1.1). This reaction has been the subject of investigation for over fifty years and the area of research is still active today; for reviews of enzymatic polycyclic cyclisations of triterpenes, including lanosterol formation, see references [1] – [3].

The cyclisation of oxidosqualene is considered to occur as a cascade of electrophilic cation–alkene addition reactions.[1–3] The substrate is held in the active site of the enzyme in a reactive conformation and is activated by complexation of the epoxide oxygen atom with an aspartic acid residue.[4,5] Oxidosqualene is stable in neutral solution, and in glacial acetic acid for about one day, and requires a powerful acid such as trichloroacetic acid for non-enzymic cyclisation to occur on a short timescale; the acidity of the activating aspartic acid is increased by hydrogen-bonding partners.[6] The initial step of the reaction is considered to be the rupture of the activated three-membered ring with participation by the proximate 6,7-double bond (Figure 1.1), leading to closure of the A-ring of lanosterol, in a concerted S_N2 substitution-like process.[7,8]

The formation of the B-ring of lanosterol occurs rapidly following formation of the A-ring, however it is not known whether cyclisation of the first two rings is concerted or if a short-lived monocyclic intermediate exists.[2] The enzymatic cyclisation of oxidosqualene proceeds via a “chair–boat–chair” conformation (Figure 1.1); the flexible nature of the oxidosqualene molecule necessitates that the enzyme

provides tight conformational control of the substrate, in order to increase efficiency by restricting competing modes of reaction of intermediate structures.

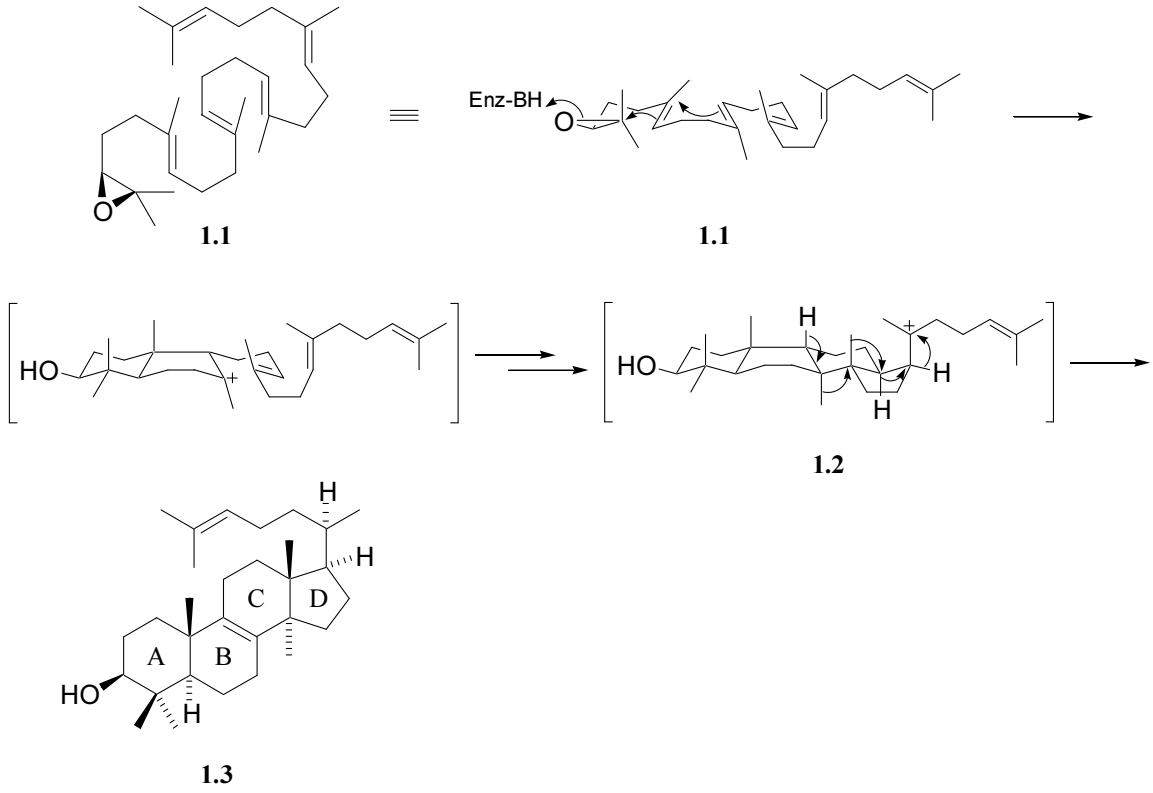

1.1 **1.1** **1.2** **1.3**

Figure 1.1. The enzyme-catalysed cyclisation of 2,3-(*S*)-oxidosqualene (**1.1**) to form lanosterol (**1.3**), via the protosteryl cation **1.2**.

Six-membered closure of the C-ring would represent the anti-Markovnikov mode of addition, forming a secondary carbocation intermediate, and the C-ring initially closes as a five-membered carbocycle[9,10] followed by ring expansion to the steroidal six-membered ring;[11] ring expansion of the C-ring may occur in concert with closure of the D-ring.[12] The D-ring cyclises with the side-chain in the β-position (above the molecular plane), which requires a smaller rotation to reach the natural 20*S* geometry of lanosterol than an α-oriented side-chain.[13,14] Following formation of the D-ring the intermediate protosteryl cation (**1.2**) undergoes a series of 1,2-methyl and hydride shifts and proton elimination to form lanosterol (Figure 1.1).

The work presented in this thesis is a computational exploration of the initiation and propagation of the enzymatic oxidosqualene cyclisation reaction. The structural and geometric nature of gas-phase model systems has been investigated to ascertain the degree of conformational and electronic control required by the enzyme. A brief outline of each of the model systems studied in this thesis is given below; a more detailed introduction is given at the start of each chapter.

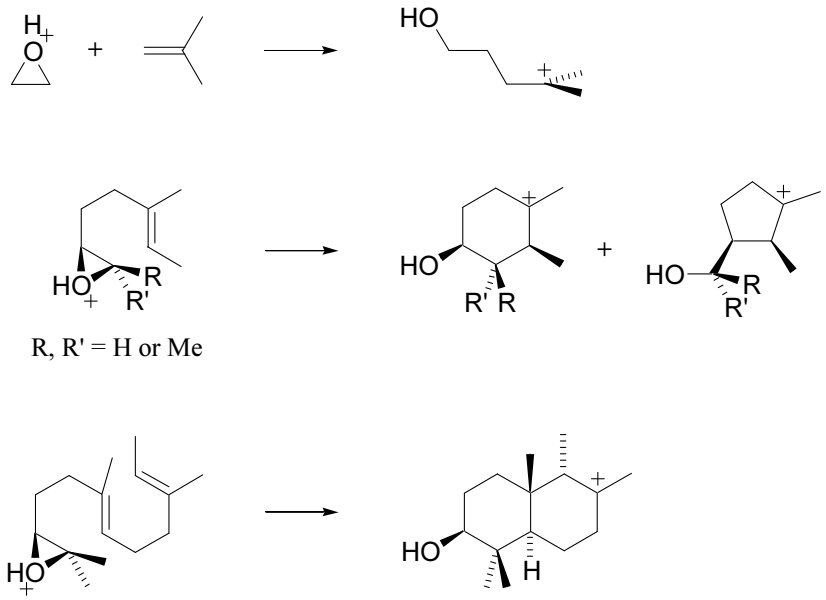

Figure 1.2. Oxidosqualene–lanosterol model systems investigated during the course of the work presented in this thesis. Top: initiation modelled by the reaction of protonated oxirane and methylpropene; middle: monocyclic A-ring model system; bottom: bicyclic B-ring model system.

The initial epoxide ring-opening reaction has been modelled by the intermolecular reaction of protonated oxirane and methylpropene (Figure 1.2); this investigation was performed in order to determine the optimal geometry and the shape of the potential energy surface for an S_N2-like epoxide–alkene reaction. The results from this study can be compared to models of lanosterol A-ring cyclisation in which the epoxide and alkene moieties are linked, and thus determine the energy cost associated with the structural restraints of the intramolecular reaction.

The stereoelectronic nature of the lanosterol A-ring has been investigated using a series of monocyclic model compounds substituted with hydrogen or methyl groups at the epoxide (Figure 1.2). The competing cyclisation reactions of these molecules *exo* and *endo* at the epoxide, forming five- and six-membered carbocycles respectively, have been followed, and the implications for the catalytic functionality of oxidosqualene cyclase are considered.

The relative timing of the formation of the A- and B-rings has been investigated using the bicyclic lanosterol model compound shown in figure 1.2. A previous computational study of this compound at the low HF/3-21G(d) level of theory[8] concluded that B-ring formation follows A-ring formation with no activation barrier; the same conclusion was reached from a computational study of the intermolecular reaction of 2-methylprop-2-ylium and 2-methylpropene.[10] A detailed investigation at the HF/6-31G(d) level of theory of the potential energy surface for cyclisation of this bicyclic model compound is reported here.

In addition to these investigations of lanosterol biosynthesis model systems, the regioselectivity of the reaction shown in figure 1.3 has been studied. This reaction is considered to proceed via the Diels–Alder adduct of the reactants, followed by elimination of carbon dioxide and hydrogen chloride.[15–17] The regioselectivity is observed to reverse between reaction at room temperature and in refluxing benzene, and an in depth study of the source of this reversal has been performed.

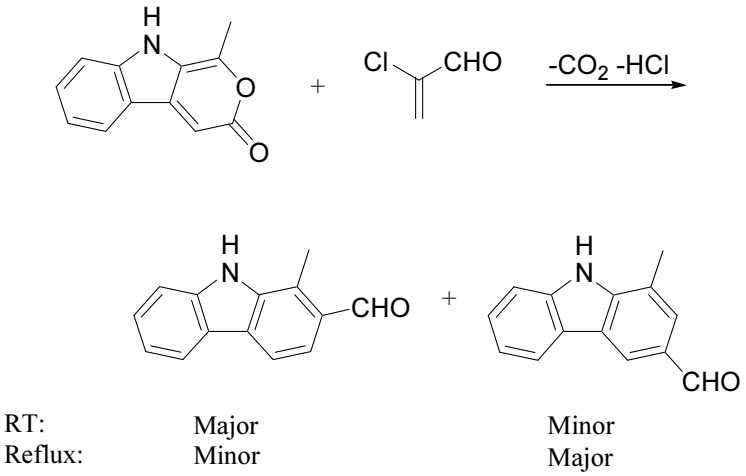

Figure 1.3. The cause of the experimentally observed reversal of regioselectivity for this reaction between room temperature and reflux has been investigated.

1.1 Computational methods

The work presented in this thesis is a computational investigation of reaction mechanisms. Calculations have been performed to find the structure of relevant stationary points on the reaction coordinate, both local minima (reactants and products) and the saddle points connecting local minima (transition states). The optimised geometries and calculated energies of these structures are used to build an image of the potential energy surface.[18] All calculations for which the results are presented in this thesis have been performed using the Gaussian 94W[19] and Gaussian 03W[20] program packages.

The quantum chemical models used in molecular modelling calculations solve an approximation of the Schrödinger wave equation (SWE) for the molecule. These models are usually a combination of a theoretical method and a basis set, which together are known as the *level of theory*. The level of theory is usually denoted by writing the abbreviation of the method used followed by the basis set and separated by a virgule, for example the HF/6-31G(d) level of theory uses the Hartree–Fock (HF) method on the 6-31G(d) basis set. When a high-level single point energy calculation

is performed on an optimised structure it is described by writing the level of theory for the energy calculation followed by the level of theory for the optimisation, for example the level of theory MP2/6-31G(d)//HF/6-31G(d) means a geometry optimisation was performed at HF/6-31G(d) followed by a single point energy calculation at MP2/6-31G(d)

The *method* represents the approximation to SWE used in the calculation. In this thesis the computational methods used are the ab initio Hartree–Fock (HF) and second order Møller–Plesset (MP2) methods, and the density functional theory Becke-3-parameter Lee–Yang–Parr (B3LYP) method.[18,21] The HF method is a common entry point and is relatively cheap in computational resources, however a major weakness of this method is that it electron correlation is not taken into account. The Møller–Plesset series of methods improve on the HF method by accounting for electron correlation, but with increased computational cost. Density functional methods account for electron correlation by introducing a correlation term based on electron density.

The *basis set* is the entire collection of basis functions, the atom-centred functions used to build the approximations of the molecular orbitals. Most basis sets are split-valence, where the core atomic orbitals are represented by one set of functions and the valence orbitals are split into inner and outer functions. A simple split-valence basis set is 6-31G, where each core atomic orbital is a combination of six Gaussian functions and the inner and outer valence orbitals are expanded in terms of three and one Gaussian respectively.[18]

Split-valence basis sets may be improved by inclusion of *d* orbital functions for heavy (non-hydrogen) main-group elements, where the valence orbitals are *s* and *p* orbitals; *p* orbital functions may also be included on hydrogen, where the valence

orbital is an *s* orbital. These *polarised basis sets* allow displacement of electron density away from the nuclei by mixing of the *p* and *d* orbitals. The polarised 6-31G(d) basis set (which may sometimes be written as 6-31G*) is constructed from the 6-31G basis set by inclusion of *d* polarisation functions.[18]

Energies obtained by calculation are electronic energies (ΔE), however thermodynamics depends on free energies (ΔG), which is derived from enthalpy (ΔH), entropy (ΔS) and temperature (T) by the equation:

$$\Delta G = \Delta H - T\Delta S$$

Enthalpy is related to energy by the equation:

$$\Delta H = \Delta E + \Delta(\mathrm{PV})$$

and this difference can usually be ignored in normal conditions.[18] The contribution of entropy to free energy can not be ignored, but it is common practice to treat ΔE and ΔG equivalently and only report electronic energies; this convention has been followed in this thesis, except in Chapter 3.2 where consideration of electronic energies gives rise to the impossible situation of transition states with apparently lower energy than an associated local minimum and free energies have been reported in this case(see Chapter 3.2).

Calculated electronic energies do not account for residual molecular vibration that persists at 0 K. The *zero-point energy* is a correction applied to the electronic energy to account for this error; the ZPE can be calculated from a frequency calculation.[21] Frequency calculations are also useful for establishing the identity of a stationary point; local minima have no imaginary freqencies, transition states have a single imaginary freqency and higher order saddle points have more than one imaginary freqency. Frequency calculations are also necessary to establish the force constants used in an *intrinsic reaction coordinate* (IRC) calculation, where the

reaction path may be followed from a saddle point to its two associated minima. Frequency calculations have known systematic errors and values derived from frequency calculations must be scaled appropriately to eliminate these errors.[21]

Chapter 2: Stereoselectivity and Regioselectivity of Diels–Alder Reactions

2.1 Introduction

The reaction shown in figure 2.1 was carried out by Professor N. S. Narasimhan of the University of Poona in Pune, India.[15–17] The alkene 2-chloroacrylaldehyde (**2.2**) was reacted with **2.1** in benzene in the presence of collidine and gives a mixture of products **2.3** and **2.4**; at room temperature the product ratio is 60% **2.3** to 40% **2.4**,[15] in refluxing benzene the reaction yields 21% **2.3** to 79% **2.4**.[15]

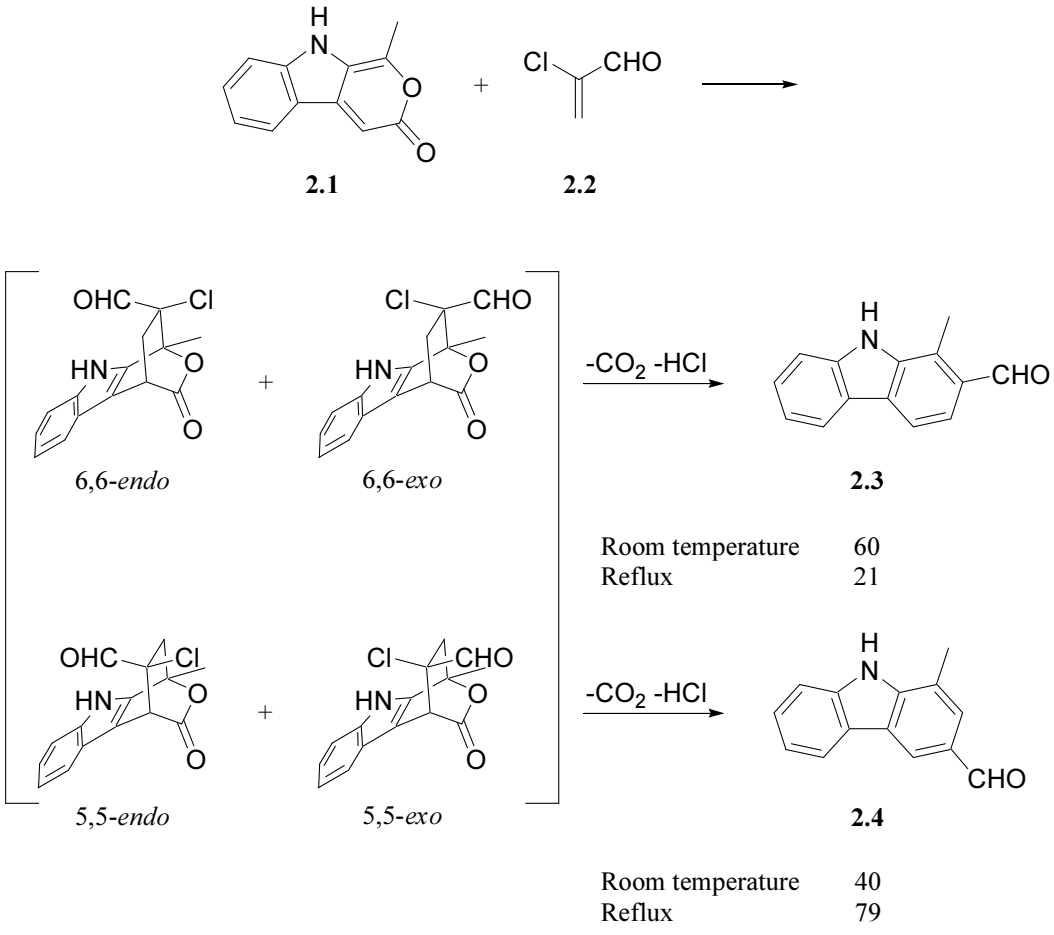

Figure 2.1. The observed product distribution at room temperature and reflux for the reaction between diene **2.1** and alkene **2.2** in benzene with the presence of collidine, and the proposed intermediate Diels–Alder adducts.

The reaction is considered to proceed via the Diels–Alder adduct, followed by elimination of carbon dioxide and hydrogen chloride to give the products. The regiochemistry is likely to be determined during the initial Diels–Alder reaction. There are four potential isomeric adducts, two regioisomeric pairs of diastereomers; upon elimination of carbon dioxide and hydrogen chloride, the 6,6-substituted diastereomers will yield product **2.3** and the 5,5-substituted adducts will give product **2.4**.

The present computational study investigates the causes of the observed reversal of regioselectivity between room temperature and reflux. To conserve limited computational resources, two model systems with the indole region of the diene removed have been investigated: the reaction of 2*H*-pyran-2-one with the simple dienophile ethene was studied to establish theory and techniques, and the potential energy surface for the reaction of 2*H*-pyran-2-one with **2.2** was examined in depth. The acquisition of a more powerful computer has allowed selected stationary points for the reaction of the full Narasimhan molecule **2.1** to be found.

This results presented here were obtained in the gas-phase at the HF/6-31G(d)//HF/6-31G(d) level of theory; computational limitations have precluded the use of higher levels of theory in the present study. It has been shown[22] that the Hartree–Fock method over-estimates the activation energy required to reach Diels–Alder transition states; the MP2 method underestimates the barrier and the closest agreement comes from calculations using the B3LYP, CCSD(T) and G2MS methods.[22] Solvent effects are expected to be low in the Diels–Alder and decarboxylation reactions as there is little charge redistribution in these pericyclic processes; however the solvent is expected to play a significant role in the base-

assisted elimination of hydrogen chloride due to the development of charge separation in the transition state.

2.2 Results and discussion: 2*H*-pyran-2-one and ethene model system

The HF/6.31G(d)//HF/6-31G(d) optimised geometries and calculated potential energy surface for the gas-phase Diels–Alder reaction of 2*H*-pyran-2-one (**2.5**) and ethene and the subsequent pericyclic decarboxylation are shown in figure 2.2.

Diels–Alder adduct **2.8** is reached via transition state **2.7**; IRC calculation of **2.7** in the reactant direction followed by geometry optimisation gives pre-reaction complex **2.6**. This complex is loose with the reactants far from the proto-bicyclo[2.2.2] structure expected for a Diels–Alder reaction. The geometry of the reactants in this complex are almost unchanged from those of the isolated reactants and they have distortion energies of 0.0065 kcal mol^{-1} (diene) and 0.018 kcal mol^{-1} (ethene). As a consequence of this looseness, the complex is only 0.7 kcal mol^{-1} lower than the sum of the reactant energies.

Gas-phase decarboxylation of adduct **2.8** is calculated to occur with an activation energy of 45.7 kcal mol^{-1}. A dipole–dipole product complex (**2.10**) has been found at ΔE = −34.9 kcal mol^{-1}; this represents an interaction energy between the products of $\delta\Delta E$ = 1.2 kcal mol^{-1}. As with reactant complex **2.6**, the product complex is not the expected proto-bicyclo[2.2.2] structure; the reactants have rotated relative to each other and the C_∞ axis of the carbon dioxide molecule is approximately parallel to the C_2 axis of cyclohexa-1,3-diene.

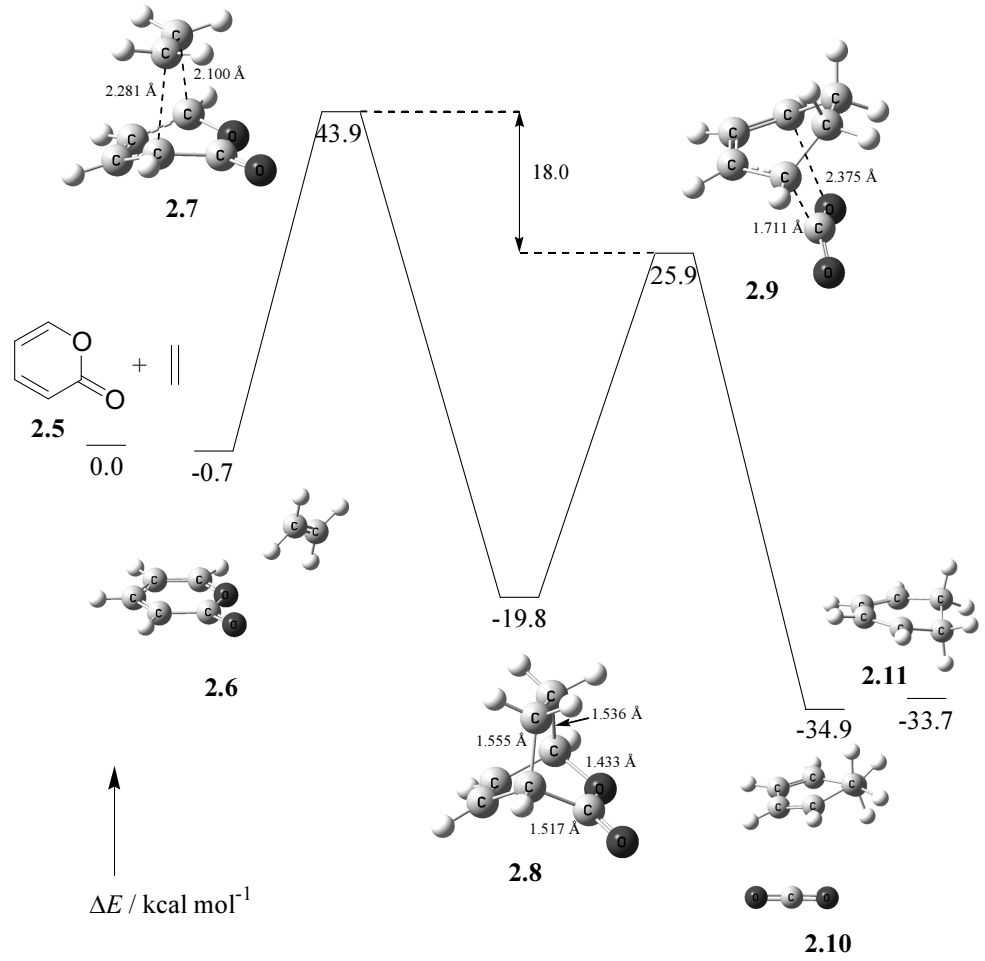

Figure 2.2. Calculated HF/6-31G(d)//HF/6-31G(d) energy profile for the Diels–Alder reaction of 2*H*-pyran-2-one (**2.5**) and ethene, and the subsequent decarboxylation to form cyclohexa-1,3-diene (**2.11**).

The results presented above for the HF/6-31G(d)//HF/6-31G(d) calculated potential energy surface of the reaction of **2.5** and ethene were obtained early in the course of the work published in this thesis; they were intended as exploratory calculations to learn the theory and methodology to be used in the course of this project. As ethene is a symmetric dienophile, this system is not particularly instructive in attempting to rationalise the regiochemistry observed for the reactions shown in figure 2.1, however it can be seen that both the initial Diels–Alder reaction and subsequent decarboxylation are exothermic processes and that the activation energy required for loss of carbon dioxide is significantly lower than the barrier for

the competing retro-Diels–Alder reaction. It therefore seems likely that elimination from the adduct will fix the regiochemistry observed by Professor Narasimhan, and that there is little equilibration to a thermodynamically preferred adduct at low temperature.

2.3 Results and discussion: 2*H*-pyran-2-one and 2-chloroacrylaldehyde model system

In the transition state for the Diels–Alder reaction of diene 2*H*-pyran-2-one (**2.5**) with dienophile 2-chloroacrylaldehyde (**2.2**), there are four orientations possible for the dienophile relative to the diene, leading to four regio- and diastereomeric adducts (structures **2.14a-d**; Figure 2.3). Loss of carbon dioxide from these adducts can either preceed or follow loss of hydrogen chloride. There are thus eight potential reaction paths leading to the products benzaldehyde (**2.19**), carbon dioxide and hydrogen chloride. The elimination reaction paths available to intermediate adduct **2.14a** are shown in figure 2.4; analogous elimination paths are possible for the other three adducts. Relevant stationary points on the reaction paths for all four alkene orientations have been found at the HF/6-31G(d)//HF/6-31G(d) level of theory and are now reported.

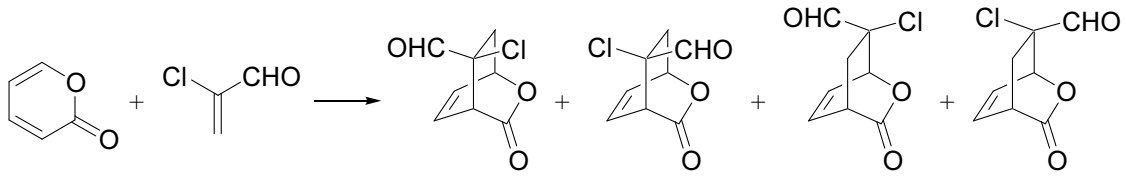

2.5 **2.2** **2.14a** **2.14b** **2.14c** **2.14d**

Figure 2.3. The four potential regio- and diastereomeric adducts that may be formed by Diels–Alder reaction of diene **2.5** and dienophile **2.2**.

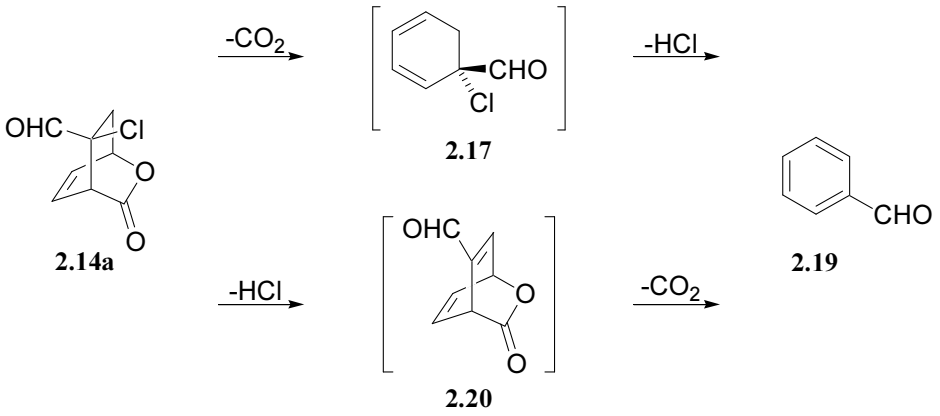

Figure 2.4. The two possible reaction paths for formation of benzaldehyde (**2.19**) from intermediate adduct **2.14a**. Equivalent reaction paths exist for the other three adducts.

Dienophile 2-chloroacrylaldehyde (**2.2**) can exist in *cisoid* or *transoid* conformational isomers. Calculations at the HF/6-31G(d) level of theory found the *cisoid* conformation to be 0.3 kcal mol^{-1} more stable than the *transoid* isomer (Figure 2.5). A C2–C3 rotational transition state, with C1–C2–C3–O dihedral angle of 97.9°, has been found connecting these two minima 7.5 kcal mol^{-1} above the *cisoid* configuration. As the *cisoid* conformation is slightly lower in energy, and is expected to give a more favourable secondary orbital interaction in the Diels–Alder transition states (Figure 2.6), all further calculations have been performed with the dienophile in *cisoid* conformation.

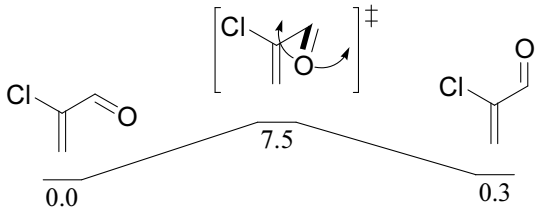

Figure 2.5. The c*isoid* and *transoid* conformational isomers of dienophile **2.2**; the two conformations are linked by a rotational transition state.

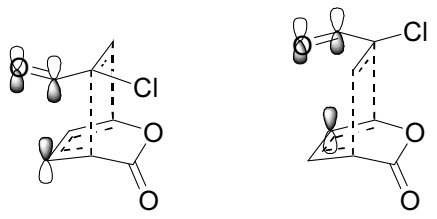

2.13a **2.13c**

Figure 2.6. The stabilising secondary orbital interactions available in the transition states for the *endo* carbonyl group of the dienophile in the *cisoid* conformation.

Diels–Alder reaction. The four potential adducts of the Diels–Alder reaction of 2-chloroacrylaldehyde (**2.2**) and 2*H*-pyran-2-one (**2.5**) are two regioisomeric pairs of *endo*/*exo* diastereomers (Figure 2.3). The calculated HF/6-31G(d)//HF/6-31G(d) potential energy surfaces of the four isomeric Diels–Alder reactions of **2.2** and **2.5** and subsequent decarboxylations are shown in figures 2.7 (5,5-*endo* adduct), 2.8 (5,5-*exo* adduct), 2.9 (6,6-*endo* adduct) and 2.10 (6,6-*exo* adduct). The regiochemistry of the 5,5-substituted adducts is equivalent to that which leads to the major product found by Narasimhan from reaction carried out in refluxing benzene and the 6,6-substituted adducts have equivalent regiochemistry to the major product from the room temperature reaction (Figure 2.1).

All four potential isomeric Diels–Alder transition states have been optimised at the HF/6-31G(d) level of theory and confirmed by frequency calculations; these transition states are proto-bicyclo[2.2.2] structures. The transition states with the carbonyl group of the dienophile in the *endo* position (**2.13a** and **2.13c**) are lower in energy than their *exo* diastereomers (**2.13b** and **2.13d** respectively), indicating that there is a more favourable secondary orbital interaction between the carbonyl and the diene than between the chlorine atom and the diene (Figure 2.6); the preference for the *endo* diastereomer is 2.1–2.5 kcal mol^{-1}.

There is also a 2.1–2.5 kcal mol^{-1} preference for the 6,6-substituted transition states over the regioisomeric 5,5-substituted transition states. It is known that Diels–Alder reactions between dienes and alkenes where each reactant has one electron-withdrawing substituent react preferentially to form the 1,2-substituted adduct;[23] this preference is thought to arise from the effect of substituent on the size of the orbital lobes at each end of the reactants. In the present system, both ends of the diene have electron-withdrawing groups and a prediction of the regiochemistry based on molecular orbital theory is problematic; however, from the calculated results presented here, it is clear that a more favourable orbital interaction in the transition states with the substituted end of the alkene adjacent to the oxygen-substituted end of the diene.

The transition state with the lowest energy is thus the 6,6-*endo* isomer (**2.13c**), which is 44.6 kcal mol^{-1} above the free reactants. This is consistent with Narasimhan's observation that the predominant product in the low temperature reaction has the regiochemistry corresponding to the 6,6-substituted adducts.

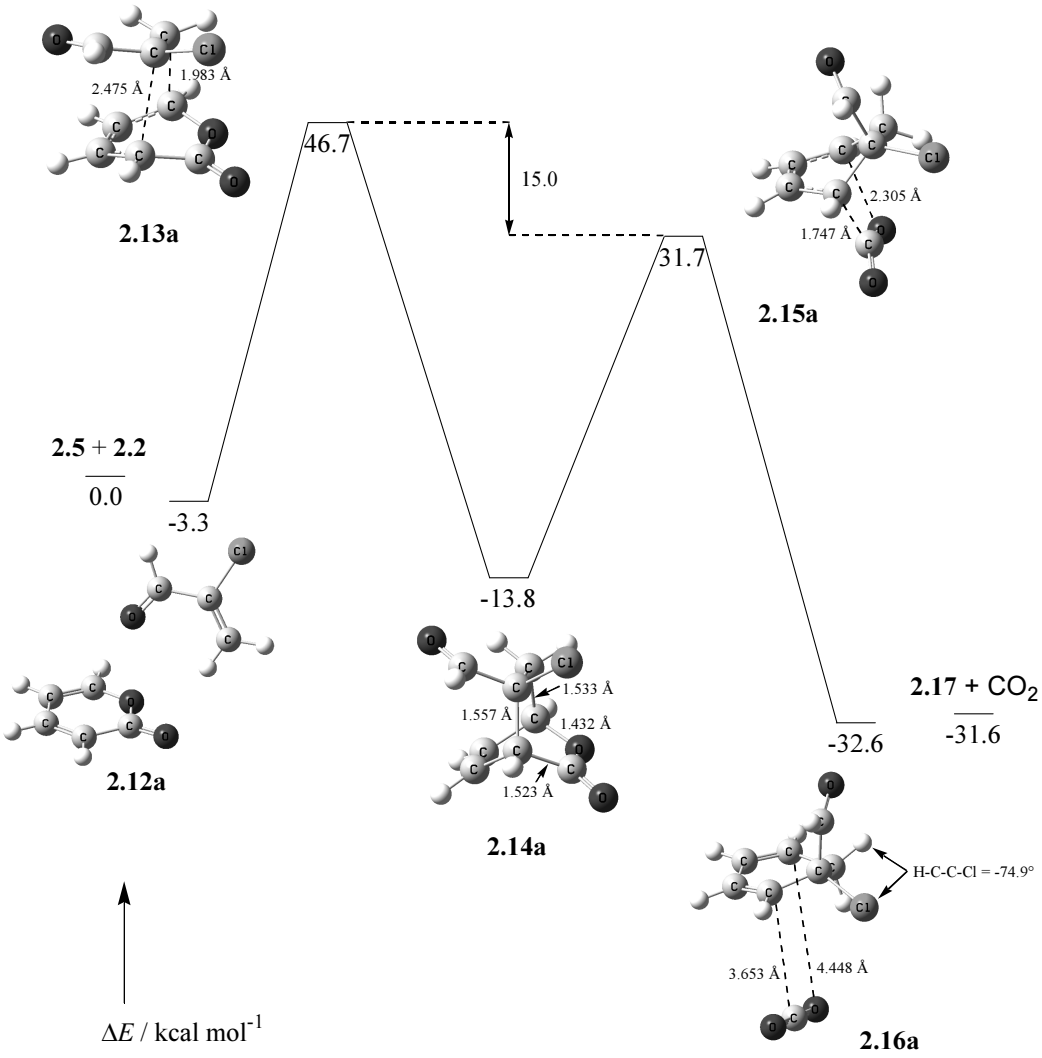

Figure 2.7. HF/6-31G(d)//HF/6-31G(d) stationary points for the 5,5-*endo* Diels–Alder reaction of **2.5** and **2.2**, and the subsequent decarboxylation of the adduct.

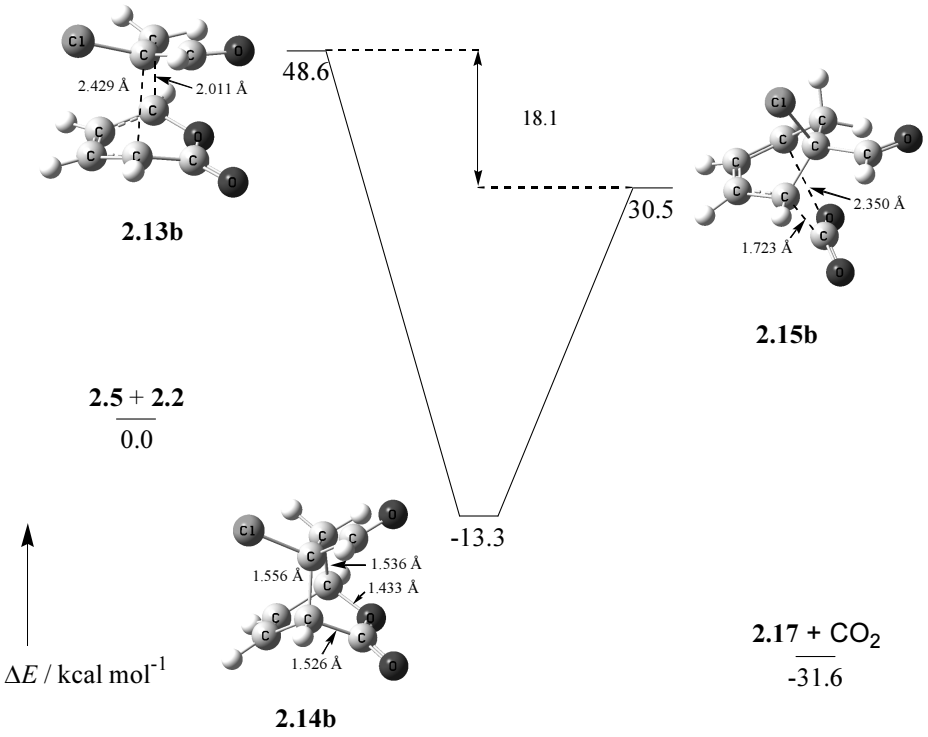

Figure 2.8. HF/6-31G(d)//HF/6-31G(d) stationary points for the 5,5-*exo* Diels–Alder reaction of **2.5** and **2.2**, and the subsequent decarboxylation of the adduct.

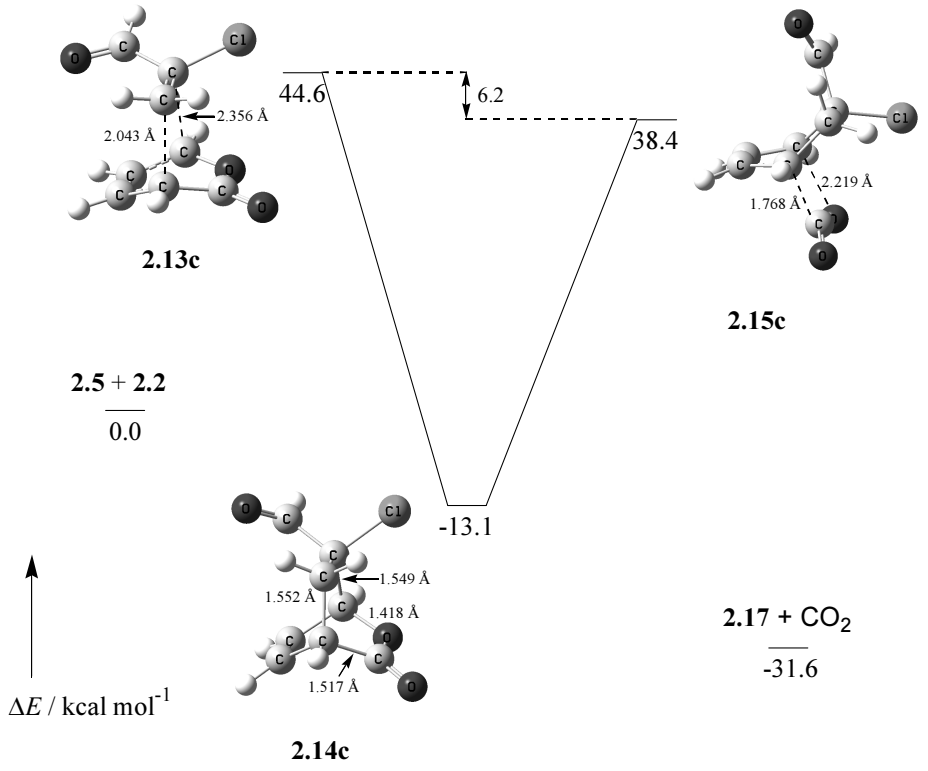

Figure 2.9. HF/6-31G(d)//HF/6-31G(d) stationary points for the 6,6-*endo* Diels–Alder reaction of **2.5** and **2.2**, and the subsequent decarboxylation of the adduct.

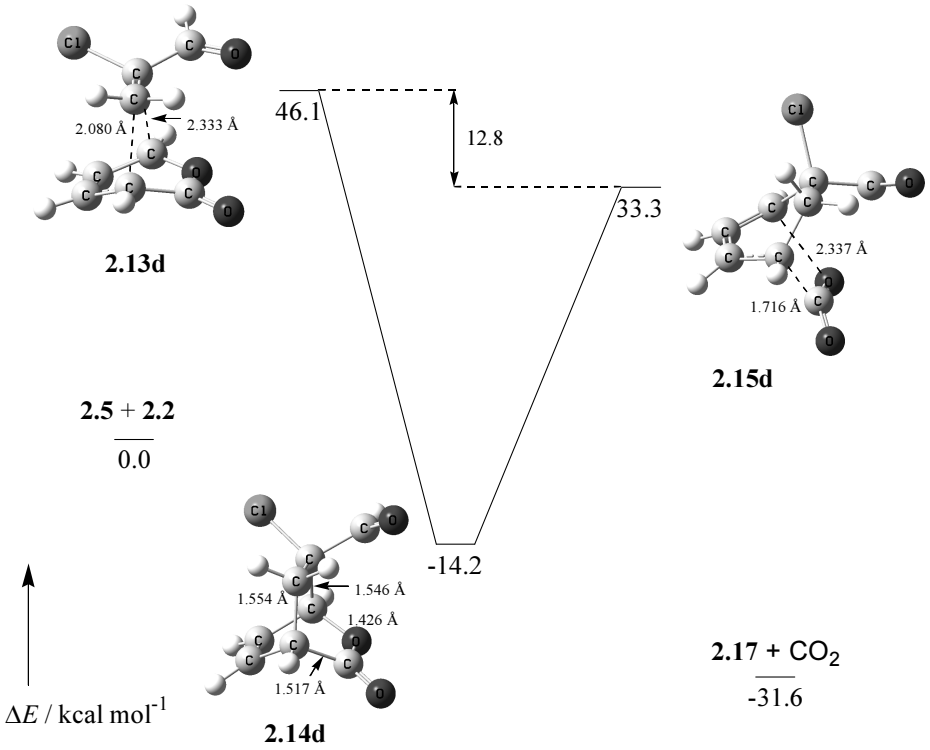

Figure 2.10. HF/6-31G(d)//HF/6-31G(d) stationary points for the 6,6-*exo* Diels–Alder reaction of **2.5** and **2.2**, and the subsequent decarboxylation of the adduct.

Following the intrinsic reaction coordinate (IRC) of 5,5-*endo* transition state **2.13a** in the direction of the reactants yielded pre-reaction dipole–dipole complex **2.12a**. As with pre-reaction complex **2.6** of 2*H*-pyran-2-one and ethene (Figure 2.2), complex **2.12a** is loose and is not in a proto-bicyclo[2.2.2] configuration (Figure 2.7). Complex **2.12a** is ΔE = −3.3 kcal mol^{-1} lower than the combined energy of the reactants at infinite separation. It is expected that similar loose reactant complexes exist on the other isomeric reaction, however, given the computational expense required to find structure **2.13a** and that the solution-phase Diels–Alder reaction is likely to pass from the reactants to the transition state directly without the presence of a pre-reaction intermediate, no attempt has been made to find the gas-phase dipole complexes for the other isomeric reactions.

From Narasimhan's observation that regioisomer **2.4** is the favoured product in refluxing benzene, it would be expected that one of the 5,5-substituted adducts is

the thermodynamically preferred product of the initial Diels–Alder reaction, and that the higher temperature at reflux allowed some degree of equilibration to take place. This expectation is not supported by the results of the present study as the lowest energy adduct found is the 6,6-*exo* isomer at $\Delta E = -14.2$ kcal mol^{-1}; the highest energy adduct is the 6,6-*endo* isomer at $\Delta E = -13.1$ kcal mol^{-1}. The two 5,5-substituted adducts occur at $\Delta E = -13.8$ kcal mol^{-1} (*endo*) and $\Delta E = -13.3$ kcal mol^{-1} (*exo*). Calculations at a higher level of theory, or of a molecular system closer to that of Narasimhan's reactions, may more accurately describe the observed experimental results.

Decarboxylation of Diels–Alder adducts. Transition states for the decarboxylation of isomeric adducts **2.14a-d** have been found at the HF/6-31G(d) level of theory (Figures 2.7 to 2.10). Transition states **2.15a-d** are all calculated to be significantly lower in energy than transition states **2.13a-d** for the competing retro-Diels–Alder reactions, in agreement with the assumption that limited equilibration occurs at low temperatures.

The adducts **2.14a-d** decarboxylate to give the same products: carbon dioxide and 1-chlorocyclohexa-2,4-diene-1-carbaldehyde (**2.17**). Adducts **2.14a** and **2.14d** give the 1*S*-enantiomer of **2.17**, and **2.14b** and **2.14c** give the 1*R*-enantiomer.

An IRC calculation of decarboxylation transition state **2.15a** lead to dipole–dipole product complex **2.16a**; this product complex has an interaction energy of 1.0 kcal mol^{-1}. The complex is loose with distortion energies of the products below 0.01 kcal mol^{-1}, however, unlike the other dipole complexes for pericyclic reactions found in the present study, complex **2.16a** is in a proto-bicyclo[2.2.2] configuration.

Elimination of HCl from decarboxylated adducts. In decarboxylation product complex **2.16a**, substituted cyclohexadiene **2.17** is in a conformation with the

aldehyde substituent oriented axially (**2.17ax**; Figure 2.11). In order to achieve optimal orbital overlap, base catalysed dehydrohalogenation by the E2 mechanism requires coplanarity of the halogen and hydrogen.[24,25] This can be from either *syn* or *anti* configurations, with the less hindered *anti*-periplanar (staggered) transition state being energetically favourable. In conformation **2.17ax** the hydrogen and chlorine atoms are not coplanar (the H–C–C–Cl dihedral angle is −74.5°) and a ring twist conformation change is required to bring the relevant bonds into a reactive position. Conformation **2.17eq** has an H–C–C–Cl dihedral angle closer to planarity at −155.9° and is reached from **2.17ax** via ring-twist transition state **2.17ts** (Figure 2.11). Conformation **2.17ax** is 0.7 kcal mol^{-1} higher in energy than **2.17eq**, likely due to a slightly higher intramolecular steric interaction of the axially oriented aldehyde over the axial chlorine.

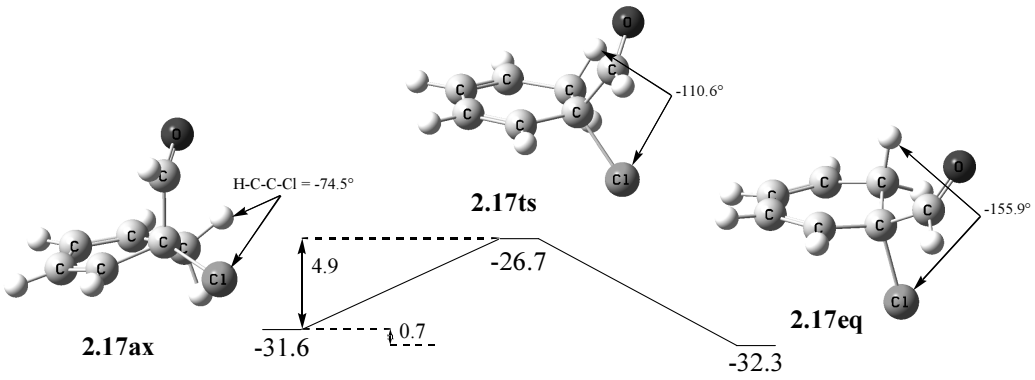

Figure 2.11. Ring-twist conformational isomers of intermediate **2.17**; relative energies are in kcal mol^{-1}.

Narasimhan[16,17] conducted his reactions in the presence of the aromatic base collidine (2,3,5-trimethylpyridine). In the present study, gas-phase transition states have been found at the HF/6-31G(d) level of theory for the E2 elimination of HCl catalysed by two nitrogenous bases: ammonia and pyridine. Intermolecular assistance for the departure of the chloride ion has not been included in the present study; it is expected that in solution the leaving ion becomes solvated or interacts with a

protonated molecule of the base to form hydrogen chloride directly. In solution, elimination reaction proceeds directly from the reactants through a transition state to the products, however in the gas phase the reaction has a "double well" energy profile and the reactants and products form intermediate ion–dipole complexes.[24,25]

Dehydrohalogenation transition state **2.18py** (pyridine base) is slightly lower in energy ($\delta\Delta E$ = −0.7 kcal mol^{-1}) than ammonia-catalysed transition state **2.18am** (Figure 2.12). This energy difference can be attributed to the aromatic ring of the pyridine molecule stabilising the developing positive charge more effectively than the ammonia molecule. This is confirmed by calculations of free ammonium and pyridinium ions, which show that protonation of pyridine is 18.6 kcal mol^{-1} more favourable than protonation of ammonia.

Base–substrate ion–dipole complexes have not been found, however transition state **2.18py** is 29.1 kcal mol^{-1} above the intermediate **2.17eq**; solvation is expected to lower the energy of the transition state by stabilising the developing charge separation. The elimination of hydrogen chloride is exothermic by ΔE = −27.6 kcal mol^{-1} and the final products of decarboxylation and dehydrohalogenation (i.e. benzaldehyde (**2.19**), carbon dioxide and hydrogen chloride) are ΔE = −59.9 kcal mol^{-1} below the Diels–Alder reactants **2.5** and **2.2** (Figure 2.12).

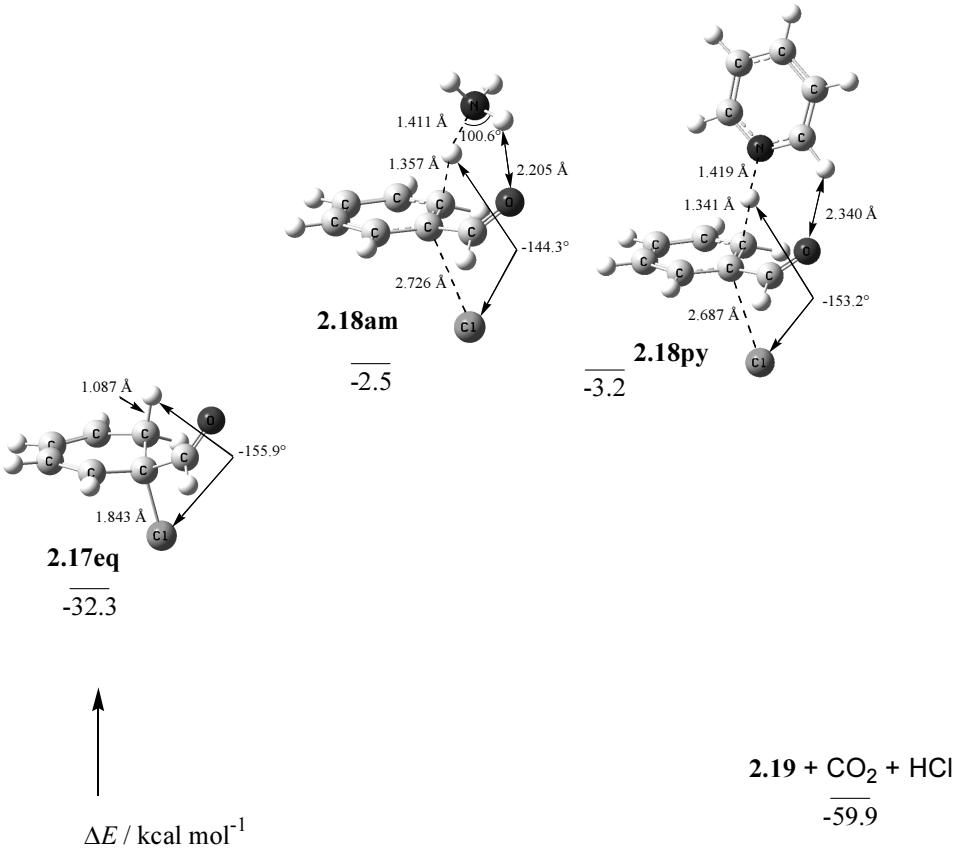

Figure 2.12. Ammonia- and pyridine-catalysed transition states for the E2 elimination of HCl from intermediate **2.17eq**. The reported transition state energies have the energy of the free base subtracted (see Appendix).

Anti-periplanar gas-phase transition states for simple nucleophile-assisted E2 elimination from substituted ethanes have a H···C–C···X dihedral angle of 180.0°.[24,25] The corresponding H···C6–C1···Cl dihedral angle is −144.3° in **2.18am** and −153.2° in **2.18py**. The deviation of these angles from the optimal values seen in substituted ethane systems can primarily be attributed to bond angle strain in the cyclic system as these values are close to the −155.9° seen in intermediate **2.17eq**.

The six-membered carbocyclic rings of the transition states are near planar (the C5–C6–C1–C2 angle is −11.6° in **2.18am** and −14.5° in **2.18py**), indicating that aromaticity is well developed in the transition state, however the carbonyl does not lie in the plane of the ring as in the conjugated planar product benzaldehyde (**2.19**). It is

likely that this deviation from coplanarity arises from a non-bonding interaction of the oxygen atom with a hydrogen atom of the base. The H···O distances are 2.205 Å in **2.18am** and 2.340 Å in **2.18py**, within the accepted distance for hydrogen bonding interactions. Other evidence for this interaction is seen in the relevant nitrogen–hydrogen bond of the base in **2.18am** (Figure 2.12): this bond is slightly longer than the other N–H bonds and the H···N–H angle is significantly narrowed (100.6° compared to ca. 114° for the other bonds). This hydrogen bonding interaction between the base and the carbonyl group may also be a contributing factor towards the non-linearity of the C6···H···N bond angle.

Ion–dipole complexes of the products have not been found, however an incomplete IRC calculation of **2.18am** suggests that late in the reaction path the dissociated Cl^- ion attacks the carbon atom of the carbonyl group and the O–H interaction, designated above as a hydrogen-bonding interaction, develops into a transfer of the proton from the NH_4^+ molecule to form chloro(phenyl)methanol. This reaction is unlikely to occur in a solution-phase reaction as the chloride ion is solvated and stabilised. Further calculations, including solvent simulations or inclusion of a stabilising group for the chloride ion such as NH_4^+, need to be performed to determine the significance of this interaction.

Elimination of HCl from adduct before decarboxylation. It has been assumed in the above discussion that decarboxylation of the Diels–Alder adduct occurs prior to HCl elimination. This assumption was made on the bases that decarboxylation of the adduct forms a planar conjugated diene, while dehydrohalogenation forms a non-conjugated bicyclo[2.2.2] diene, and that elimination of HCl requires participation of a base, while elimination of carbon dioxide is a unimolecular pericyclic reaction and therefore expected to occur rapidly

following formation of the adduct. To test the validity of this assumption, the reaction path in which dehydrohalogenation of adduct **2.14a** precedes decarboxylation has been investigated.

Transition states for ammonia- and pyridine-catalysed E2 elimination of hydrogen chloride from 5,5-*endo* adduct **2.14a** are shown in figure 2.13. The rigid bicyclo[2.2.2] structure can not rotate to allow *anti*-periplanar elimination and therefore only *syn* elimination transition states have been found. The H···C6–C5···Cl dihedral angles are slightly deviant from planarity, being 6.4° and 7.6° in the ammonia and pyridine transition states respectively. This deviation is likely a steric effect caused by interaction of the base and departing atoms with the lactone region of the substrate.

Transition state **2.18py** for elimination from the decarboxylated adduct is lower than **2.18am**, considered to be a result of more efficient stabilisation of the positive charge by pyridine. The order of stability is reversed for elimination directly from the adduct, with transition state **2.20py** 2.0 kcal mol^{-1} higher in energy than ammonia-catalysed transition state **2.20am**. This difference is possibly a steric effect of the larger pyridine molecule over the ammonia molecule interacting with the bulkier bicyclo[2.2.2] substrate.

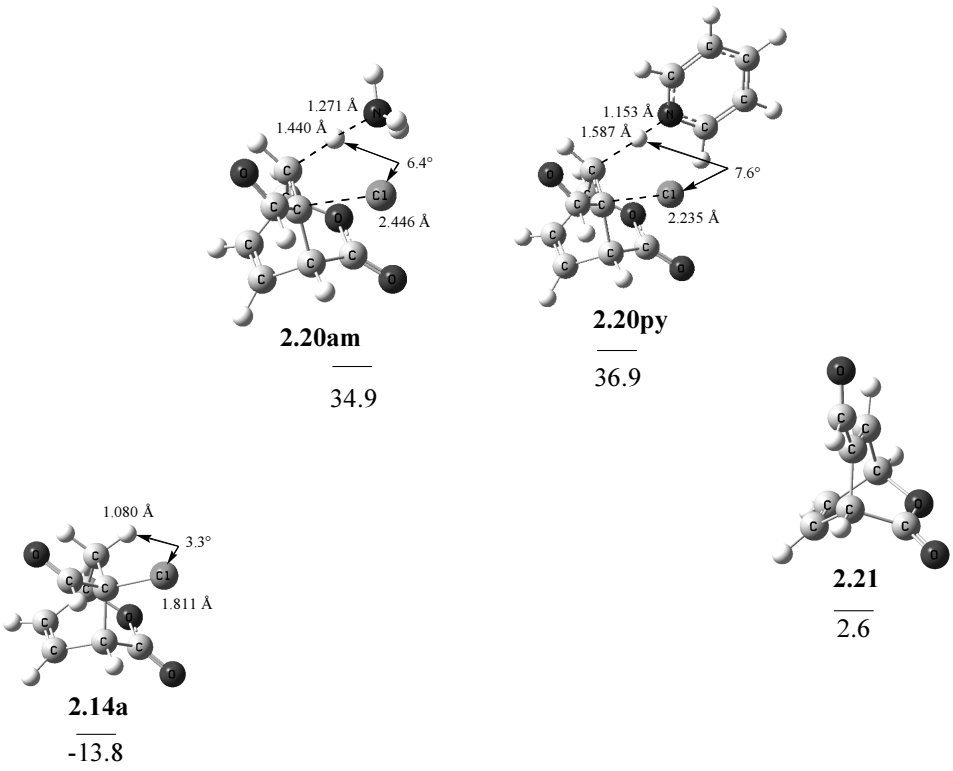

Figure 2.13. Transition states for ammonia- and pyridine-catalysed E2 elimination of HCl from Diels–Alder adduct **2.14a**.

The base–substrate and product–product dipole complexes linked by these transition states have not been found, however **2.20am** is 48.7 kcal mol^{-1} and **2.20py** is 50.7 kcal mol^{-1} higher than Diels–Alder adduct **2.14a**. These transition state energies are 3.2 kcal mol^{-1} and 5.2 kcal mol^{-1} higher than the activation barrier for the competing decarboxylation reaction that proceeds via transition state **2.15a** (Figure 2.7). The higher transition state energy for dehydrohalogenation and the bimolecular nature of the reaction suggests that the regioselectivity of the Diels–Alder reactions is fixed by loss of carbon dioxide rather than loss of hydrogen chloride.

A transition state (**2.22**) for pericyclic loss of carbon dioxide from dehydrohalogenated adduct **2.21** to form benzaldehyde has also been found (Figure 2.14). This transition state is reached with an activation energy of 28.7 kcal mol^{-1}, which is considerably less than the activation barriers for decarboxylation of the

Diels–Alder adducts shown in figures 2.7 to 2.10. This lower barrier to reaction reflects the favourable formation of an aromatic six-membered ring over the cyclohexadiene system of **2.17**.

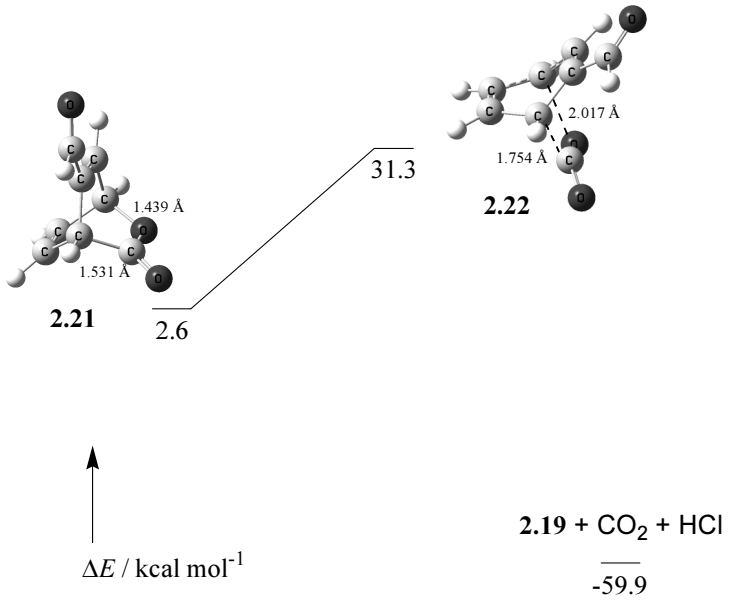

Figure 2.14. Transition state for decarboxylation of dehydrohalogenated intermediate **2.21** to form benzaldehyde.

2.4 Results and discussion: full Narasimhan system

The potential energy surface of the reaction of 1-methylpyrano[3,4-*b*]indol-3(9*H*)-one (**2.1**) and 2-chloroacrylaldehyde (**2.2**) has been investigated at the HF/6-31G(d) level of theory. Due the large size of these molecules and the limited availability of computational resources, only the stationary points considered most important have been found. Transition states and adducts for all four regio- and diastereomers of the initial Diels–Alder reaction have been found, however further calculations have been performed for only the *endo* isomers. Dipole–dipole complexes have not been found as these are expected to be loose and only present in the gas phase. Following the results presented in Chapter 2.3 above, it has been assumed that decarboxylation of the adduct is preferred over dehydrohalogenation,

and the competing reaction path in which elimination of hydrogen chloride occurs first has not been explored.

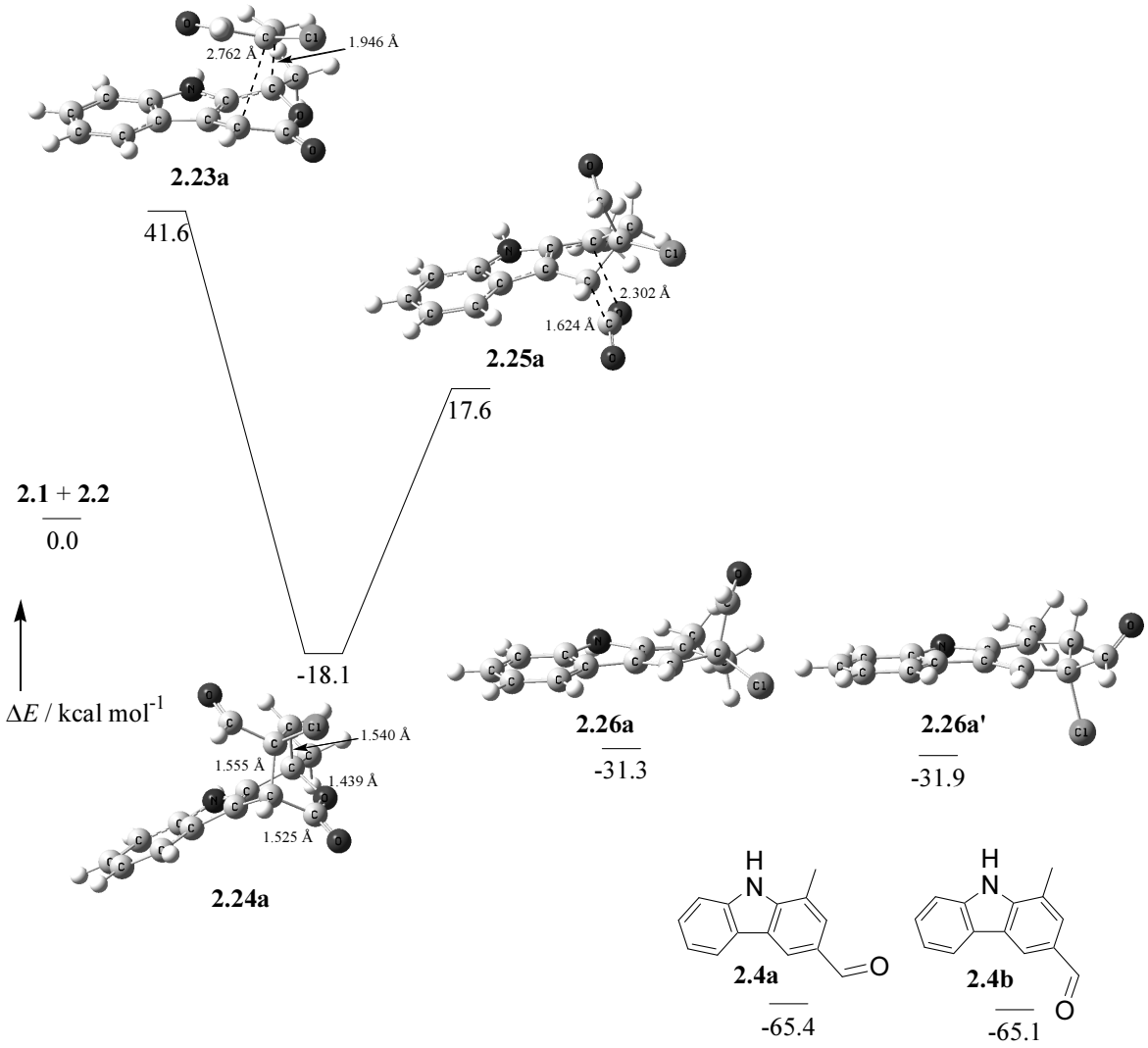

Figure 2.15. Selected stationary points on the HF/6-31G(d)//HF/6-31G(d) potential energy surface for the 5,5-*endo* Diels–Alder reaction of diene **2.1** and dienophile **2.2**, and the subsequent eliminations to form product **2.4**.

Stationary points found for the 5,5-*endo* reaction of **2.1** and **2.2** are shown in figure 2.15 and for the 6,6-*endo* reaction in figure 2.16; Diels–Alder transition states and adducts for the *exo* isomers are shown in figure 2.17. As with the 2*H*-pyran-2-one model system (Chapter 2.3), the *endo* transition states are ca. 2 kcal mol^{-1} lower than their *exo* diastereomers, and the 6,6 regioisomers are lower than the 5,5

regioisomers by approximately the same amount. The 6,6-*endo* adduct (**2.24b**) is the kinetically favoured intermediate and is expected to lead to the favoured product at low temperature. This is consistent with the experimental results of Narasimhan, who observed that the major product at room temperature was **2.3** (Figure 2.1), with regiochemistry corresponding to that of the 6,6-substituted adducts.

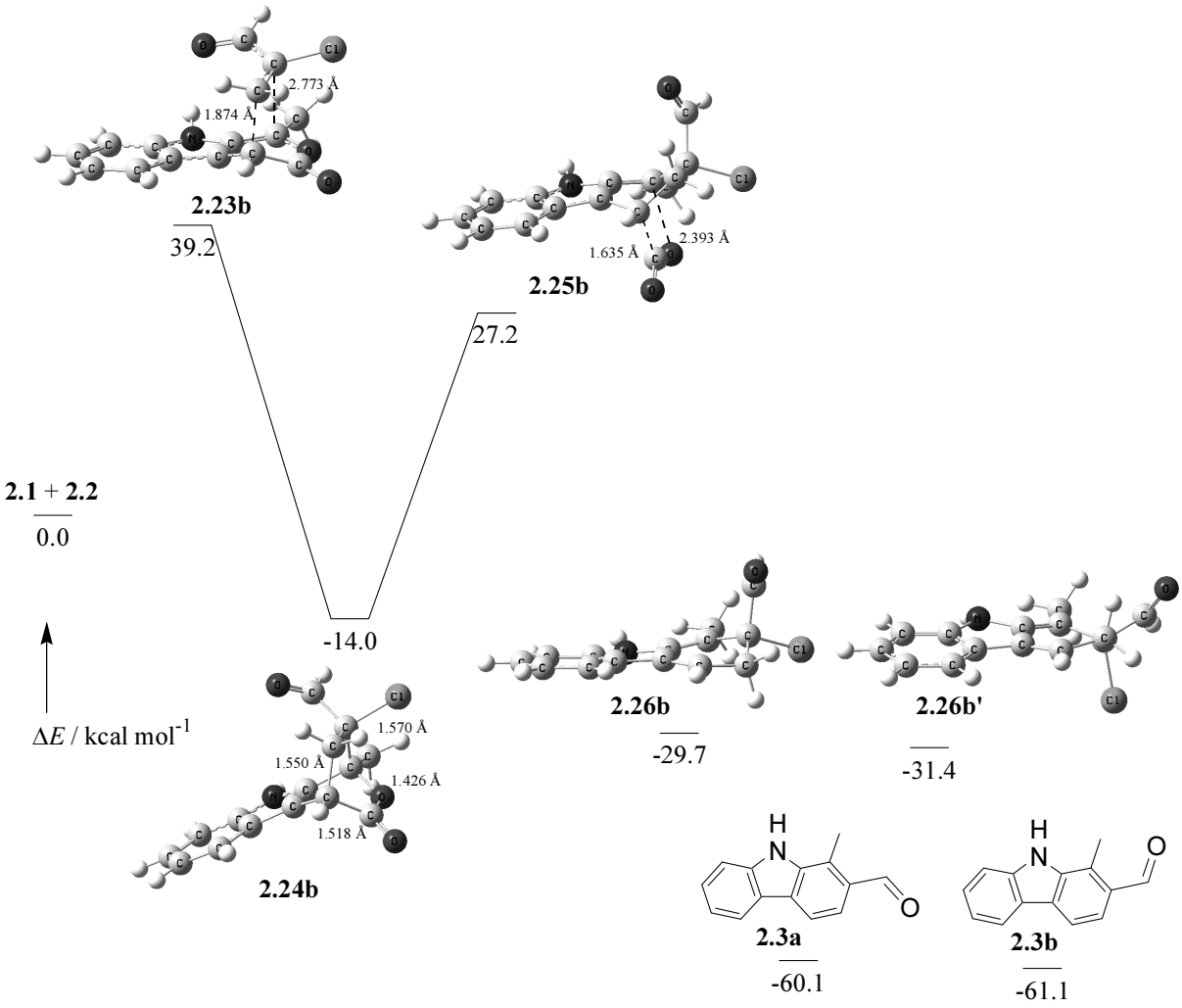

Figure 2.16. Selected stationary points on the HF/6-31G(d)//HF/6-31G(d) potential energy surface for the 6,6-*endo* Diels–Alder reaction of diene **2.1** and dienophile **2.2**, and the subsequent eliminations to form product **2.3**.

Both 5,5-sustituted adducts, corresponding to the regiochemistry of the major product at reflux, are lower in energy than the 6,6-substituted adducts. The 5,5-*endo* adduct (**2.24a**) is at $\Delta E = -18.1$ kcal mol^{-1} and the 5,5-*exo* adduct (**2.24c**) is at $\Delta E =$

−16.8 kcal mol^{-1}, while the most stable 6,6-substituted adduct is the *exo* diastereomer (**2.24d**) at ΔE = −14.8 kcal mol^{-1}. The higher energy of the 6,6-substituted adducts may arise from a steric interaction of the carbonyl or chlorine substituent with the methyl group or the aromatic region of the molecule. These results are consistent with the expectation that the major product found at high temperatures is formed from the thermodynamically favoured adduct.

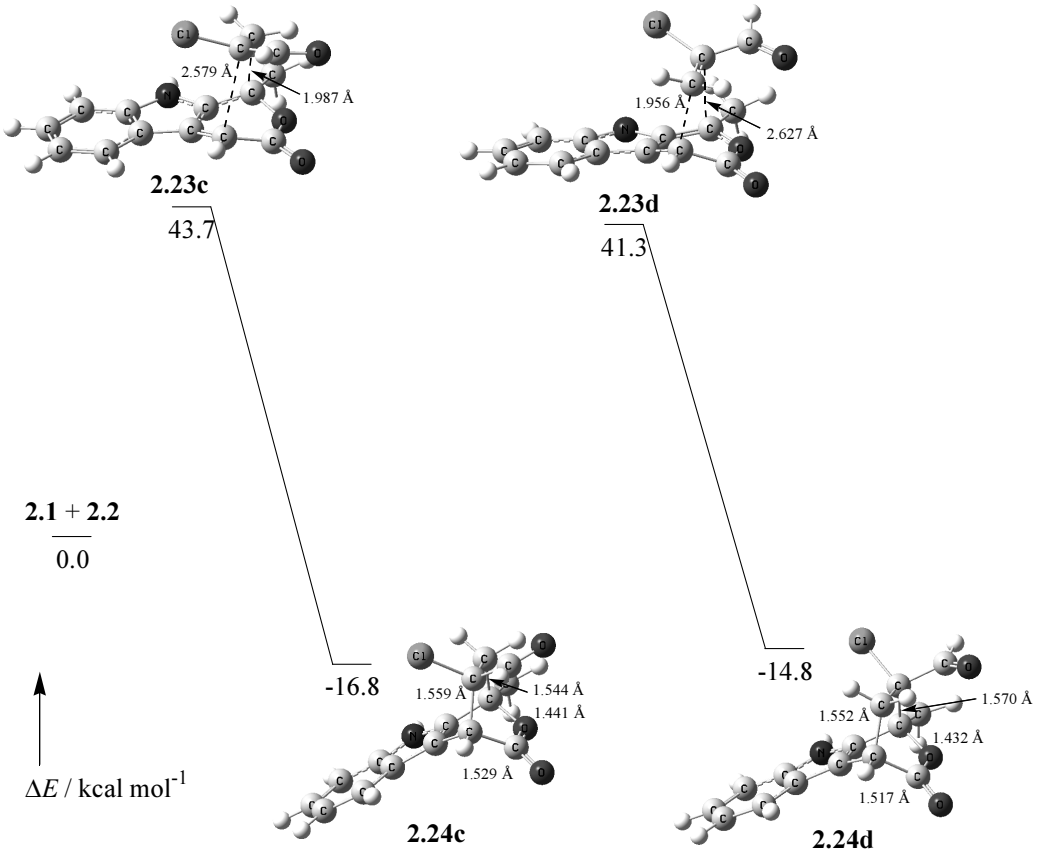

Figure 2.17. HF/6-31G(d) transition states and adducts for the *exo* isomers of the Diels–Alder reaction between diene **2.1** and dienophile **2.2**.

2.5 Conclusion

A detailed study of the gas-phase HF/6-31G(d)//HF/6-31G(d) potential energy surface for the Diels–Alder reaction of 2*H*-pyran-2-one (**2.5**) with dienophile 2-chloroacrylaldehyde (**2.2**), and subsequent decarboxylation and dehydrohalogenation, has been performed as a model for the reactions carried out by Professor Narasimhan.

The important transition states and minima for the reaction of the full Narasimhan system have also been found. The Diels–Alder reaction and carbon dioxide elimination reaction are both pericyclic cycloaddition or retro-cycloaddition processes with loose dipole–dipole complexes. The observed regiochemistry is expected to be determined by the kinetic adduct (lowest energy transition state) at room temperature and by the thermodynamic adduct (lowest energy adduct) at reflux.

The two lowest energy Diels–Alder transition states of the 2-*H*-pyran-2-one model system are calculated to be the two 6,6-substituted regioisomers. Elimination of carbon dioxide and hydrogen chloride from these adducts gives the 1,2-substituted product, the regioselectivity observed by Professor Narasimhan at room temperature. The most stable adduct of the 2-*H*-pyran-2-one model system is calculated to be the 6,6-*exo* isomer, which does not correspond to the regiochemistry of the predominant product at reflux. Thus, at the HF/6-31G(d)//HF/6-31G(d) level of theory, the calculated results for the 2-*H*-pyran-2-one model system correctly predict the observed regiochemistry for the room temperature reaction, but are not in agreement with the observed regiochemistry of the reaction at reflux.

The order of transition state energies calculated for the Diels–Alder reaction of the Narasimhan diene (**2.1**) is the same as that calculated for the 2-*H*-pyran-2-one system. The 6,6-substituted transition states are the lowest in energy, corresponding to the regiochemistry of the major product at room temperature. The most stable adduct for the reaction of **2.1** is calculated to be the 5,5-*endo* regioisomer; elimination of carbon dioxide and hydrogen chloride from this adduct gives the 1,3-substituted product, which is observed to be the predominant regioisomer from reaction in refluxing benzene. Therefore, the HF/6-31G(d)//HF/6-31G(d) calculated potential energy surface for the reaction of **2.1** and alkene **2.2** is in agreement with the

regiochemistry observed by Professor Narasimhan at both room temperature and reflux.

Chapter 3: Ring-Opening Reaction of Protonated Oxirane and Methylpropene

3.1 Introduction

The cyclisation of 2,3-(*S*)-oxidosqualene (**1.1**) to form the tetracyclic steroid precursor lanosterol (**1.3**) is catalysed by the enzyme oxidosqualene cyclase[1,2] (Figure 1.1). The substrate is held by the active site of the enzyme in a reactive conformation and the epoxide is activated by an acidic amino acid residue.[4] The initial step of the cyclisation is considered to be the ring opening of the activated epoxide, in concert with S_N2-like nucleophilic attack by the proximate 6,7-double bond, leading to closure of the lanosterol A-ring.

The steric restrictions introduced by the linked epoxide and alkene moieties of oxidosqualene are likely to prevent the molecule from achieving optimal orbital overlap during the closure of the A-ring. To determine the optimal conformation of a ring-opening epoxide–alkene reaction of this type, and thence estimate the energy cost of the steric requirements of the oxidosqualene system, the initial step of the reaction was modeled by the gas-phase reaction of protonated oxirane (**3.1**) and methylpropene (**3.2**) shown in figure 3.1.

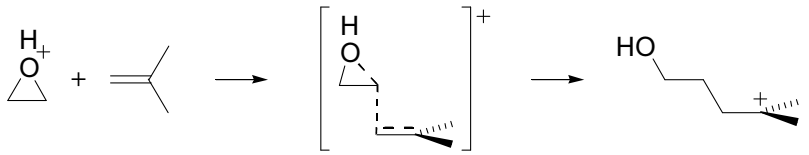

3.1 **3.2** **3.3**

Figure 3.1. The nucleophilic ring-opening reaction of protonated oxirane (**3.1**) and methylpropene (**3.3**) studied as a model of the initial step of oxidosqualene cyclisation.

Nucleophilic substitution reactions can proceed via a number of different mechanisms, the most common of which are the S_N1 and S_N2 mechanisms.[24] Nucleophilic substitution of protonated epoxides by the S_N1 mechanism would require unimolecular opening of the three-membered ring to an intermediate containing a carbocation centre adjacent to a hydroxyl group. Previous ab initio molecular modelling studies have shown that a local minimum of this general structure does not exist on the potential energy surface of **3.1** at the HF/6-31G(d)[26] and MP2/6-31G(d)[27] levels of theory, and that unimolecular ring opening of **3.1** leads to rearrangement to form a protonated aldehyde in a concerted, single step process (Figure 3.2). The absence of a stable carbocation intermediate on the calculated potential energy surface of **3.1** means that it is unlikely to undergo nucleophilic substitution by S_N1 mechanism.

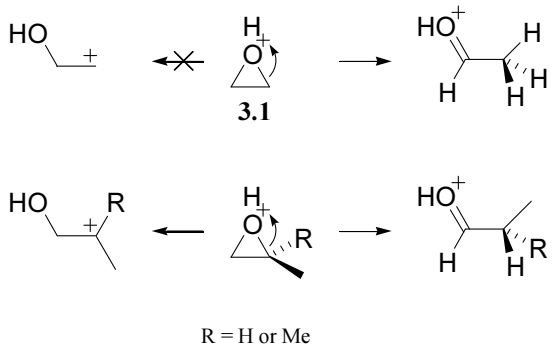

Figure 3.2. Unimolecular ring opening of **3.1** leads to molecular rearrangement in a concerted single-step process. Substituted oxiraniums may open to form stable carbocationic intermediates.

Secondary and tertiary carbocationic intermediates have been found on the potential energy surface for the rearrangement of protonated 2-methyloxirane[28] (MP2/6-31G(d) level of theory) and protonated 2,2-dimethyloxirane[29] (B3LYP/6-31G(d) level of theory), suggesting that S_N1-like, ring-opening substitution of those compounds may be possible for these compounds in the gas phase (Figure 3.2).

Oxidosqualene (**1.1**) is a substituted epoxide and it may be expected that ring opening of the enzyme-activated oxirane to form an intermediate secondary carbocation is possible, however experimental[4] and theoretical[8] studies have shown that the opening of the activated epoxide and the formation of the A-ring occur in concert. The present study of the ring-opening substitution of **3.1** by **3.2** therefore only considers the backside bimolecular nucleophilic (S_N2) reaction, as other modes of reaction are not relevant to oxidosqualene cyclisation.

3.2 Results for MP2(Full)/6-31G(d) optimised structures

Relevant stationary points on the potential energy surface for the nucleophilic ring-opening reaction of protonated oxirane (**3.4**) and methylpropene (**3.5**) have been optimised at the MP2(Full)/6-31G(d) level of theory. Transition state **3.7** has been confirmed by frequency calculations, and IRC calculations performed on this structure led to reactant dipole–dipole complex **3.6** and carbocationic product **3.8**. A conformational isomer of the product (**3.10**) has been found and this can be reached from **3.8** via transition state **3.9**, representing a rotation of the C2–C3 bond.

Reaction energy profile. At the MP2(Full)/6-31G(d)//MP2(Full)/6-31G(d) level of theory reactant complex **3.6** has a calculated electronic energy of $\Delta E = -9.3$ kcal mol^{-1} relative to the isolated reactants (Table 3.1). Transition state **3.7** has an electronic energy of $\Delta E = -9.4$ kcal mol^{-1} relative to the isolated reactants, which represents an impossible negative activation barrier from complex **3.6** of $\delta\Delta E = -0.1$ kcal mol^{-1}. Rotational transition state **3.9** also has a calculated electronic energy lower than one of its associated minima, being $\delta\Delta E = 0.2$ kcal mol^{-1} lower than **3.8**. These apparently negative activation energies are retained in single-point energy calculations of the structures at the B3LYP/6-31+G(d,p) level of theory (Table 3.1).

This incongruity of an apparent negative activation barrier also appears in the work of Holubka and coworkers,[30] who studied the ring-opening nucleophilic reaction of unprotonated and protonated ethylene oxide with ammonia at the MP4SDTQ/6-31G(d)//HF/6-31G(d) level of theory (Figure 3.3), but was not noted or explained in their paper. For the reaction of ammonia with oxirane the product is reported to be 1.3 kcal mol^{-1} higher in energy than the transition state, and for the reaction of ammonia with protonated oxirane the dipole complex is reported to be 0.2 kcal mol^{-1} higher than the transition state.[30]

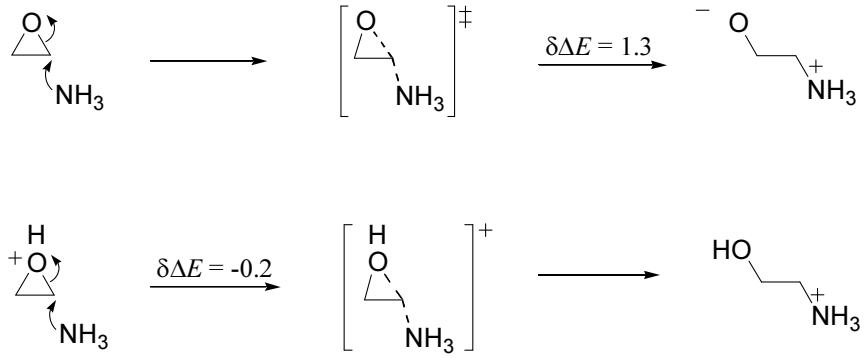

Figure 3.3. The reaction of oxirane and protonated oxirane with ammonia studied at the MP4SDTQ/6-31G(d)//HF/6-31G(d) level of theory by Holubka and coworkers (see ref. [30]), who reported transition states with a lower electronic energy than one of the associated minima.

The inversion of stationary point levels is an observed and recognised phenomenon of very flat potential energy surfaces[31] and is considered to arise from the partially corrected energies (zero point-corrected electronic energies only) commonly reported. The phenomenon is only significant when comparing stationary points with very small energy differences in a flat transition state region of a potential energy surface. Stating energy values which take account of the vibrational energy contribution of enthalpy and entropy (i.e. Gibbs free energy, ΔG) for potential energy surfaces in which this anomaly appears avoids reporting transition states with an

apparent energy lower than an associated local minimum. For this reason, energies reported in this section (Chapter 3.1, MP2(Full)/6-31G(d) optimised structures) are Gibbs free energies found with frequency calculations in Gaussian 94[19] using the ReadIsotopes option[21,32] at 298.15 K and 1 atm, with the naturally most abundant atomic isotopes, and using a scaling factor of 0.9646.[21] Calculated electronic energies and Gibbs free energies are given in Table 3.1.

Table 3.1. Energies and relative energies of MP3(Full)/6-31G(d) optimised structures. Both transition states have calculated electronic energies lower than one of their associated minima, however this anomaly is not present in the calculated Gibbs free energies.

	E [a,b]		ΔE [c]			
Structure	MP2(Full)/6-31G(d)	B3LYP/6-31+G(d,p)	MP2(Full)/6-31G(d)	B3LYP/6-31+G(d,p)	G [a,d]	ΔG [c]
3.4	−153.547092	−154.034915	0.0[e]	0.0[e]	−153.571437	0.0[e]
3.5	−156.539630	−157.138559			−156.567008	
3.6	−310.101596	−311.184885	−9.3	−7.2	−310.139124	−0.4
3.7 (TS)	−310.101770	−311.187132	−9.4	−8.6	−310.137838	0.4
3.8	−310.154161	−311.240352	−42.3	−42.0	−310.188680	−31.5
3.9 (TS)	−310.154398	−311.242076	−42.5	−43.0	−310.187971	−31.1
3.10	−310.154801	−311.244059	−42.7	−44.3	−310.190698	−32.8

[a] Values in hartrees. [b] Includes scaled zero-point correction (see Appendix). [c] Values in kcal mol^{-1}. [d] Gibbs free energy calculated at MP2(Full)/6-31G(d) and includes corrections scaled by 0.9646 (see ref. [21]). [e] Sum of energies for protonated oxirane (**3.4**) and methylpropene (**3.5**).

When corrections for electronic and thermal enthalpies and entropies are made, reactant complex **3.6** is at ΔG = −0.4 kcal mol^{-1} with respect to the free reactants (Figure 3.4). Transition state **3.7** is reached with an activation barrier of $\delta\Delta G$ = 0.8 kcal mol^{-1} and the reaction is exothermic to give product **3.8** at ΔG = −31.5 kcal mol^{-1}. Product rotational transition state **3.9** has an activation barrier of

$\delta\Delta G$ = 0.4 kcal mol^{-1} and the conformational isomer of the cationic product (**3.10**) is at ΔG = −32.8 kcal mol^{-1}.

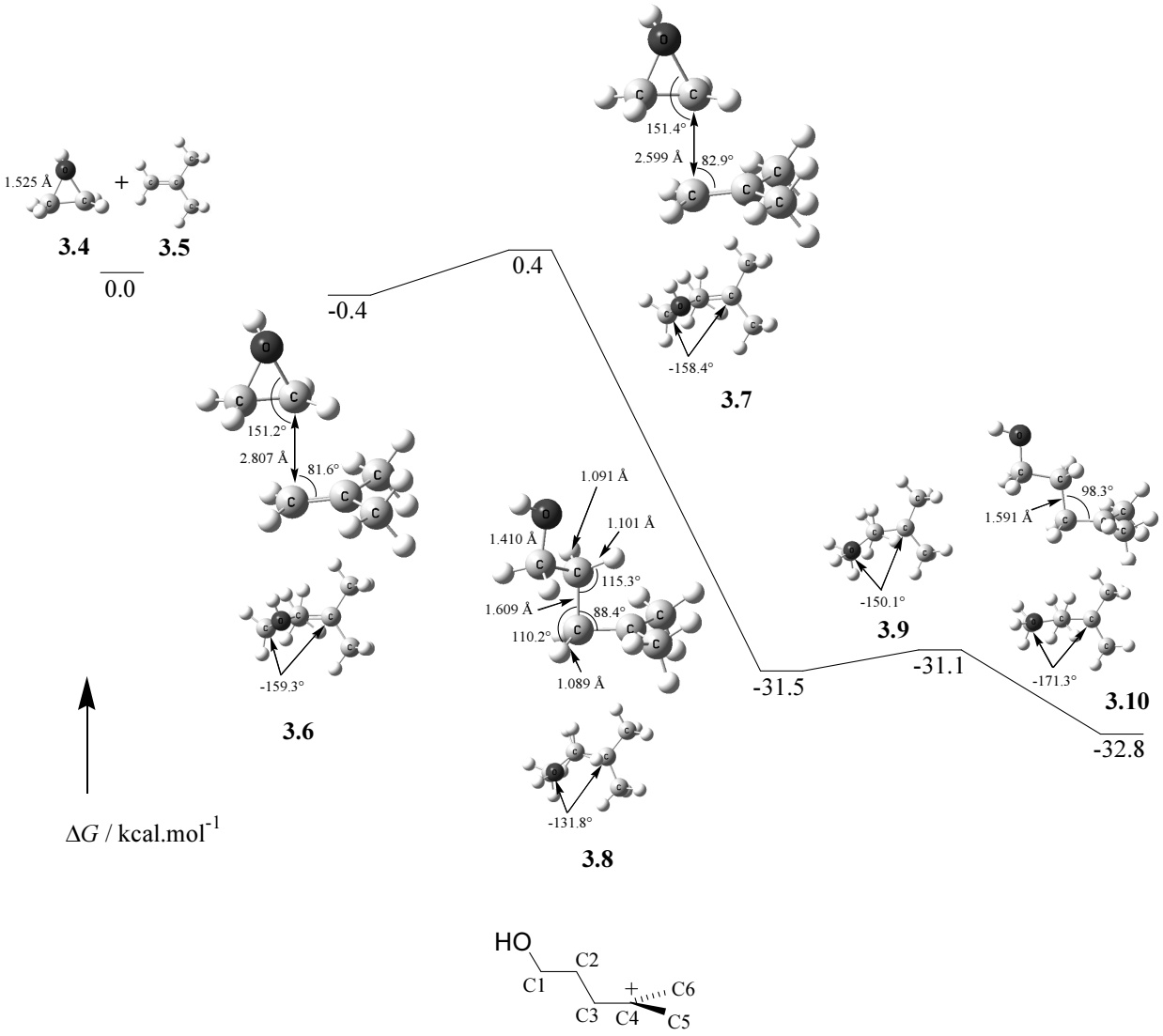

Figure 3.4. MP2(Full)/6-31G(d)//MP2(Full)/6-31G(d) optimised structures and potential energy surface. Also shown is a schematic of the product showing the atomic numbering system used in the text.

Previous computational studies[26,30,33,34] that examined the nucleophilic ring opening of both activated and unactivated epoxides have found that unactivated reactions are endothermic with a high activation barrier of ca. 15–20 kcal mol^{-1}. Activation of the epoxide by complexation with a Brønsted–Lowry acid generally leads to an exothermic reaction with a barrier of ca. 10 kcal mol^{-1} and reactions of a

protonated epoxide are highly exothermic with an activation energy of less than 5 kcal mol^{-1}. This trend is consistent with the expectation that reactivity increases with increasing stability of the leaving group.

The calculated activation energy of just ΔG = 0.8 kcal mol^{-1} required to reach transition state **3.7** is in agreement with this trend and is likely to be negligible in a solution-phase or enzyme-catalysed reaction such as in the biosynthesis of lanosterol. In the present study, with a neutrally charged nucleophile, protonation of the epoxide oxygen atom further lowers the barrier by eliminating the energy cost associated with charge separation in the transition state.

The low barriers associated with ring-opening reactions of epoxides in comparison to the equivalent reactions of their acyclic analogues can primarily be attributed to relief of strain of the three-membered ring in the transition state. Simple three- and four-membered rings have ring-strain energies of ca. 25–30 kcal mol^{-1} relative to their six-membered analogues.[35] However, despite the almost identical ring strain of three- and four-membered rings, ring-opening reactions of three-membered rings, such as in the present study, generally have a much lower activation barrier than the equivalent reaction at a four-membered ring due to the presence of an additional accelerating factor.[36,37]

The activation barrier for the alkene-assisted rupture of the oxirane in transition state **3.7** is lower than that for oxidosqualene models in which the two moieties are linked (see Chapters 4 and 5) because there is no ring strain or steric interaction associated with the formation of the A-ring.

Structure geometries. The reactant complex **3.6** shows only small distortions from the reactants **3.4** and **3.5** indicating the attraction between the two reactants is

loose. Transition state **3.7** is early and closely resembles the reactant complex, consistent with the low barrier to reaction and the Hammond postulate.

Both complex **3.6** and transition state **3.7** are non-planar through the dihedral angle about the forming carbon–carbon bond (Figure 3.4); the C1–C2–C3–C4 dihedral angle is −159.3° in **3.6** and −158.4° in **3.7**. The nucleophilic substitution reaction can be considered to be the attack of the π orbital of **3.5** to a σ^* of **3.4**, and, as such, the C1–C2–C3–C4 torsional angle would be expected to be 180° for optimal orbital overlap.

The deviation of the C1–C2–C3–C4 dihedral angle from planarity in both **3.6** and **3.7** can be explained as a steric effect, where the alkene is rotated away from the face of the epoxide *syn* to the proton. An optimisation at the MP2(Full)/6-31G(d) level of theory of **3.6** but modified by fixing the C2–C3–C4–C5 dihedral angle at 180° gave a structure $\delta\Delta E$ = 0.02 kcal mol^{-1} higher than **3.6**. This is comparable to the result calculated for protonated methyloxirane,[28] in which the *syn* protonated stereoisomer is 0.2 kcal mol^{-1} higher in energy than the *anti* isomer at the MP2/6-31G(d) level of theory (Figure 3.5). The shorter distance between the proton and the methyl group in protonated methyloxirane than between the *syn*-proton and the alkene in **3.6** accounts for the smaller energy difference calculated for the present system.

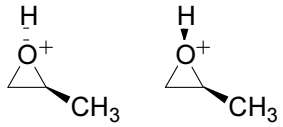

0.0 0.2

Figure 3.5. The MP2/6-31G(d) calculated energy difference for *anti* and *syn* protonated methyloxirane (see ref. [28]).

The angle of approach of **3.4** to **3.5** at the sp^2 hybridised C3 (i.e. the C2–C3–C4 angle) is 81.6° in reactant complex **3.6** and 82.9° in transition state **3.7**, less than

90° (Figure 3.4). Since the alkene acts as a nucleophile, it would be expected that the most important frontier orbital interaction would be between the π orbital of **3.5** and a vacant σ^* anti-bonding orbital of **3.4** (Figure 3.6). The reduction in the C2–C3–C4 angle below 90° in **3.6** and **3.7** occurs because the donating π orbital (and therefore the reaction centre) is not centred on an individual atom but is a molecular orbital centred between C3 and C4. This forms an asymmetric three centre (C2, C3, C4) interaction in the reactant complex and the transition structure. As the reaction proceeds from **3.6** to **3.8**, the π orbital of the former alkene develops into an atom-centred sp^3 orbital (on C3) and a vacant p orbital (on carbocationic C4). Therefore, through the course of the reaction the reaction centre moves towards C3 and the C2–C3–C4 angle moves closer to 90° (Figure 3.4).

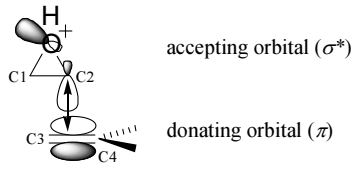

Figure 3.6. Schematic of the frontier orbital interaction in **3.7**. Note that the HOMO π orbital is not centred on an atom and that the LUMO σ^* orbital is bent towards C1.

In a normal backside S_N2 reaction the X–C–Nu angle is 180° in both the reactant complex and transition state,[24,38] where X is the leaving group and Nu is the nucleophile. At the MP2(Full)/6-31G(d) level of theory, the O–C2–C3 angle is 151.2° in reactant complex **3.6** and 151.4° in transition state **3.7** (Figure 3.4).

There are three likely contributing factors to this decrease in the O–C–Nu angle. Firstly, the geometry of the three-membered epoxide ring restricts the ability of the oxygen to leave at an angle of 180°. Retaining a linear O–C2–Nu through the course of the reaction would require an increase in the O–C1 bond length, however relief of ring strain actually causes this bond length to decrease as the reaction

proceeds, from 1.525 Å in **3.4** to a more normal acyclic carbon–oxygen distance of 1.410 Å in product **3.8** (Figure 3.4).

The second contributing factor to a non-linear O–C–Nu angle is the shape of the oxygen–carbon σ^* acceptor orbital. The formation of a three-membered ring causes such a distortion of the atoms from their preferred geometry that the atomic orbitals are unable to achieve linear overlap, forming so-called "bent bonds".[39] This is seen for the bonding orbitals in X-ray diffraction experiments as the electron density concentrated outside the line of the bond. The accepting lobe of the σ^* molecular orbital is thus not colinear with the formal oxygen–carbon bond, but is bent towards the other epoxide carbon atom (C1; Figure 3.6) leading to an O–C–Nu approach angle of less than 180°.

A third contributing factor to the decrease in the O–C–Nu angle is unique to reactions in which the nucleophile is an alkene or alkyne. As described above, the donating orbital of the nucleophile is the π orbital, which is not atom-centred, and this shift in the reaction centre to a point between C3 and C4 causes a slight reduction in the O–C2–C3 angle in the reactant complex and the transition state. Previous computational studies[26,30,33,34,36,40] of the ring-opening nucleophilic substitution reactions of protonated and unprotonated epoxides with conventional atom-centred nucleophiles have found the O–C–Nu angle to be less than 180° but larger than the O–C2–C3 angle in **3.7**; for example, in the reaction of protonated oxirane and ammonia[30] the O–C–N angle is ca. 171° in the transition state at the HF/6-31G(d) level of theory.

IRC calculation of transition structure **3.7** at MP2(Full)/6-31G(d) level of theory leads, on the product side, to local minimum **3.8** (Figure 3.4)**.** Product **3.8** has a C1–C2–C3–C4 dihedral angle of −131.8°, such that the carbon skeleton C2–C3 and

C4–C5 bonds are almost eclipsed with carbon–hydrogen bonds (the C–C–C–H dihedral angles are −14.9° and −12.4° respectively). Unlike **3.6** and **3.7**, steric arguments can not be used to explain the deviation of this torsional angle from a staggered 180° as the hydroxyl group is not in a position where it could interact with the rest of the molecule.

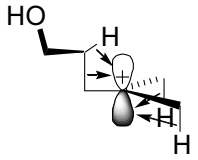

Figure 3.7. The important hyperconjugative interactions in structure **3.8**.

The most likely explanation for the non-planarity of the carbon skeleton of **3.8** is hyperconjugative stabilisation of the C4 carbocation by the C2–H bond. This bond is elongated, indicating a decrease in electron density in the bond, and the H–C2–C3 angle is widened, bringing it closer to parallel with the vacant *p* orbital of the carbocation (Figure 3.7). The distortions of the C2–H bond can not be attributed to steric interactions with the C4 atom as they do not occur in the similarly eclipsed C3–H bond.

Other hyperconjugative interactions with the carbocation are observed. The C5 and C6 methyl groups have rotated so that the hydrogen atoms are able to hyperconjugate with the carbocation. The C3–C4–C5–H dihedral angle is reduced to 98.8° and the C3–C4–C6–H dihedral angle is −102.3° (in **3.7** these angles are 115.6° and −117.4° respectively). Both the C5–H and C6–H bonds have lengthened to 1.102 Å and are bent towards the carbocation approximately 5° from the standard tetrahedral angle. There is also evidence of delocalization of the positive charge into the carbon skeleton, with elongation of the C2–C3 bond to 1.609 Å and the C2–C3–C4 bond angle reduced to 88.4°.

As mentioned above, there is a conformational isomer of the product (**3.10**) formed via transition state **3.9** by rotation about the C2–C3 bond. Structure **3.10** has a C1–C2–C3–C4 dihedral angle of −171.3°, and is thus sterically favoured in comparison to product **3.8**, but exhibits less hyperconjugative stabilisation of the carbocation. Only the C5 methyl group is rotated to allow hyperconjugation. The C2–C3 bond is shorter and not as tilted towards the carbocation in comparison to **3.8**, and this is consistent with less electron delocalisation from this bond; similarly there is no evidence of γ-electron donation from a C2–H bond.

Both **3.8** and **3.10** are conformations with compromise between the sterically favoured antiperiplanar (staggered) carbon skeleton and hyperconjugative stabilisation of the carbocation. Reaction product **3.8** shows more hyperconjugation but is more sterically hindered and rotational isomer **3.10** shows less hyperconjugation but has a more sterically favourable conformation.

3.3 Results for HF/6-31G(d) optimised structures

The HF/6-31G(d)//HF/6-31G(d) potential energy surface and optimised stationary point structures are shown in figure 3.8. At this level of theory, calculated electronic energies do not produce an apparent negative activation barrier on the potential energy surface and energies reported here are relative electronic energies (ΔE), including scaled zero-point corrections.

A dipole–dipole complex (**3.13**) of the reactants has been found with an interaction energy of ΔE = −5.7 kcal mol^{-1}, which is then calculated to react via transition state **3.14** with a barrier of $\delta\Delta E$ = 1.6 kcal mol^{-1}. The geometries of methylpropene and protonated oxirane show little change in complex **3.13**. Transition state **3.14** can be considered to be reactant-like, consistent with the low activation barrier and the Hammond postulate.

Both **3.13** and **3.14** are non-planar through the carbon skeleton; the C1–C2–C3–C4 dihedral angle is −173.6° in **3.13** and −174.6° in **3.14**. The deviation of these angles from planarity can be rationalised using the same reasoning as for the MP2(Full)/6-31G(d) optimised structures **3.6** and **3.7** reported above, i.e. as the alkene rotating away from the face of the epoxide *syn* to the proton. These angles are significantly closer to planarity than those in the corresponding MP2(Full)/6-31G(d) optimised structures, and this may be due to the MP2 method accounting for slight electronic stabilisation in the complex and transition state. The C2–C3–C4 angle in both **3.13** and **3.14** are close to the 90° expected for reaction of a C3 atom-centred *p* orbital instead a C3–C4 π molecular orbital, the corresponding MP2 calculated values for this angle in the **3.6** and **3.7** are 81.6° and 82.9°.

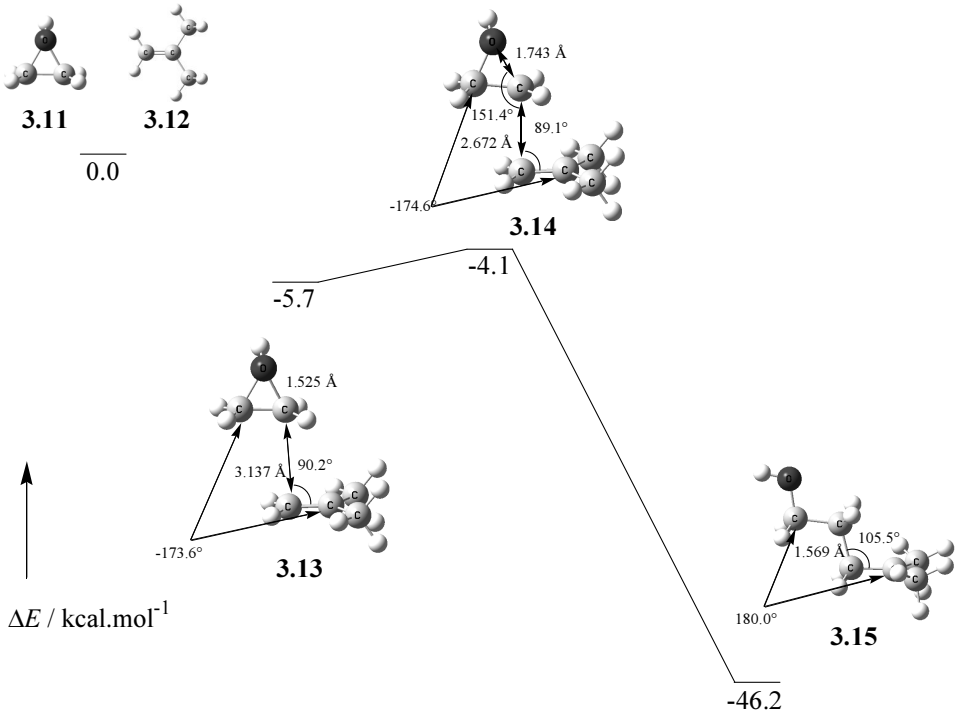

Figure 3.8. HF/6-31G(d) optimised stationary points for the reaction of protonated oxirane and methylpropene.

IRC calculation of transition state **3.14** leads to structure **3.15** as the product of the reaction. The reaction is exothermic by 46.2 kcal mol^{-1} relative to reactants **3.11**

and **3.12**. Unlike the MP2(Full)/6-31G(d) product **3.8**, structure **3.15** is planar through the carbon skeleton with a C1–C2–C3–C4 dihedral angle of 180.0° and shows little evidence of hyperconjugative stabilisation of the carbocation. This is because the MP2 method introduces electron correlation to the approximation of the Hamiltonian that is absent in the HF method. With no consideration of electronic stabilisation of the C4 carbocation, the HF/6-31G(d) optimised product **3.15** assumes the most sterically favoured conformation of a completely planar, staggered chain of carbon atoms.

3.4 Conclusion

The ring-opening reaction of protonated oxirane and methylpropene can be considered as an S_N2-type nucleophilic reaction. It is calculated to occur readily with a low activation barrier and high exothermicity. This thermodynamic profile can be attributed to the inherent reactivity of three-membered rings, primarily arising from relief of ring-strain, and protonation of the epoxide oxygen increasing the power of the leaving group and eliminating charge separation in the transition state.

At the MP2(Full)/6-31G(d) level of theory, the geometry of the reactant complex and transition state is strongly influenced by a low-energy steric interaction between the protonated epoxide and the alkene. Hyperconjugative stabilisation of the carbocation product has an important effect on the calculated geometry, forcing the molecule to adopt a sterically unfavoured conformation. At the HF/6-31G(d) level of theory the steric influence on the conformation of the complex and transition state is still present, however the method does not account for electron correlation and hyperconjugative interactions in the product are not found at this level of theory.

Chapter 4: Cyclisation of Monocyclic Oxidosqualene Models

4.1 Introduction

In animals and fungi, the steroid precursor lanosterol (**1.3**) is formed by cationic cyclisation of 2,3-(*S*)-oxidosqualene (**1.1**; Figure 1.1). This remarkable biosynthesis forms four carbocyclic rings and seven new stereocentres in a process catalysed by the single enzyme oxidosqualene cyclase.[1–3] The substrate is activated in the enzyme active site by complexation of the epoxide oxygen with an acidic aspartic acid residue, and the initial step of the reaction is considered to be the ring-opening of the protonated epoxide in concert with the intramolecular attack of the 6,7-double bond to form the lanosterol A-ring[4] (Figure 1.1).

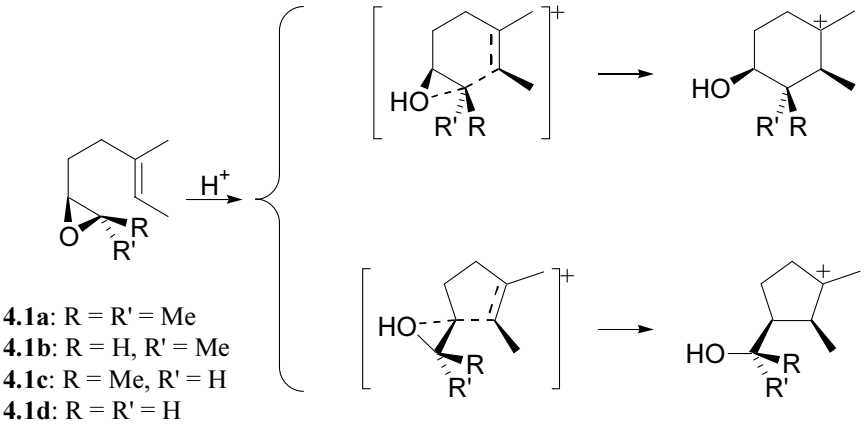

Figure 4.1. The proton-catalysed six- and five-membered cyclisations of the oxidosqualene model systems **4.1a–d** investigated in the present study.

The A-ring forms as a six-membered ring in a chair conformation, however there is a potential competing reaction to form a five-membered product. In order to understand how the enzyme affects the conformational requirements and energy of the substrate, the proton-catalysed five- and six-membered cyclisations of the series of

oxidosqualene model compounds **4.1a–d** (Figure 4.1) has been investigated in a gas-phase computational study and the results of this study are now presented.

In 1976 Baldwin[41] proposed a series of empirical rules governing the relative facility of competing ring forming reactions. These rules were based on the stereochemical requirements for the transition states to give the most favourable orbital overlap.[42]

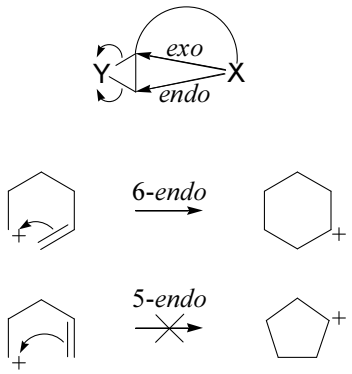

Figure 4.2. Baldwin's rules for nucleophilic ring closure at three-membered rings (top) and cationic ring closure at alkenes. Baldwin states that three-membered rings generally prefer *exo* closure.

Baldwin stated that nucleophilic openings of three-membered rings to form cyclic structures generally prefer *exo* modes of intramolecular attack, such that formation of the smaller ring is favoured (Figure 4.2). This generalisation is supported by experimental evidence for epoxynitriles,[43] and experimental[44] and computational[45,46] evidence of epoxyalcohols. An exception to this rule is seen in the preferential formation of the *endo* five-membered cyclic ether in the cyclisation of *cis*- and *trans*-3,4-epoxypentan-1-ol;[44,47] this result is perhaps explained by considering the high ring strain of the four-membered *exo* transition states, however it is to be noted that 3-oxiran-2-ylpropanenitriles readily form four-membered *exo* cyclisation products.[43] For electrophilic cyclisations of alkenes, Baldwin states that

endo closure of six-membered rings is favoured and that *endo* closure of five-membered rings from simple cations is not known (Figure 4.2).

The cyclisations of oxidosqualene and the model compounds investigated in the present study can be considered as either a nucleophilic substitution of an epoxide or as an electrophilic addition to an alkene. The enzyme-catalysed cyclisation of oxidosqualene does not follow Baldwin's rule for cyclisation of an epoxide, but the reaction occurs in the active site of an enzyme and the regiochemical control exerted by the enzyme means that it can not be considered typical of this type of cyclisation reaction. The present study seeks to determine the applicability of Baldwin's rules to cyclisation of alkenyloxiranes in general.

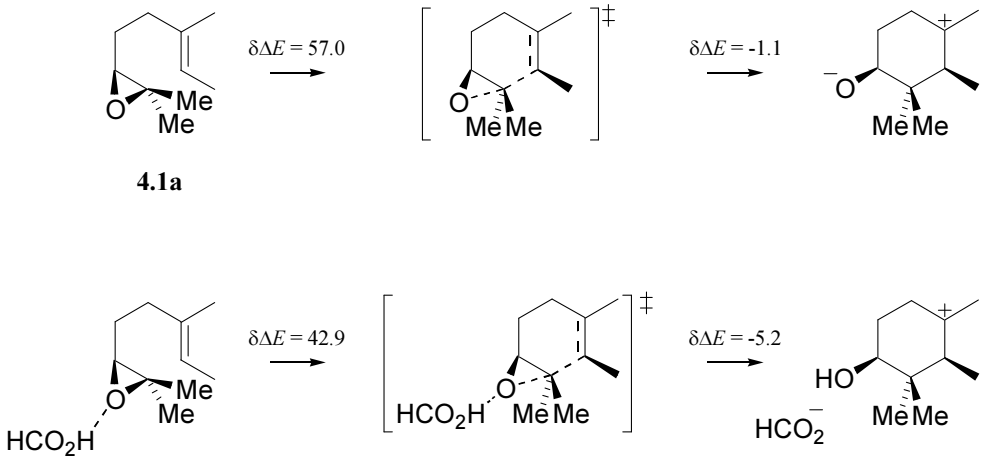

Figure 4.3. The uncatalysed and methanoic acid-catalysed six-membered cyclisations of **4.1a** investigated by Gao et al. at the B3LYP/6-31+G(d)//HF/6-31G(d) level of theory (see ref. [8]).

An earlier computational study[8] of oxidosqualene model systems investigated the uncatalysed and methanoic acid-catalysed six-membered cyclisation of **4.1a** (Figure 4.3). At the B3LYP/6-31+G(d)//HF/6-31G(d) level of theory, the transition state for the uncatalysed reaction is reached with an activation energy of 57.0 kcal mol^{-1} and leads to a zwitterionic intermediate 1.1 kcal mol^{-1} below the transition state. Activation of the oxirane by methanoic acid lowers the barrier to 42.9 kcal

mol^{-1} and the energy of the product to ΔE = 37.7 kcal mol^{-1}. A highly endothermic reaction such as those calculated by Pan, Gao et al. is typical of gas-phase charge separation reactions.[8]

4.2 Results

Stationary points on the potential energy surfaces for the five- and six-membered cyclisation of oxidosqualene models **4.1a–d** have been found in the gas phase at the HF/6-31G(d) level of theory and are presented here. Density functional single-point energy calculations have been performed on these optimised structures at the B3LYP/6-31+G(d) level of theory.

Protonation can occur from either face of the epoxide ring to give stereoisomeric oxiranium structures. It has been reported[28] that protonation of the least hindered face of methyloxirane to give the *anti* stereoisomer is 0.2 kcal mol^{-1} more stable than the *syn*-protonated stereoisomer at the MP2/6-31G(d)//MP2/6-31G(d) level of theory. Protonation of **4.1a**, **4.1c** and **4.1d** on the less hindered face of the epoxide *anti* to the 3-methylpent-3-en-1-yl substituent is therefore expected to be favoured over *syn* protonation, and all calculations reported here have been performed on the *anti*-protonated stereoisomers of these molecules. The *trans*-monomethyl epoxide **4.1b** has more equally hindered faces, however calculations have been performed only for the stereoisomer protonated *anti* to the 3-methylpent-3-en-1-yl group.

Cyclisation of dimethyloxirane oxidosqualene model. A schematic of the B3LYP/6-31+G(d)//HF/6-31G(d) reaction profile for proton-assisted five- and six-membered cyclisation of **4.1a** is shown in figure 4.4. Both reactions are calculated to be single-step processes with carbon–oxygen bond cleavage occurring in concert with carbocyclic ring closure in an intramolecular S_N2-like reaction. Cyclohexyl formation

occurs via transition state **4.3**, while the reaction for cyclopentyl formation passes through transition state **4.4**. Intrinsic reaction coordinate (IRC) calculations of both transition states lead to the same reactant structure (**4.2**), and to product structures **4.5** (six-membered) and **4.6** (five-membered).

Pre-folded conformation **4.2** is the reactant for both five- and six-membered ring formation and can be considered as either a chair-like pre-cyclohexyl or a puckered pre-cyclopentyl ring (Figure 4.4). The double bond is oriented so that the nucleophilic alkene carbon (C7) is available to react with either C2 (six-membered cyclisation) or C3 (five-membered cyclisation); the C2···C7 distance is 3.762 Å and the C3···C7 distance is 3.466 Å. The O–C2 bond distance is 1.575 Å, somewhat longer than the O–C3 distance of 1.511 Å. The difference in oxygen–carbon bond distances can be attributed to the higher degree of substitution of C2 by electron-donating alkyl groups, thereby preferentially stabilising the partial positive charge on that side of the oxirane.

Gas-phase six-membered cyclisation of **4.2** is calculated to be considerably more favourable than five-membered cyclisation at the B3LYP/6-31+G(d)//HF/6-31G(d) level of theory; transition state **4.3** is only 0.8 kcal mol^{-1} above **4.2** while an activation energy of 5.6 kcal mol^{-1} is required to reach **4.4**. This represents a preference for substitution at the more highly substituted carbon atom, a reaction mode that is usually considered unfavourable for S_N2 substitutions on steric grounds but is common in protonated epoxides; in basic or neutral conditions epoxides undergo S_N2 reactions at the less highly substituted carbon.[24] It is likely that ring opening of a protonated oxirane leads to a larger concentration of charge on the reaction centre in the transition state than occurs in S_N2 reactions of analogous acyclic species or unprotonated epoxides, and that the preference for reaction at the more

substituted carbon atom arises from increased stabilisation of the transitory positive charge by the substituent alkyl groups.

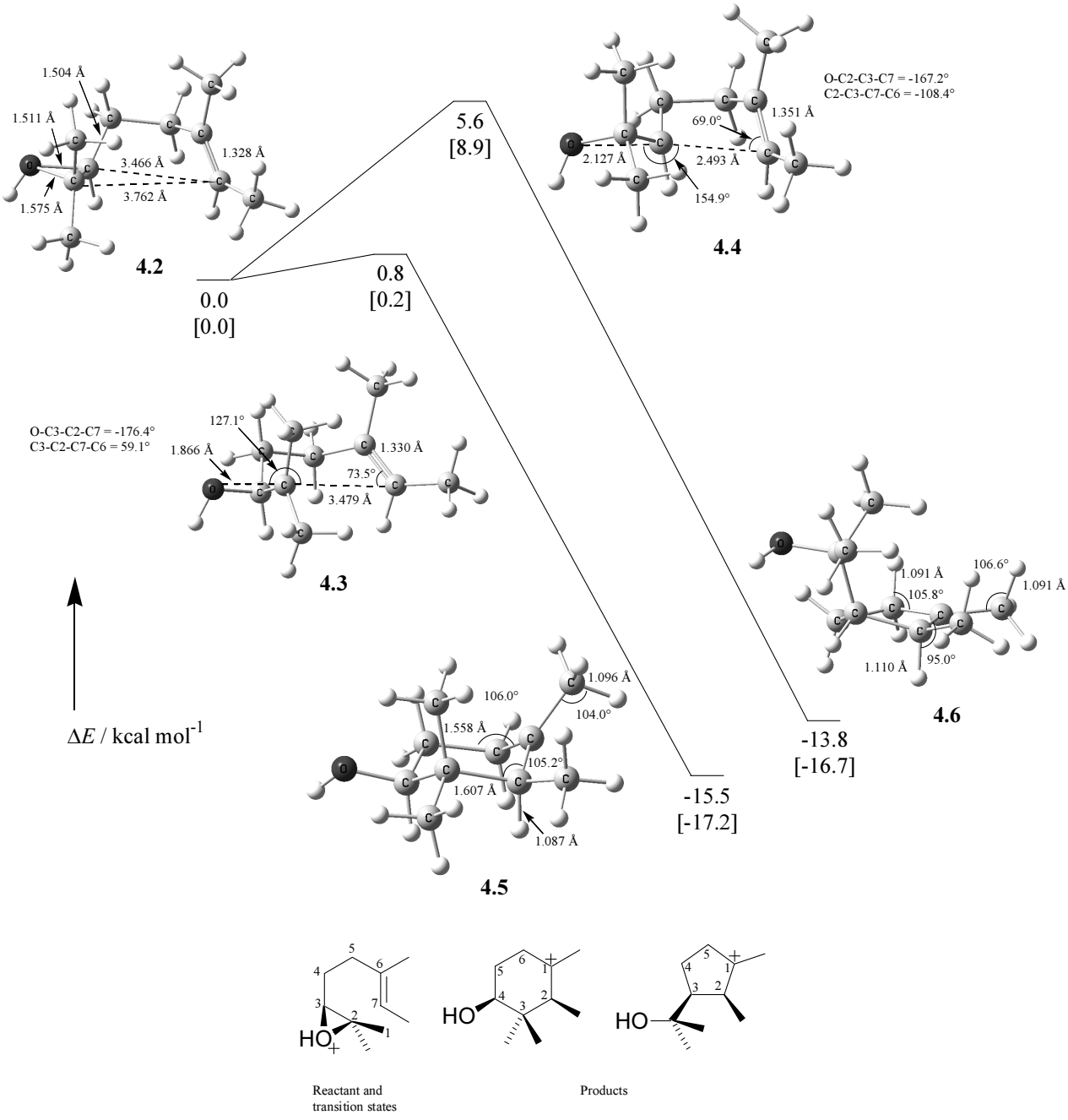

Figure 4.4. Reaction energy profiles and optimised stationary points for the five- and six-membered cyclisation of the dimethyl-substituted oxidosqualene model at the B3LYP/6-31G(d)//HF/6-31G(d) level of theory. HF/6-31G(d)//HF/6-31G(d) energies are given in square brackets.

As well as the strong kinetic preference for six-membered cyclisation via **4.3**, cyclohexyl product **4.5** is thermodynamically more stable than cyclopentyl product **4.6**; formation of **4.5** is exothermic by −15.5 kcal mol^{-1} and formation of **4.6** is exothermic by −13.8 kcal mol^{-1} at the B3LYP/6-31+G(d)//HF/6-31G(d) level of theory.

Carbocationic six-membered cyclisation product **4.5** is in a chair conformation with two of the methyl groups and the hydroxyl group oriented in the sterically preferred equatorial position (Figure 4.4). The HF/6-31G(d) optimised structure displays evidence of hyperconjugative stabilisation of the C1 cation similar to that seen in high-level ab initio calculations of 1-methylcyclohexylium[48,49] (**4.7**; Figure 4.5). The C2–C3 bond is elongated (1.607 Å) and the C2–C3–$C1^+$ angle is narrowed to 105.2°; the C7 methyl group is rotated so that a carbon–hydrogen bond is aligned with the vacant *p* orbital and this carbon–hydrogen bond is elongated and bent towards the carbocation (C7–H distance is 1.096 Å; $C1^+$–C7–H angle is 104.0°).

Unlike in 1-methylcyclohexylium conformation **4.7**, hyperconjugative stabilisation of **4.5** by carbon–carbon bonds is not symmetric; the C5–C6 bond is not significantly longer than a normal carbon–carbon bond at 1.558 Å long. It is likely that this preference for hyperconjugation from the C2–C3 bond is due to the substituted nature of this bond, i.e. the electron-donating methyl groups on C2 and C3 help to stabilise the loss of electron density from hyperconjugation.

1-Methylcyclohexylium exists in two distinct chair conformations, termed "hyperconjomers", linked by a ring-bending transition state[48,49] (Figure 4.5); a conformational isomer with the vacant *p* orbital oriented equatorially (**4.7**) shows evidence of hyperconjugation from β-γ carbon–carbon bonds, and an isomer with the *p* orbital oriented axially (**4.8**) is stabilised by hyperconjugation from axial carbon–

hydrogen bonds β to the carbocation. Hyperconjomer **4.7** is calculated to be ca. 1–3 kJ mol^{-1} more stable than **4.8** in the gas phase,[48] whereas experimental[50] and theoretical[49] studies show **4.8** to be the predominant form in solution. Product conformation **4.5** is the equatorial carbon–carbon stabilised hyperconjomer; it is likely that a conformational isomer with an axial *p* orbital exists, however no attempt has been made to find such a structure.

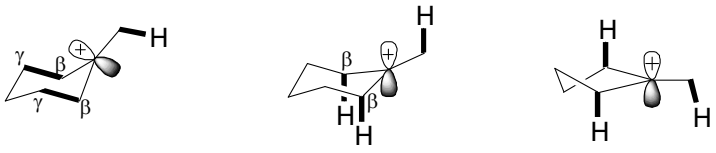

4.7 **4.8** **4.9**

Figure 4.5. Conformational isomers of 1-methylcyclohexylium (see refs. [48–50]) and 1-methylcyclopentylium (see ref. [51]). Hyperconjugating bonds are shown in bold.

In five-membered cyclisation product **4.6** the $C1^+$ and C2 methyl groups are in a pseudo-equatorial position, however, as a consequence of the geometry of transition state **4.4**, the bulky 1-hydroxy-1-methylethyl group on C3 is in a pseudo-axial position. The five-membered ring is in an envelope conformation, with C3 out of the plane of the other four carbon atoms (the C2–C1–C5–C4 dihedral angle is −0.5°). A conformational change, so that the C3 substituent moves to a pseudo-equatorial position, is expected to reduce steric interaction between this group and the rest of the molecule resulting in a lower energy structure.

The C_2-symmetrical 1-methylcyclopentylium (**4.9**; Figure 4.5) shows evidence of hyperconjugative stabilisation of the formal $C1^+$ cation by pseudo-axial hydrogen atoms on both intra-annular β-carbon atoms (C2 and C5) and by a hydrogen atom of the methyl group.[51] Five-membered product **4.6** displays structural features attributed to hyperconjugative stabilisation from the analogous carbon–hydrogen bonds but

shows a stronger hyperconjugation from the hydrogen atom on the more substituted C2 carbon atom. The C2–H bond is 1.110 Å and is bent appreciably towards the carbocation, giving a $C1^{+}$–C2–H angle of 95.0°; by contrast, the C5–H and C6–H bonds are both 1.091 Å and form angles to the carbocation of 105.8° and 106.6° respectively. As with the asymmetric hyperconjugation of six-membered product **4.5**, this preference for hyperconjugation from the C2–H bond over the C5–H bonds in **4.6** can be explained by the electron-donating C2 alkyl substituent partially compensating for the loss of electron density arising from donation to the carbocation.

Cyclisation of *trans*- and *cis*-monomethyloxirane oxidosqualene model. At the B3LYP/6-31+G(d)//HF/6-31G(d) level of theory, the reactive conformation of protonated *trans*-substituted epoxide (**4.10**; Figure 4.6) is 1.7 kcal mol^{-1} more stable than the *cis* isomer **4.15** (Figure 4.7). If the structures of these reactants are considered as proto-chair conformations, the C1 methyl group of **4.10** can be seen to be in a pseudo-equatorial position, while in the higher energy structure **4.15** the methyl is in the more sterically hindered pseudo-axial position. This 1.7 kcal mol^{-1} energy difference between the *cis* and *trans* isomers is comparable to experimental[52–55] and theoretical[55–58] values for axial and equatorial methylcyclohexane.

The epoxy carbon atoms of **4.10** and **4.15** are substituted more equally than those of **4.2** and the similar degree of stabilisation of the positive charge is reflected in the similar carbon–oxygen bond lengths. The C2···C7 distance of *cis* epoxide **4.15** is 3.773 Å, similar to the analogous distance of **4.2**, while the C2···C7 distance of *trans* epoxide **4.10** is 3.680 Å. It is likely the larger separation of these atoms in **4.2** and **4.15** is a result of steric interaction between the *cis* “axial” methyl group and the proto-A-ring.

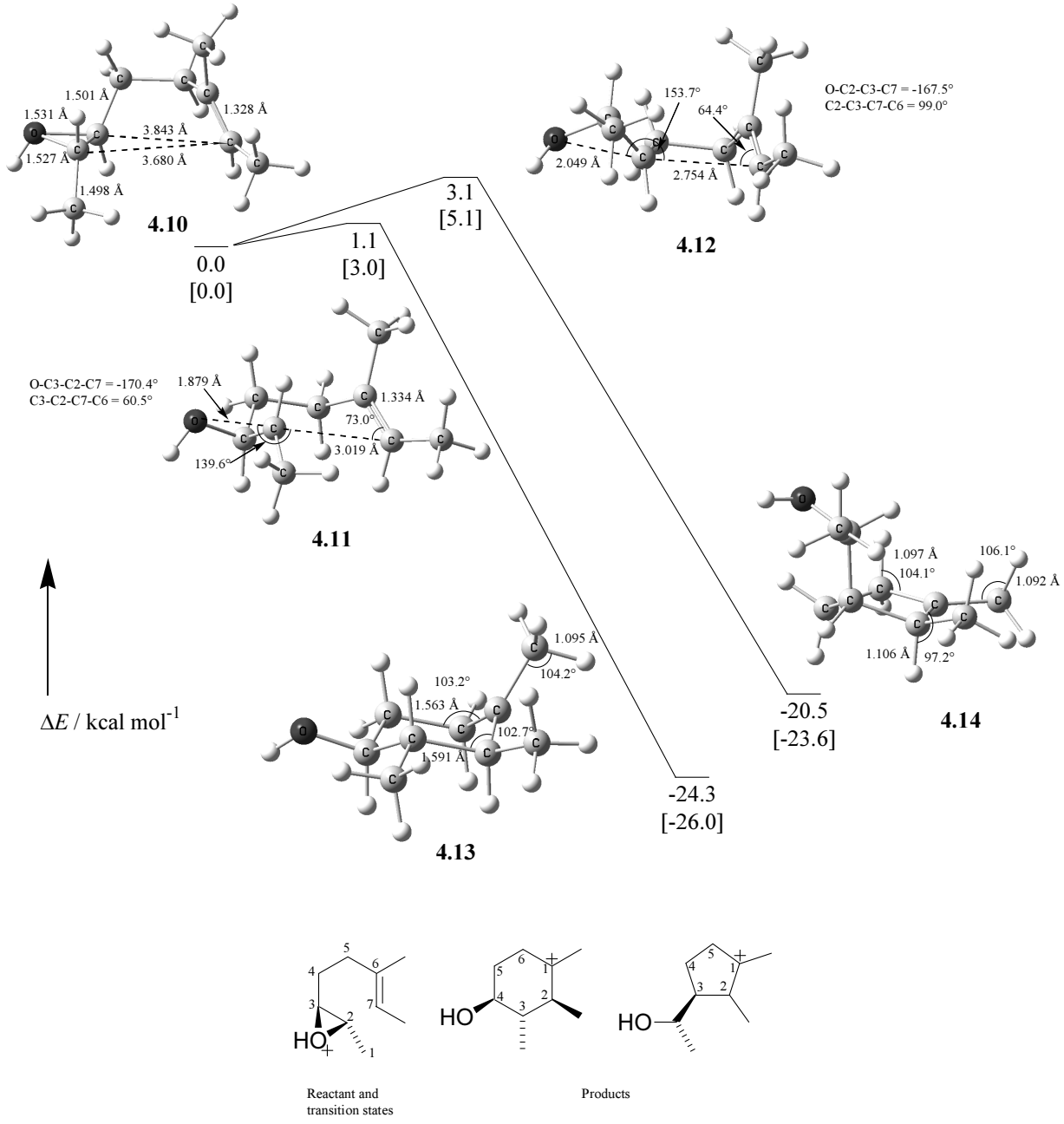

Figure 4.6. Reaction energy profiles and optimised stationary points for the five- and six-membered cyclisation of the *trans* monomethyl-substituted oxidosqualene model at the B3LYP/6-31G(d)//HF/6-31G(d) level of theory. HF/6-31G(d)//HF/6-31G(d) energies are given in square brackets.

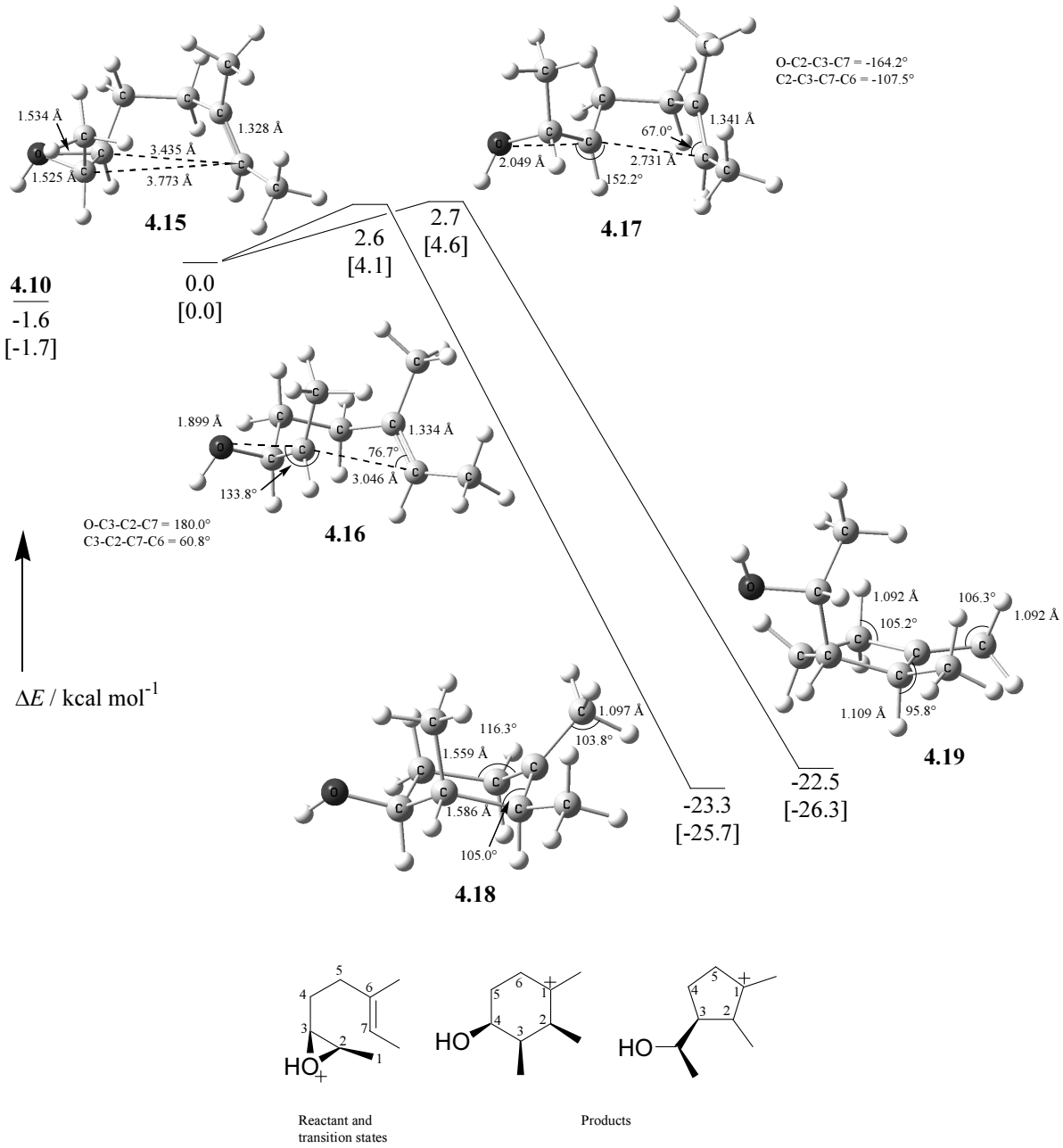

Figure 4.7. Reaction energy profiles and optimised stationary points for the five- and six-membered cyclisation of the *cis* monomethyl-substituted oxidosqualene model at the B3LYP/6-31G(d)//HF/6-31G(d) level of theory. HF/6-31G(d)//HF/6-31G(d) energies are given in square brackets.

Protonated *trans* epoxide **4.10** cyclises to a six-membered ring via transition state **4.11** with an activation energy of 1.1 kcal mol^{-1}, and to a cyclopentyl product via transition state **4.12** with a barrier of 3.1 kcal mol^{-1}. The *cis* isomer **4.15** requires 2.6 kcal mol^{-1} to reach six-membered transition state **4.16**, and five-membered transition

state **4.17** is 2.7 kcal mol^{-1} above the protonated epoxide. The competing reactions of closure to a five- or six-membered product have closer activation barriers in comparison to the competing reactions of dimethyl-substituted **4.2**, and this can be attributed to the similar stabilisation of the transitory positive charge on both of the epoxide carbon atoms by the substituent alkyl groups.

The activation energy required to reach six-membered *cis* transition state **4.16** is 1.5 kcal mol^{-1} higher than that required to reach the isomeric *trans* structure **4.11**, and this difference is likely to arise from steric interaction of the C1 methyl group axial to the incipient cyclohexyl ring. The C1 methyl group is more distant from the rest of the molecule in the five-membered transition states and consequently the barriers to five-membered transition states **4.12** and **4.17** are closer. As the transition states for six-membered cyclisation are early and reactant-like, it can be assumed that the energy contribution of the axial methyl group in **4.16** over the equatorial methyl in **4.11** is approximately the same as in the reactants at ca. 1.7 kcal mol^{-1}. It can therefore be seen that formation of a six-membered ring from protonated monomethyl-substituted epoxide is favoured by ca. 1.8–2.0 kcal mol^{-1} over five-membered cyclisation.

Cyclisation of oxidosqualene model with no terminal methyl groups. The energy profile for competing five- and six-membered cyclisations of protonated **4.1d** is shown in figure 4.8. The reactant in conformation **4.20** can be considered as a proto-chair and the C1···C6 distance is 3.642 Å; this distance is similar to the corresponding distance in *trans* monomethyl epoxide reactant **4.10**, strengthening the suggestion that the longer distance in **4.2** and **4.15** is a result of steric interaction of the *cis* methyl group "axial" to the proto-ring. Consistent with the calculated

structures **4.2**, **4.10** and **4.15** the more highly substituted C2–O bond is longer than the C1–O bond, reflecting a higher degree stabilisation of the positive charge.

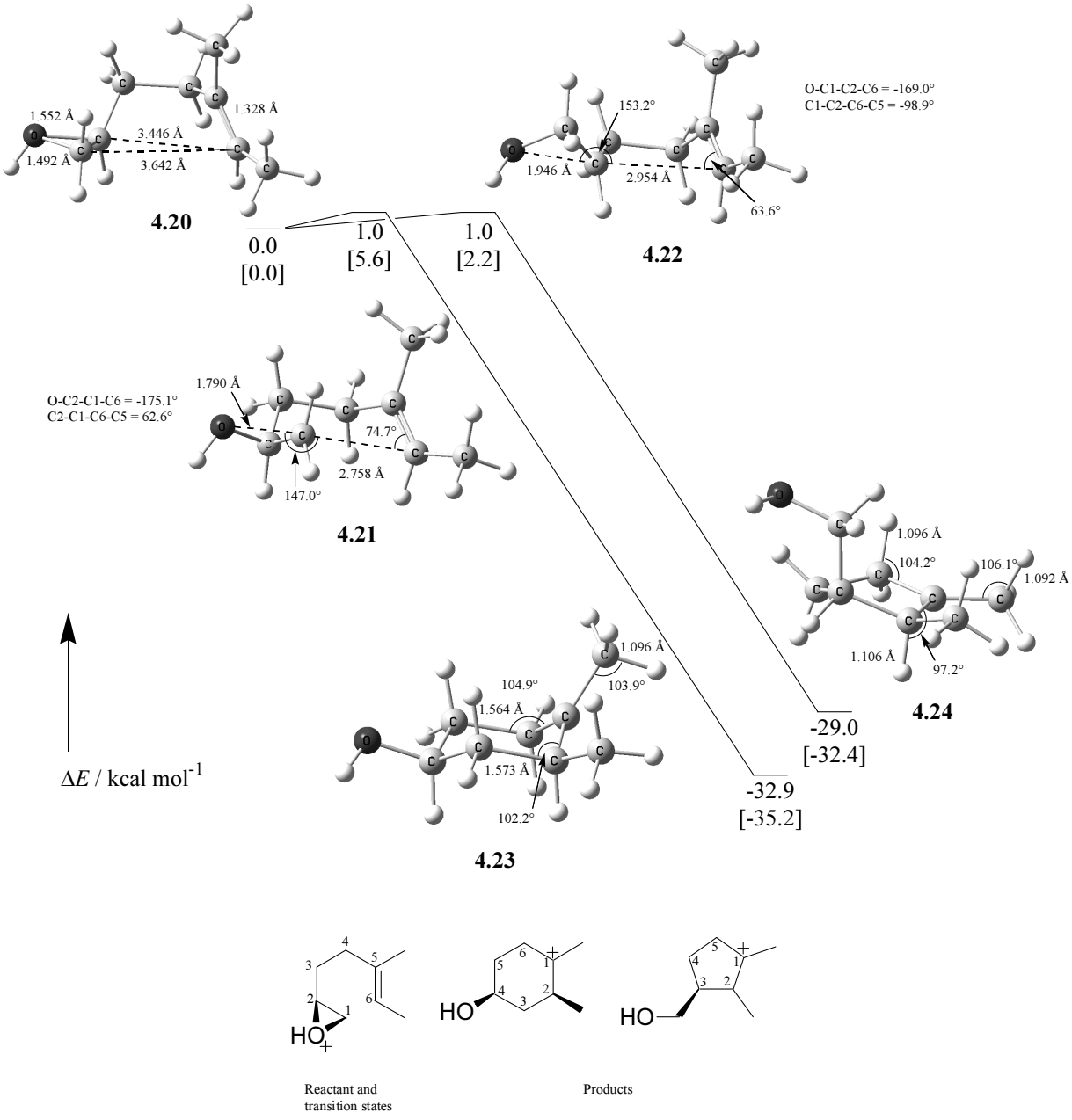

Figure 4.8. Reaction energy profiles and optimised stationary points for the five- and six-membered cyclisation of the oxidosqualene model with no terminal methyl groups at the B3LYP/6-31G(d)//HF/6-31G(d) level of theory. HF/6-31G(d)//HF/6-31G(d) energies are given in square brackets.

Protonated oxidosqualene analogue **4.20** lacks terminal methyl groups and, as discussed above, it would be expected that the preferred reaction would occur at the

more substituted carbon atom to produce the five-membered product. At the B3LYP/6-31+G(d)//HF/6-31G(d) level of theory, however, it is calculated that the transition states for six-membered (**4.21**) and five-membered (**4.22**) cyclisation are both reached with an activation energy of 1.0 kcal mol^{-1}. That the reaction does not occur preferentially at the more substituted carbon atom suggests that an additional stabilising factor is present in six-membered ring formation; this is discussed in further detail below.

4.3 Discussion

Transition state energies. It has been seen that, in the acid-catalysed cyclisation reactions of the series **4.1a–d**, a number of factors determine the activation energies required to reach the competing five- and six-membered transition states. In particular, stabilisation of the transitory positive charge favours reaction at the carbon atom more highly substituted with electron-donating alkyl groups and an additional stabilising factor favours six-membered over five-membered ring formation.

This additional stabilising factor for six-membered cyclisation can be understood by considering Baldwin's rules[41] for ring closure reactions and their basis in the stereochemical requirements for optimal orbital overlap.[42] However, the cyclisation reactions of enzyme-activated oxidosqualene and the protonated analogues investigated in the present study are not substitutions of epoxides by the simple nucleophiles discussed by Baldwin, nor are they simple cationic cyclisations of alkenes (Figure 4.2); it is not immediately clear which, if any, of Baldwin's rules are applicable.

Baldwin's rule for the opening of three-membered rings in cyclisation reactions is not particularly precise, stating that they "generally prefer *exo* modes" of reaction. The results of the present study are contrary to this rule, with a clear

preference for the *endo* formation of a six-membered ring over the *exo* formation of a five-membered ring. Baldwin's rule for cationic closures of an alkene is much more stringent, asserting that "the 5-*endo*-*trig* case is, for simple cations, not known". All reactions considered in the present study are *endo* at the alkene and, despite the electrophilic moiety of the reactants not being a simple cation, the preference for six-membered over five-membered cyclisation can be seen to follow Baldwin's rule for cation–alkene closures.

It was suggested above that opening of a protonated epoxide causes a larger concentration of positive charge at the reaction centre than occurs in analogous reactions of unprotonated epoxides or acyclic species; this suggestion was made to account for the preference of reaction at the more substituted end of the protonated epoxide. It is likely that this increase in the transitory positive charge on the epoxide carbon atom causes it to behave in some ways as a conventional cation, thus accounting for the adherence to Baldwin's rule for cationic closures at alkenes. However, this adherence is not absolute; the constraints associated with the leaving group attached the system in a strained three-membered ring are also present (Baldwin's "general preference" for *exo* opening of a three-membered ring) and this accounts for the relatively low additional energy cost for closure of the *exo* five-membered ring over the *endo* six-membered ring of ca. 1.8–2.0 kcal mol^{-1}.

It is clear that the six-membered transition states for the series of protonated alkenyloxiranes investigated in the present study must have a more favourable frontier orbital interaction than the five-membered transition states. When the geometries of the transition states are compared to the geometry of the transition state for the reaction of methylpropene with protonated oxirane (**3.7**; Figure 4.9), as presented in chapter 3 of this thesis, an analysis of the important parameters can be made.

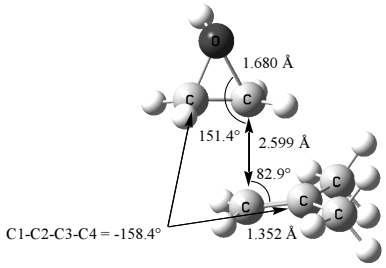

3.7

Figure 4.9. MP2(Full)/6-31G(d) optimised transition state for the reaction of protonated oxirane and methylpropene.

In **3.7** the O–C2–C3 angle of nucleophilic attack at the epoxide is 151.4°; in chapter 3 it was noted that this angle is significantly smaller than the 180° expected for the analogous angle in nucleophilic substitutions of less strained systems and this difference was attributed primarily to the "bent" bonds of the three-membered ring. The equivalent angles in five-membered transition states of the present study lie in the range 152.2°–154.9°, while the angles for the three six-membered transition states with at least one terminal methyl group lie in the range 127.1°–139.6°. The larger deviation from the ideal conformation seen in the six-membered transition states would be expected to raise the energy requirement of these structures and, as thus it appears that this angle is flexible with low energy costs for bending. The angle of nucleophilic attack in **4.21** is 147.0° and the molecule is able to achieve this more favourable conformation because there are no steric interactions associated with terminal methyl groups.

The C1–C2–C3–C4 dihedral angle shows significant differences between **3.7** and both the five- and six-membered cyclisation transition states. In structure **3.7** this angle is −158.4° and the deviation from planarity of this angle was ascribed to a steric effect costing less than 0.2 kcal mol^{-1} (Chapter 3). This energy cost is considerably lower than the preference for six-membered ring formation seen in the present study,

and it is therefore likely that variation of this dihedral angle induces only small energy changes in the transition state and does not significantly affect the regioselectivity of the reaction.

The parameter considered most important to the stereoelectronic preference for six-membered ring formation in the present study is the C2–C3–C4 bond angle, i.e. the angle for electrophilic addition to the alkene. This angle in the unlinked transition state **3.7** is 82.9°, in the six-membered intramolecular transition states it is 73.0°–76.7° and for the five-membered reaction it is 63.6°–69.0°, and the greater deviation from the ideal geometry in the cyclopentyl transition states accounts for the additional energy cost of these reactions. That the angle of attack at the alkene is the most important parameter affecting transition state energy shows that the most important orbital interaction occurs at the alkene reaction centre, and is consistent with the reaction following Baldwin's rule for cationic cyclisations of alkenes and not the rule for nucleophilic cyclisations of three-membered rings.

The present study considered only the competing reactions *endo* at the alkene. In order to gain a complete understanding of the present systems it is necessary to study the potential reactions *exo* at the alkene (Figure 4.10). Baldwin does not give rules for cationic closure *exo* at an alkene, however it is not thought that these reactions are significant in the present study as the products are secondary carbocations and give ring systems with a higher degree of strain than the *endo* reactions.

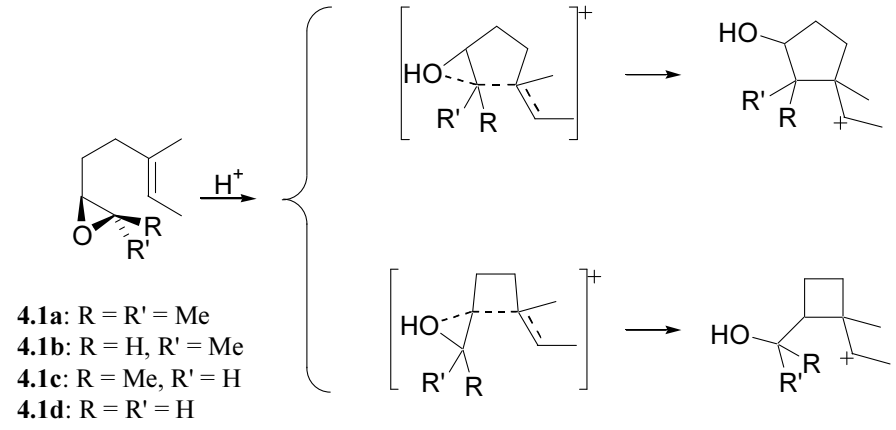

4.1a: R = R' = Me
4.1b: R = H, R' = Me
4.1c: R = Me, R' = H
4.1d: R = R' = H

Figure 4.10. The potential reactions of **4.1a–d** *exo* at the alkene.

Product energies. For all four oxidosqualene model compounds investigated, the six-membered carbocationic product is lower in energy than the five-membered product. There are three likely reasons for the higher stability of the six-membered product: (1) the inherent stability of a largely strain-free six-membered ring in a chair conformation over a five-membered ring with some bonds in an eclipsed configuration; (2) an unfavourable conformation of the five-membered products with the bulky C3 substituent in a pseudo-axial position; and (3) hyperconjugating carbon–carbon bonds, as seen in the six-membered products, are known to provide a higher stabilising effect than carbon–hydrogen bonds, as in the five-membered products.[48,49]

When comparing the exothermicities of the acid-catalysed cyclisations of the series **4.1a–d**, it can be seen that cyclisation of epoxides with a higher degree of substitution are less exothermic than epoxides with less substitution. Dimethyl-substituted **4.2** gives products exothermic by ca. 13–16 kcal mol^{-1}, monomethyl reactants **4.10** and **4.15** give products exothermic by ca. 20–24 kcal mol^{-1} and **4.20** gives products exothermic by ca. 29–33 kcal mol^{-1}. The main contributing factor to this trend is thought to be that a greater degree of substitution of the protonated epoxide helps to stabilise the positive charge; as all the products have similarly

stabilised cations the higher stabilisation of the substituted reactants lowers their energy relative to the products and decreases the exothermicity.

4.4 Conclusion

The cyclisation reactions of the series of protonated epoxides **4.1a–d** are concerted, single-step processes with carbon–oxygen bond cleavage occurring in concert with intramolecular nucleophilic attack by the proximate double bond to form a carbocyclic ring. The exothermic reactions proceed via early, reactant-like transition states with low activation barriers. The relative activation energies calculated to be required to reach competing five- and six-membered transition states depend on a number of factors.

Ring opening of protonated epoxides occurs readily due to relief of ring strain from the three-membered ring and the stability of the leaving group. The reactions in the present study are calculated to be S_N2-like in character at the epoxide, however the facility of the ring opening of a protonated epoxide leads to a higher concentration of positive charge on the epoxide carbon atom in the transition state than occurs in similar reactions of unprotonated epoxides or acyclic species. This transitory positive charge is stabilised to a higher degree on the more substituted carbon, accounting for the preference for reaction at the more hindered centre.

An additional stabilising factor for closure of the six-membered ring over the five-membered ring can be understood by consideration of Baldwin's rules. The facile rupture of the protonated three-membered ring and the increase in the positive charge on the epoxide reaction centre cause the reactant to behave somewhat like a cation, and therefore the selectivity for a six-membered ring is seen to follow Baldwin's rule for cation–alkene cyclisations. A weaker leaving group, such as in an unprotonated epoxide or an epoxide complexed to a weak Brønsted–Lowry acid, may

lead the reaction to behave more as a nucleophile–epoxide cyclisation, which by Baldwin's rules favours five-membered ring formation.

An analysis of the geometry of the transition states in comparison with the transition state for the reaction of unlinked methylpropene and protonated oxirane shows that the most important geometric parameter determining transition state energy is the angle of attack at the alkene. This confirms that the reaction behaves more like an electrophilic addition to an alkene than a nucleophilic substitution of an epoxide.

The strong kinetic and thermodynamic preference for the formation of the six-membered ring from dimethyl-substituted oxirane **4.2** suggests that the similarly substituted oxidosqualene will readily form a six-membered A-ring. The catalytic influence imparted by the enzyme is likely to consist of conformational control of the prefolded substrate, and activation of the epoxide by a sufficiently strong amino acid that the initial reaction acts more as an electrophilic addition to an alkene (and therefore favouring six-membered cyclisation) than as a nucleophilic substitution of an epoxide (which would favour five-membered cyclisation).

An important feature of the products is hyperconjugative stabilisation of the carbocation. The cyclohexylium products show structural evidence of hyperconjugation from the intra-annular β-γ carbon–carbon bonds and from a carbon–hydrogen bond of the C7 methyl group. The cyclopentylium products are stabilised by electron donation from carbon–hydrogen bonds β to the cation, both within the ring and from the C6 methyl group. A greater degree of hyperconjugation is seen from more highly substituted bonds, as the substituents help compensate for the loss of electron density from hyperconjugation.

Chapter 5: Cyclisations of Bicyclic Oxidosqualene Model

5.1 Introduction

The biosynthesis of the tetracyclic steroid precursor lanosterol (**1.3**) involves the cationic cyclisation of the triterpene oxidosqualene (**1.1**; Figure 1.1). This cyclisation reaction is catalysed by the enzyme oxidosqualene cyclase and forms four carbocyclic rings and seven new stereocentres.[1–3] The enzyme holds the substrate in a reactive conformation and activates the epoxide with an aspartic acid residue.[4] The initial step of the cyclisation is the ring opening of the activated epoxide in concert with nucleophilic attack by the proximate 6,7-double bond to form the A-ring.

The formation of the B-ring of lanosterol is thought to occur rapidly following formation of the A-ring, however it is not known whether cyclisation of the first two rings is concerted or if a short-lived monocyclic intermediate exists.[2] The B-ring of lanosterol cyclises in a boat conformation and a later rearrangement, following formation of the C- and D-rings, produces a conformation change to the steroidal chair conformation.

Following the investigation of models of the initiation and A-ring cyclisation (see Chapters 3 and 4), a computational study of a bicyclic lanosterol model system has been performed and is now presented here. Proposed step-wise and concerted mechanisms for the cyclisation of oxidosqualene model **5.1** are shown in figures 5.1 and 5.2 respectively. The present study seeks to determine the relative timing, activation energy requirements and geometry for gas-phase cyclisation of **5.1**.

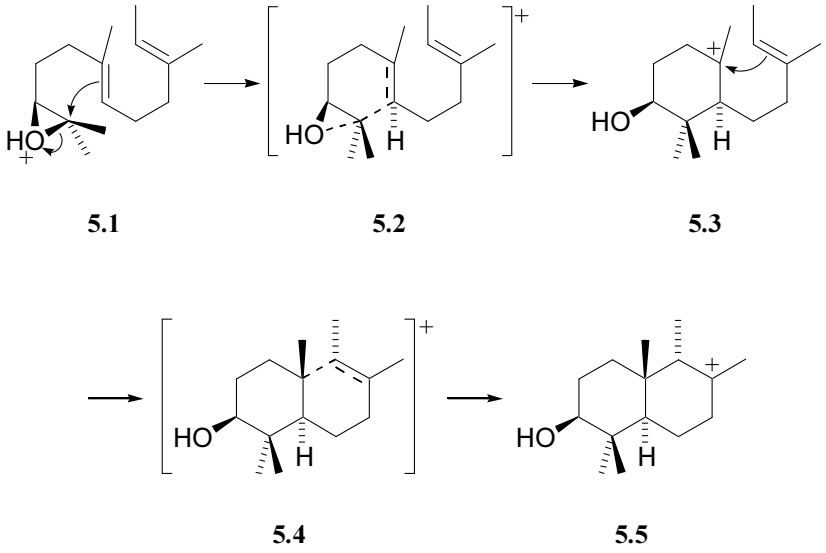

5.1 **5.2** **5.3**

5.4 **5.5**

Figure 5.1. Proposed mechanism for cyclisation of bicyclic lanosterol model **5.5** with sequential A- and B-ring formation.

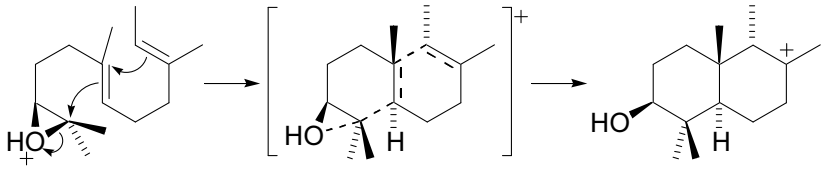

5.1 **5.5**

Figure 5.2. Proposed mechanism for cyclisation of bicyclic lanosterol model **5.5** with concerted A- and B-ring formation.

5.2 Results and discussion

HF/3-21G optimised structures. A previous computational study of this bicyclic model system has been performed at the HF/3-21G level of theory by Pan, Gao and coworkers.[8] They found two stationary points on the potential energy surface: monocyclic intermediate **5.6** and bicyclic product **5.8a**. Pan, Gao, et al. approximated the reaction profile between these two local minima by optimising discrete points between the minima with the incipient C11–C6 bond fixed at intermediate distances, and they reported that the reaction **5.6** → **5.8a** is exothermic by 6.7 kcal mol^{-1} (they did not include zero-point corrections in their reported

energies). A structure with C6–C11 distance fixed at 2.90 Å, which was not an optimised transition state, was reported to be at ΔE = 0.7 kcal mol^{-1} relative to **5.6**; despite this structure having a higher energy than both local minima they concluded that closure of the B-ring is concerted with A-ring cyclisation (i.e. proceeding without barrier).

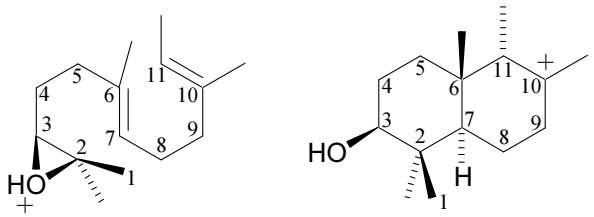

5.1 **5.5**

Figure 5.3. Atomic labelling scheme used in the text.

Preliminary exploratory calculations for the present study were carried out at the HF/3-21G level of theory and the two stationary points found by Pan, Gao, et al. (**5.6** and **5.8a**) were found independently (Figure 5.4). A transition state (**5.7**) was found with C6–C11 distance of 2.926 Å and an uncorrected activation barrier of 0.7 kcal mol^{-1} (it is 1.0 kcal mol^{-1} with inclusion of the electronic zero-point energy); **5.7** was confirmed as the transition state that connects **5.6** and **5.8a** by frequency and IRC calculations. Optimised transition state **5.7** is not the same structure as the intermediary structure reported by Pan, Gao et al. A second conformation of the bicyclic product (**5.8b**) also exists at the HF/3-21G level of theory and is shown in figure 5.4; structure **5.8b** was not found by Pan, Gao, et al. A monocyclic minimum and a cyclisation transition state leading to **5.8b** have not been found at this low level of theory but are expected to exist as a parallel reaction path to that leading to **5.8a**. The existence of discrete intermediates and transition states for the closure of the B-ring at the HF/3-21G//HF/3-21G level of theory suggests that, contrary to the

conclusion of Pan and Gao, the formation of the B-ring is not concerted with A-ring cyclisation at this level of theory.

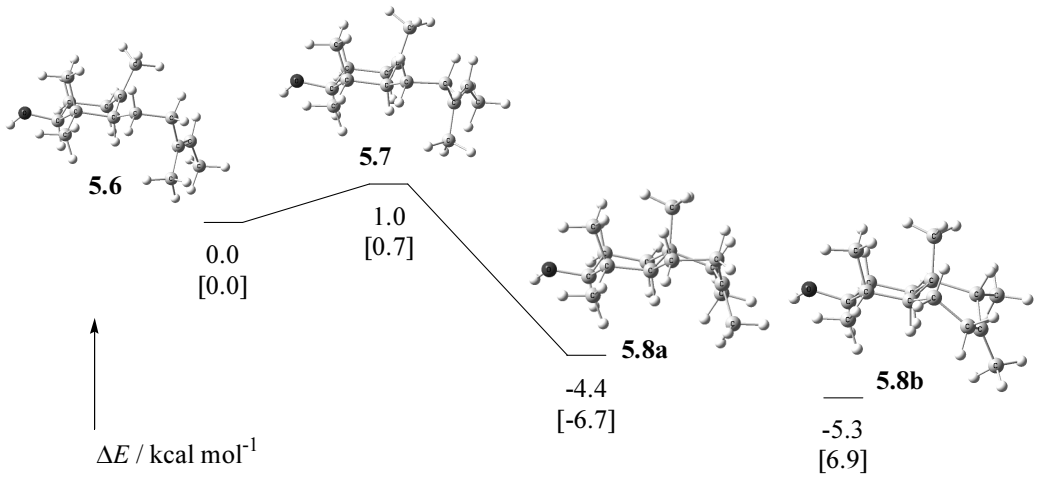

Figure 5.4. HF/3-21G//HF/3-21G optimised structures and reaction profile for B-ring closure of **5.1**. Energies in brackets are uncorrected for the zero-point energy.

HF/6-31G(d) optimised structures. The potential energy surface for the cyclisation of oxidosqualene model compound **5.1** has been investigated in depth at the HF/6-31G(d) level of theory. Two parallel reaction paths have been found for the gas-phase cyclisation of **5.1** to bicyclic product **5.5**; optimised structures and relative energies for reaction paths A and B are shown in figures 5.5 and 5.6 respectively. These two reaction paths arise from two twist-boat conformations of the proto-B-ring and B-ring which differ primarily in the dihedral angle about the C8–C9 bond. In both reaction pathways, the cyclisations of the A- and B-rings are calculated to be sequential and non-concerted, i.e. distinct monocyclic (A-ring) intermediates have been found, which then pass over a second transition state to form the bicyclic product. Transition states representing a rotation about the C8–C9 bond have been found which link the two reaction paths at each local minimum (Figure 5.7). The relative energies of all stationary points found for both reaction paths and the linking transition states are shown in figure 5.8.

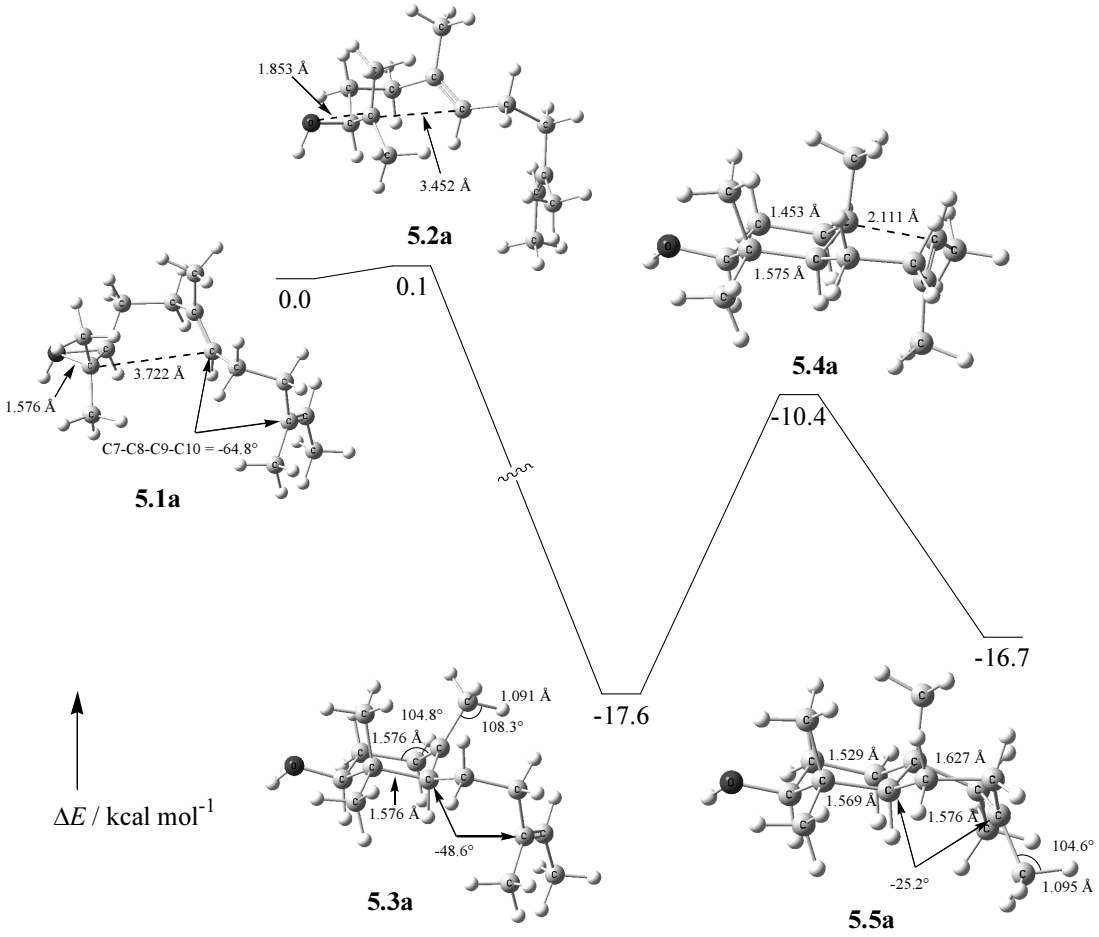

Figure 5.5. HF/6-31G(d)//HF/6-31G(d) optimised stationary points and relative energies for reaction path A of the cyclisation of **5.1**.

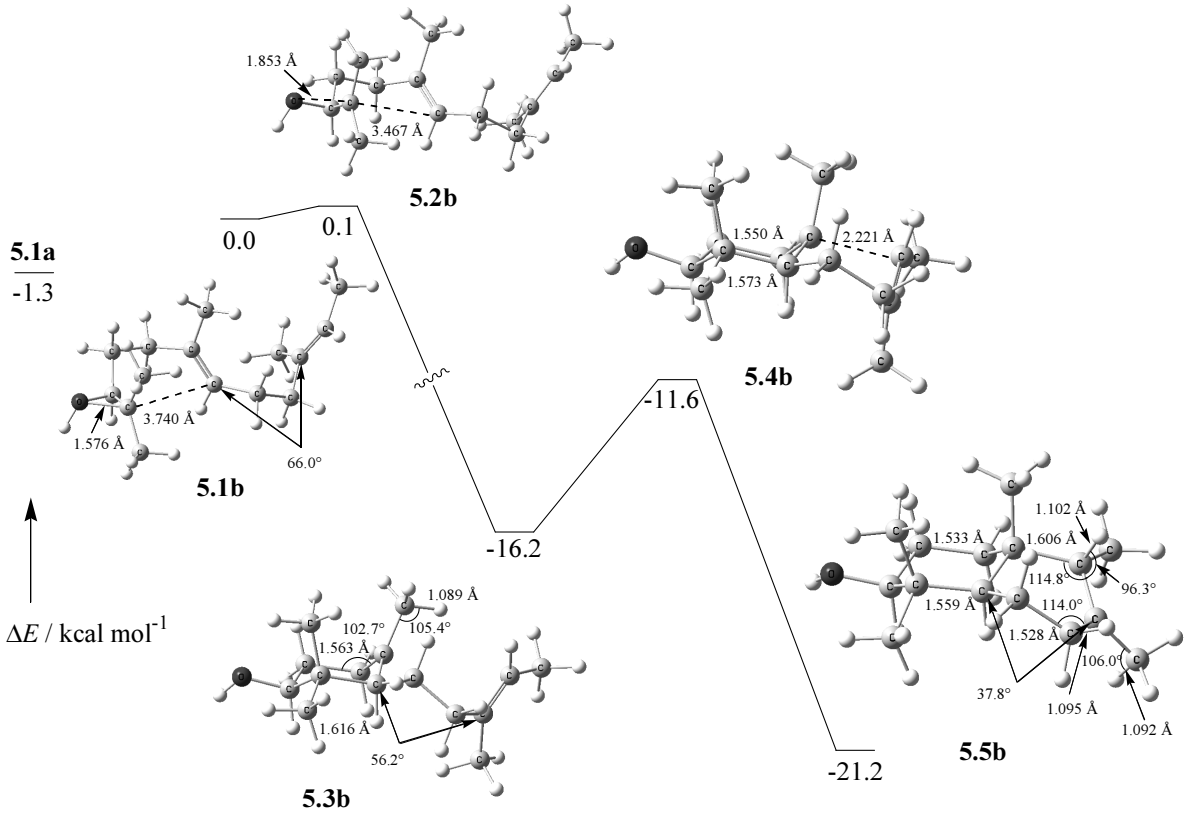

Figure 5.6. HF/6-31G(d)//HF/6-31G(d) optimised stationary points and relative energies for reaction path B of the cyclisation of **5.1**.

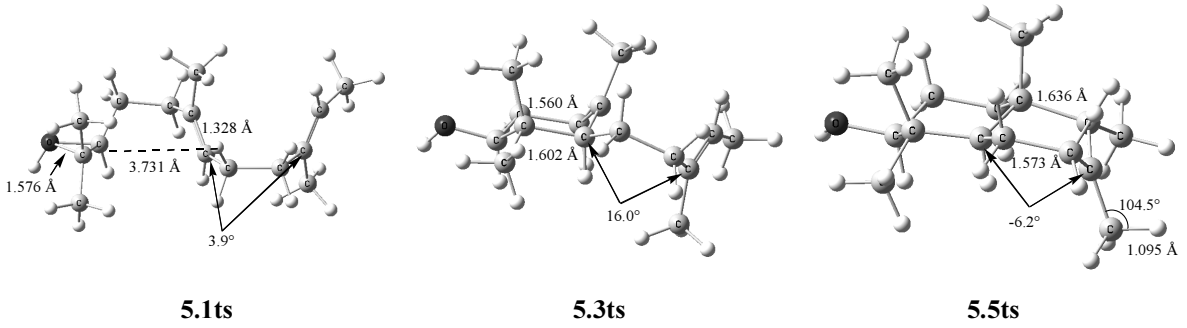

Figure 5.7. Bond rotation and ring-twist transition states that connect local minima on the two cyclisation reaction paths.

Prefolded reactant conformation **5.1a** (path A) is 1.3 kcal mol^{-1} lower in energy than conformation **5.1b** (path B) at the HF/6-31G(d)//HF/6-31G(d) level of theory. The activation barriers for A-ring cyclisation from both reactant conformations are very low at ca. 0.15 kcal mol^{-1}. Transition state **5.1ts**, which links **5.1a** and **5.1b** by rotation about the C8–C9 bond, is 6.1 kcal mol^{-1} above **5.1a**. As the

activation barrier for conformational change is significantly higher than the activation barriers for A-ring cyclisation it is necessary to consider each reaction path separately.

Monocyclic intermediate **5.3a** is 17.6 kcal mol^{-1} below path A reactant **5.1a** and intermediate **5.3b** is 16.2 kcal mol^{-1} below path B reactant **5.1b**. The two conformations of the intermediate are linked by bond rotational transition state **5.3ts** with an activation barrier of 4.6 kcal mol^{-1} from **5.3a** and 1.8 kcal mol^{-1} from **5.3b**.

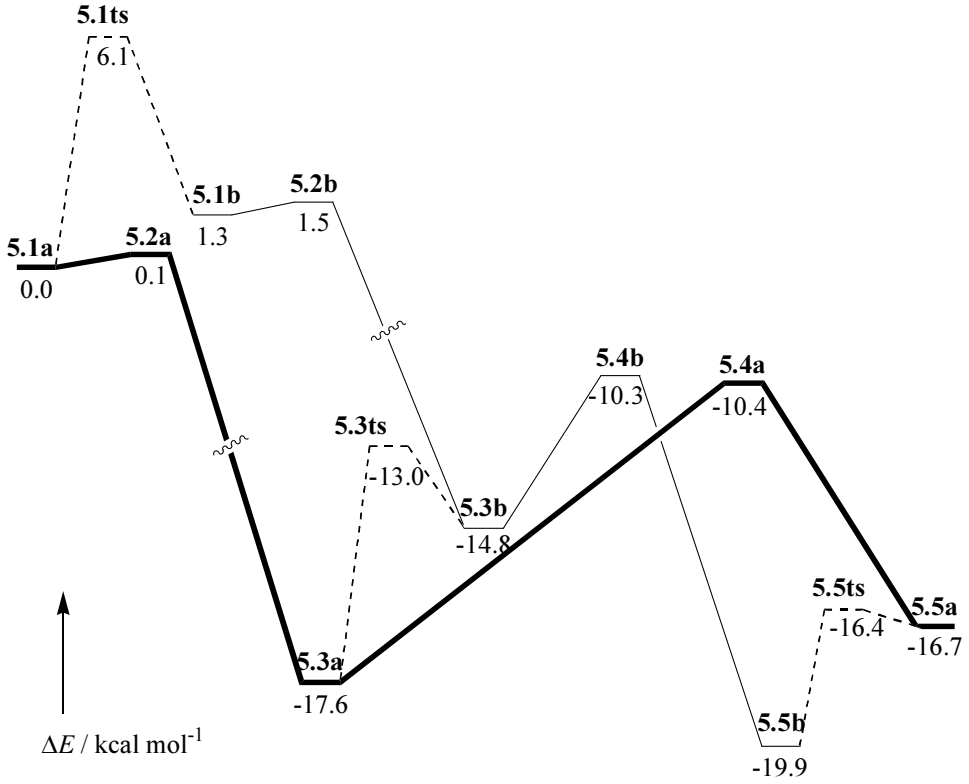

Figure 5.8. Schematic of the potential energy surface for the cyclisation reaction paths of **4.1**. Reaction path A is shown by thick lines, reaction path B by thin lines and conformation-change transition states between local minima by dashed lines.

The cyclisation of the A-ring by both reaction paths is very similar to the six-membered cyclisation of monocyclic model **4.5** presented in Chapter 4 of this thesis. Six-membered cyclisation of **4.5** has an activation barrier of 0.2 kcal mol^{-1} and is exothermic by 17.2 kcal mol^{-1} at the HF/6-31G(d)//HF/6-31G(d) level of theory. Furthermore, the geometries of the stationary points of the monocyclic model are

similar to those of the A-ring of the bicyclic model system. The structural and energetic similarity of A-ring cyclisation in both reaction paths of the bicyclic model, and in the monocyclic model, suggests that A-ring closure is unlikely to vary significantly in larger (tri- or tetracyclic) model systems and that the model systems presented in this thesis accurately describe A-ring formation.

Formation of the B-ring occurs via transition states **5.4a** and **5.4b** on reaction paths A and B respectively. IRC calculations of these saddle points led to monocyclic intermediates **5.3a** and **5.3b**, suggesting that B-ring cyclisation can occur immediately following A-ring closure and that a conformational change in the intermediate is not necessary to bring the C10–C11 double bond into a reactive position. The barriers for B-ring cyclisation are 7.2 kcal mol^{-1} to **5.4a** and 4.6 kcal mol^{-1} to **5.4b**. These activation energies are not negligible, and are significantly greater than the barrier for B-ring formation at the HF/3-21G level of theory.

It has previously been suggested[2] that in the enzyme active site, with a preorganised conformation and with the presence cation-stabilising groups, the B-ring of lanosterol forms in barrierless concert with, or rapidly following, the A-ring. The comparatively high activation barriers found for gas-phase B-ring closure for a sequential mechanism (7.2 kcal mol^{-1} for **5.4a** and 4.6 kcal mol^{-1} for **5.4b**) are not consistent with this view and much effort was expended to find a concerted or low-barrier mechanism for B-ring closure. All attempts to find such a mechanism were unsuccessful and it is thought that the relevant transition states and intermediates do not exist in the gas phase at the HF/6-31G(d) level of theory, suggesting that a barrier to B-ring formation is a real feature of the potential energy surface and that a brief monocyclic intermediate may exist during lanosterol biosynthesis.

B-ring formation by path B is exothermic with bicyclic product **5.5b** $\delta\Delta E$ = −5.0 kcal mol^{-1} lower than monocyclic intermediate **5.3b**, however closure of the B-ring by reaction path A is an endothermic process with **5.5a** $\delta\Delta E$ = 0.7 kcal mol^{-1} above **5.3a**. Product conformations **5.5a** and **5.5b** are linked by ring-twist transition state **5.5ts**. The presence of a planar carbocation in the B-ring, requiring a bond angle of approximately 120°, means that neither **5.5a** nor **5.5b** is able to assume either a true boat or true twist conformation of the B-ring; both are in twist-boat conformations.

Monocyclic intermediates **5.3a** and **5.3b** show similar hyperconjugation to that seen in monocyclic model **4.5**, but there is no evidence of hyperconjugation in the A-ring of the bicyclic product due to the transfer of the positive charge to the B-ring. The B-rings of **5.5a** and **5.5b** differ in the hyperconjugative stabilisations of the carbocation. Structure **5.5a** shows increased bond lengths and decreased bond angles consistent with hyperconjugation from both carbon–carbon and carbon–hydrogen bonds, but **5.5b** only shows carbon–hydrogen hyperconjugation. The C6–C11 bond of **5.5b** is longer than a standard carbon–carbon bond at 1.606 Å but the dihedral angle of this bond with the vacant *p* orbital is ca. 45° and the C6–C11–C10 angle is 114.8°, suggesting that the elongation of this bond is due to steric or other factors and not hyperconjugative stabilisation of the cation.

Jenson and Jorgensen[10] have reported a computational study of the gas-phase reaction of 2-methylprop-2-ylium and 2-methylpropene (Figure 5.9) to investigate the fundamental energetics of a tertiary cation → tertiary cation reaction, as occurs in the cyclisation of the B-, C- and D-rings of lanosterol. They found that reactant ion–dipole complexes are present as shallow minima on the HF/6-31G(d)//HF/6-31G(d) and B3LYP/6-31G(d)//B3LYP/6-31G(d) potential energy surfaces with a C2–C3 distance of 3.6 Å in the HF/6-31G(d) optimised complex. The barrier to collapse is

ca. 0.5 kcal mol^{-1} and the 2,4,4-trimethylpent-2-ylium cation product is ca. 15 kcal mol^{-1} below the minimum.

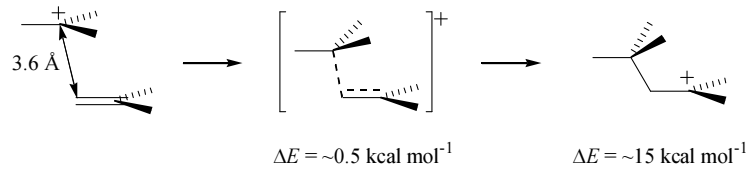

Figure 5.9. Reaction of 2-methylprop-2-ylium and 2-methylpropene studied by Jenson and Jorgensen (see ref. [10]).

Comparison of Jenson and Jorgensen's results with those presented above for the cyclisation of the B-ring of shows that the ring strain and steric interactions present in the cyclic system significantly affect the energetics of the reaction by raising the activation barrier by ca. 4.1–6.9 kcal mol^{-1} and decrease the exothermicity by ca. 9.4–15.1 kcal mol^{-1}. Jenson and Jorgensen suggested that the tenuous prereaction minima found in the reaction of 2-methylprop-2-ylium and 2-methylpropene may not exist at higher levels of theory, and should not be considered significant as ion–dipole complexes. The results of the present study suggest that the constraints imposed by an intramolecular reaction have a significant influence on the energetics of such a cation–alkene reaction, and that prereaction minima are an important feature of the potential energy surface that must be overcome by catalytic functionalities of the enzyme.

The reaction energy profile for the cyclisation of the A-ring in both the monocyclic model system (Chapter 4) and the present bicyclic model system does not differ greatly from the reaction energy profile for the analogous acyclic reaction of protonated oxirane and methylpropene (Chapter 3); all of these epoxide–alkene reactions have an activation barrier of ca. 1 kcal mol^{-1} and are exothermic by ca. 20–30 kcal mol^{-1}. In comparison, the intramolecular cyclisation of the B-ring presented

here is significantly different from the analogous intermolecular reaction studied by Jenson and Jorgensen; the transition state for B-ring closure is ca. 5 kcal mol^{-1} higher than the unlinked cation–alkene reaction and the reaction is ca. 10 kcal mol^{-1} less exothermic.

This difference between the A- and B-ring when compared to their intramolecular analogues is likely due to the formation of a largely strain-free chair A-ring while the B-ring is a twist-boat conformation with associated bond strain and steric interactions. A twist conformation of cyclohexane is ca. 5 kcal mol^{-1} higher in energy than a chair conformation, and a boat cyclohexane is ca. 1.5 kcal mol^{-1} higher than a twist conformation.[24]

5.3 Conclusion

At the HF/6-31G(d) level of theory, two parallel reaction paths exist for the gas-phase cyclisation of oxidosqualene model compound **5.1** to bicyclic product **5.5**. Both reaction paths have similar energy profiles and differ primarily in the conformation of the proto-B-ring and B-ring. Bond-rotation and ring-twist transition states have been found connecting the two reaction paths at each local minimum. It is unlikely that both reaction paths are relevant in the biosynthesis of lanosterol, as a consequence of the conformational constraint provided by the enzyme.

In both reaction paths, formation of the A-ring and B-ring is sequential and non-concerted. The barriers to cyclisation of the B-ring are significantly higher than that calculated by Jenson and Jorgensen for the analogous intermolecular reaction, and this increase in activation energy is likely to be a result of ring strain and steric interactions. The barrier to B-ring cyclisation is likely to be a real feature of the potential energy surface which must be overcome by the catalytic functionality of the enzyme. Future computational studies that include stabilising groups around the

model compound, mimicking the cation-stabilising ability of the enzyme, may provide a closer representation of the biosynthetic process and help determine if a brief monocyclic intermediate exists during oxidosqualene cyclisation.

Chapter 6: Conclusion

The computational studies of oxidosqualene model systems presented in this thesis have further elucidated the nature of the cyclisation of the A- and B-rings during the biosynthesis of lanosterol. The gas-phase nature of these calculations has allowed optimal geometries and energetics to be found, shedding light on the degree of conformational control and stabilisation provided by the enzyme.

In all model systems studied, the formation of the new carbon–carbon bond has been found to be concerted with rupture of the protonated epoxide; this is consistent with all previous experimental and computational studies of the oxidosqualene system. Formation of the A-ring, or the analogous intermolecular reaction, has a low activation barrier from the prearranged reactant minimum and a high exothermicity. This general reaction profile can be attributed to the facility of the opening a protonated epoxide, arising from relief of ring strain, the stability of the hydroxyl leaving group and the absence of the development of charge separation through the course of the reaction.

A model compound with equivalent substitution of the epoxide to that in oxidosqualene has a strong kinetic and thermodynamic preference to form the six-membered ring over the potential competing five-membered ring. This preference comes from three reasons: the inherent stability of a six-membered ring over a five-membered ring, the preference for nucleophilic substitution of protonated epoxides at the most substituted carbon atom and a stronger adherence of the system to Baldwin's rule for electrophilic closure at an alkene than to Baldwin's rule for nucleophilic closure of an epoxide.

The obedience to Baldwin's rule for electrophile–alkene reactions likely arises from the early and facile opening of the protonated epoxide, which causes a large

concentration of positive charge on the epoxide carbon atom. This concentration of positive charge accounts for the unexpected preference of protonated epoxides to undergo ring-opening S_N2 substitution at the more highly substituted, and thus more highly stabilised, carbon atom. The formation of the A-ring can therefore be considered more as an electrophilic addition to an alkene than as a nucleophilic substitution on an epoxide.

The low activation barrier for the concerted epoxide opening and carbon–carbon bond formation in the protonated model systems presented in this thesis, and the strong preference for formation of the six-membered A-ring over the five-membered ring, implies that the role of the enzyme during the initial step of lanosterol formation is two-fold. The first role of the enzyme is to provide sufficient conformational control over the flexible substrate so that the epoxide and 6,7-double bond are in position to react. The second role of the enzyme is to complex the epoxide of oxidosqualene with an amino acid residue of high enough acidity that the activated epoxide behaves similar to a protonated epoxide, leading to preference of reaction at the more highly substituted carbon atom and as an electrophilic ring closure at an alkene, as described by Baldwin's rules.

At the HF/6-31G(d) level of theory, the closure of the B-ring has been found to not be concerted with formation of the A-ring, and there is a significant barrier to reach the transition state from the monocyclic intermediate. A previous study by Jenson and Jorgensen[10] found that the analogous intermolecular cation–alkene reaction occurs with a very low barrier, and the significant barrier seen in the intramolecular B-ring closure must arise from ring strain and steric interactions. It seems likely that, in the enzyme-catalysed cyclisation of oxidosqualene, B-ring

cyclisation is not concerted with A-ring formation and a brief monocyclic intermediate exists.

References

1. Abe, I.; Rohmer, M.; Prestwich, G. D. *Chem. Rev.* **1993**, *93*, 2189.
2. Wendt, K. U.; Schulz, G. E.; Corey, E. J.; Liu, D. R. *Angew. Chem., Int. Ed. Engl.* **2000**, *39*, 2812.
3. Yoder, R. A.; Johnston, J. N. *Chem. Rev.* **2005**, *105*, 4730.
4. Corey, E. J.; Cheng, H.; Baker, C. H.; Matsuda, S. P. T.; Li, D.; Song, X. *J. Am. Chem. Soc.* **1997**, *119*, 1277.
5. Corey, E. J.; Cheng, H.; Baker, C. H.; Matsuda, S. P. T.; Li, D.; Song, X. *J. Am. Chem. Soc.* **1997**, *119*, 1289.
6. Schulz-Gasch, T.; Stahl, M. *J. Comput. Chem.* **2003**, *24*, 741.
7. Corey, E. J.; Staas, D. D. *J. Am. Chem. Soc.* **1998**, *120*, 3526.
8. Gao, D.; Pan, Y.-K.; Byun, K.; Gao, J. *J. Am. Chem. Soc.* **1998**, *120*, 4045.
9. Corey, E. J.; Virgil, S. C.; Cheng, H.; Baker, C. H.; Matsuda, S. P. T.; Singh, V.; Sarshar, S. *J. Am. Chem. Soc.* **1995**, *117*, 11819.
10. Jenson, C.; Jorgensen, W. L. *J. Am. Chem. Soc.* **1997**, *119*, 10846.
11. Vrček, V.; Saunders, M.; Kronja, O. *J. Org. Chem.* **2003**, *68*, 1859.
12. Hess, B. A., Jr. *J. Am. Chem. Soc.* **2002**, *124*, 10286.
13. Corey, E. J.; Virgil, S. C. *J. Am. Chem. Soc.* **1991**, *113*, 4025.
14. Corey, E. J.; Virgil, S. C.; Sarshar, S. *J. Am. Chem. Soc.* **1991**, *113*, 8171.
15. Narasimhan, N. S., Personal Communication.
16. Narasimhan, N. S.; Gokhale, S. M. *J. Chem. Soc., Chem. Commun.* **1985**, 86.
17. Narasimhan, N. S.; Gokhale, S. M. *J. Indian Inst. Sci.* **2001**, *81*, 135.
18. Hehre, W. J. *A Guide to Molecular Mechanics and Quantum Chemical Calculations*; Wavefunction, Inc.: Irvine, CA, United States of America, 2003.

19. Frisch, M. J.; Trucks, G. W.; Schlegel, H. B.; Gill, P. M. W.; Johnson, B. G.; Robb, M. A.; Cheeseman, J. R.; Keith, T.; Petersson, G. A.; Montgomery, J. A.; Raghavachari, K.; Al-Laham, M. A.; Zakrzewski, V. G.; Ortiz, J. V.; Foresman, J. B.; Cioslowski, J.; Stefanov, B. B.; Nanayakkara, A.; Challacombe, M.; Peng, C. Y.; Ayala, P. Y.; Chen, W.; Wong, M. W.; Andres, J. L.; Replogle, E. S.; Gomperts, R.; Martin, R. L.; Fox, D. J.; Binkley, J. S.; Defrees, D. J.; Baker, J.; Stewart, J. P.; Head-Gordon, M.; Gonzalez, C.; Pople, J. A. *Gaussian 94, Revision E.1,* Gaussian, Inc., Pittsburgh PA, 1995.

20. Frisch, M. J.; Trucks, G. W.; Schlegel, H. B.; Scuseria, G. E.; Robb, M. A.; Cheeseman, J. R.; Montgomery, J. A., Jr.; Vreven, T.; Kudin, K. N.; Burant, J. C.; Millam, J. M.; Iyengar, S. S.; Tomasi, J.; Barone, V.; Mennucci, B.; Cossi, M.; Scalmani, G.; Rega, N.; Petersson, G. A.; Nakatsuji, H.; Hada, M.; Ehara, M.; Toyota, K.; Fukuda, R.; Hasegawa, J.; Ishida, M.; Nakajima, T.; Honda, Y.; Kitao, O.; Nakai, H.; Klene, M.; Li, X.; Knox, J. E.; Hratchian, H. P.; Cross, J. B.; Adamo, C.; Jaramillo, J.; Gomperts, R.; Stratmann, R. E.; Yazyev, O.; Austin, A. J.; Cammi, R.; Pomelli, C.; Ochterski, J. W.; Ayala, P. Y.; Morokuma, K.; Voth, G. A.; Salvador, P.; Dannenberg, J. J.; Zakrzewski, V. G.; Dapprich, S.; Daniels, A. D.; Strain, M. C.; Farkas, O.; Malick, D. K.; Rabuck, A. D.; Raghavachari, K.; Foresman, J. B.; Ortiz, J. V.; Cui, Q.; Baboul, A. G.; Clifford, S.; Cioslowski, J.; Stefanov, B. B.; Liu, G.; Liashenko, A.; Piskorz, P.; Komaromi, I.; Martin, R. L.; Fox, D. J.; Keith, T.; Al-Laham, M. A.; Peng, C. Y.; Nanayakkara, A.; Challacombe, M.; Gill, P. M. W.; Johnson, B.; Chen, W.; Wong, M. W.; Gonzalez, C.; Pople, J. A. *Gaussian 03, Revision B.04,* Gaussian, Inc., Pittsburgh PA, 2003.

21. Foresman, J. B.; Frisch, Æ. *Exploring Chemistry with Electronic Structure Methods*; Second ed.; Gaussian, Inc.: Pittsburgh, PA, United States of America, 1996.

22. Coxon, J. M.; Froese, R. D. J.; Ganguly, B.; Marchand, A. P.; Morokuma, K. *Synlett* **1999**, 1681.

23. Norman, R. O. C.; Coxon, J. M. *Principles of Organic Synthesis*; Third ed.; Blackie Academic & Professional: Glasgow, United Kingdom, 1993.

24. Smith, M. B.; March, J. *March's Advanced Organic Chemistry: Reactions, Mechanisms, and Structure*; Fifth ed.; John Wiley & Sons, Inc.: New York, NY, United States of America, 2001.

25. Glad, S. S.; Jensen, F. *J. Org. Chem.* **1997**, *62*, 253.

26. Ford, G. P.; Smith, C. T. *J. Am. Chem. Soc.* **1987**, *109*, 1325.

27. Bock, C. W.; George, P.; Glusker, J. P. *J. Org. Chem.* **1993**, *58*, 5816.

28. Coxon, J. M.; Maclagan, R. G. A. R.; Rauk, A.; Thorpe, A. J.; Whalen, D. *J. Am. Chem. Soc.* **1997**, *119*, 4712.

29. Coxon, J. M.; Thorpe, A. J.; Smith, W. B. *J. Org. Chem.* **1999**, *64*, 9575.

30. Holubka, J. W.; Bach, R. D.; Andrés, J. L. *Macromolecules* **1992**, *25*, 1189.

31. Lee, I.; Kim, C. K.; Li, H. G.; Lee, B.-S.; Lee, H. W. *Chem. Phys. Lett.* **2000**, *320*, 307.

32. Frisch, Æ.; Frisch, M. J.; Trucks, G. W. *Gaussian 03 User's Reference*; Gaussian, Inc.: Carnegie, PA, United States of America, 2003.

33. Lau, E. Y.; Newby, Z. E.; Bruice, T. C. *J. Am. Chem. Soc.* **2001**, *123*, 3350.

34. Laitinen, T.; Rouvinen, J.; Peräkylä, M. *J. Org. Chem.* **1998**, *63*, 8157.

35. Dudev, T.; Lim, C. *J. Am. Chem. Soc.* **1998**, *120*, 4450.

36. Banks, H. D. *J. Org. Chem.* **2003**, *68*, 2639.

37. Sawicka, D.; Wilsey, S.; Houk, K. N. *J. Am. Chem. Soc.* **1999**, *121*, 864.

38. Glukhovtsev, M. N.; Pross, A.; Radom, L. *J. Am. Chem. Soc.* **1995**, *117*, 2024.

39. Wiberg, K. B. *Acc. Chem. Res.* **1996**, *29*, 229.

40. Wolk, J. L.; Hoz, T.; Basch, H.; Hoz, S. *J. Org. Chem.* **2001**, *66*, 915.

41. Baldwin, J. E. *J. Chem. Soc., Chem. Commun.* **1976**, 734.

42. Johnson, C. D. *Acc. Chem. Res.* **1993**, *26*, 476.

43. Stork, G.; Cohen, J. F. *J. Am. Chem. Soc.* **1974**, *96*, 5270.

44. Coxon, J. M.; Hartshorn, M. P.; Swallow, W. H. *Aust. J. Chem.* **1973**, *26*, 2521.

45. Na, J.; Houk, K. N.; Shevlin, C. G.; Janda, K. D.; Lerner, R. A. *J. Am. Chem. Soc.* **1993**, *115*, 8453.

46. Coxon, J. M.; Thorpe, A. J. *J. Org. Chem.* **1999**, *64*, 5530.

47. Coxon, J. M.; Morokuma, K.; Thorpe, A. J.; Whalen, D. *J. Org. Chem.* **1998**, *63*, 3875.

48. Rauk, A.; Sorensen, T. S.; Maerker, C.; Carneiro, J. W. d. M.; Sieber, S.; Schleyer, P. v. R. *J. Am. Chem. Soc.* **1996**, *118*, 3761.

49. Rauk, A.; Sorensen, T. S.; Schleyer, P. v. R. *J. Chem. Soc., Perkin Trans. 2* **2001**, 869.

50. Kirchen, R. P.; Ranganayakulu, K.; Sorensen, T. S. *J. Am. Chem. Soc.* **1987**, *109*, 7811.

51. Mesić, M.; Novak, I.; Sunko, D. E.; Vančik, H. *J. Chem. Soc., Perkin Trans. 2* **1998**, 2371.

52. Booth, H.; Everett, J. R. *J. Chem. Soc., Chem. Commun.* **1976**, 278.

53. Booth, H.; Everett, J. R. *J. Chem. Soc., Perkin Trans. 2* **1980**, 255.

54. Abraham, R. J.; Ribeiro, D. S. *J. Chem. Soc., Perkin Trans. 2* **2001**, 302.

55. Wiberg, K. B.; Hammer, J. D.; Castejon, H.; Bailey, W. F.; DeLeon, E. L.; Jarret, R. M. *J. Org. Chem.* **1999**, *64*, 2085.

56. Freeman, F.; Kasner, M. L.; Hehre, W. J. *THEOCHEM* **2001**, *574*, 19.

57. Ribeiro, D. S.; Rittner, R. *J. Org. Chem.* **2003**, *68*, 6780.

58. Jones Weldon, A.; Vickrey, T. L.; Tschumper, G. S. *J. Phys. Chem. A* **2005**, *109*, 11073.

Appendix: Optimised Molecular Structures

This appendix gives the coordinates of the optimised molecular structures for stationary points presented in this thesis, specified as z-matrices in *Gaussian 03* input format (see references [21] and [32]). Interatomic distances are in angstroms, and bond and dihedral angles are in degrees. The geometry specification is preceded by a line giving the molecular charge and spin multiplicity.

Also given are ab initio calculated energies, zero-point corrections (scaled, see ref. [21]) and imaginary frequencies. Energies and ZPCs are given in hartrees and imaginary frequencies in cm^{-1}.

Molecular structures are given in the order in which they are encountered in the body of this thesis. Structures which appear in more than one section of this thesis are included with the structures of the first section in which they appear.

A.1 Stereoselectivity and regioselectivity of Diels–Alder reactions

Table A.1. 2*H*-Pyran-2-one and ethene model system at HF/6-31G(d)//HF/6-31G(d).

Ethene
E = −78.0317181 ZPC: 0.050032 Imag. Freq.: N/A
0 1
C
C 1 1.31702000
H 1 1.07601585 2 121.79525164
H 1 1.07601585 2 121.79525164 3 180.00000000
H 2 1.07601585 1 121.79525164 3 180.00000000
H 2 1.07601585 1 121.79525164 3 0.00000000

2*H*-Pyran-2-one (**2.5**)
E = −341.3784884 ZPC: 0.079677 Imag. Freq.: N/A
0 1
C
C 1 1.32699450

C	2	1.44674935	1	117.43102060		
O	1	1.33936401	2	123.10932828	3	0.00000000
O	4	2.19177724	1	151.40926254	2	0.00000000
H	1	1.07112407	2	125.24956384	3	180.00000000
H	2	1.07162283	1	120.77114166	4	180.00000000
H	3	1.07504179	2	119.36263825	1	−180.00000000
H	3	2.12234611	2	145.15499139	1	0.00000000
C	3	1.33473731	2	120.20492251	1	0.00000000
C	5	1.18379789	4	33.07647459	1	−0.00269676

Prereaction complex **2.6**

E = −419.4120717 ZPC: 0.130425 Imag. Freq.: N/A

0 1

C						
C	1	1.46055010				
C	2	2.37455771	1	87.34351133		
C	1	1.33507572	2	120.64087280	3	−0.09257915
C	2	4.23305560	1	125.53209702	4	110.18258651
O	2	1.18508868	1	125.92771044	4	179.80175099
H	1	1.07192173	4	123.36074116	3	179.99443874
H	3	1.07103254	2	140.34819124	1	179.93067788
H	4	1.07500720	1	120.40568861	2	−179.91880677
H	3	2.08902086	2	120.53303699	1	0.21432891
H	5	1.07665807	2	151.14639570	1	−16.80818463
H	5	1.07538822	2	51.89681335	1	59.65532818
H	5	2.09504187	2	99.00493899	1	−137.33954430
H	5	2.08803773	2	52.36156678	1	−161.97488637
O	3	1.33927945	2	28.69302941	1	−179.54838114
C	3	1.32712319	2	94.37658280	1	0.12470657
C	5	1.31734070	2	75.45087817	1	−148.21364374

Diels–Alder transition state **2.7**

E = −419.3435129 ZPC: 0.132905 Imag. Freq.: −822.9391

0 1

C						
C	1	1.46080745				
C	2	2.33581822	1	83.24987490		
C	1	1.39107524	2	118.57925624	3	31.22516125
C	1	2.28688525	4	99.91012175	3	61.02458697
O	2	1.18819652	1	126.43919823	4	−152.31712719

H	1	1.07298148	4	121.36828889	3	176.18419355
H	3	1.07139387	2	140.39878490	1	176.31327570
H	4	1.07490737	1	120.36256482	2	158.18723964
H	3	2.14375251	2	119.53436894	1	−29.66027825
H	5	1.07244295	1	90.48934219	4	71.08229643
H	5	1.07403834	1	92.90286254	4	−173.52084192
H	5	2.12769927	1	110.99275656	4	−23.68562766
H	5	2.11723158	1	112.44198272	4	−78.46501679
O	2	1.34721359	1	113.70063022	4	28.69827599
C	4	1.37277923	1	117.29371030	2	−31.07908126
C	5	1.38555063	1	106.48370737	4	−50.91073548

Adduct **2.8**

E = −419.4504116 ZPC: 0.138300 Imag. Freq.: N/A

0 1

C						
C	1	1.51727557				
C	2	2.33055309	1	77.81461454		
C	1	1.51631152	2	106.71831191	3	54.08021514
C	1	1.55519295	4	107.83421847	3	59.83481873
O	2	1.18294005	1	126.22804020	4	−126.61764467
H	1	1.07891703	4	114.05967021	3	−174.48759078
H	3	1.07766292	2	136.75705261	1	−175.82375246
H	4	1.07426494	1	121.54558831	2	126.44799686
H	4	2.12933027	1	137.52181888	2	−54.41474373
H	5	1.08280643	1	108.94613958	4	64.24132060
H	5	1.08395131	1	109.62591085	4	−178.48208685
H	3	2.16099363	2	116.40225878	1	44.52934564
H	3	2.14679462	2	90.39353941	1	86.45018309
O	2	1.33485896	1	111.78490291	4	54.92358848
C	4	1.31819410	1	113.26702455	2	−53.71612143
C	3	1.53630033	2	91.40610051	1	57.91660207

Decarboxylation transition state **2.9**

E = −419.3727920 ZPC: 0.133552 Imag. Freq.: −477.7122

0 1

C						
C	1	1.71108735				
C	1	1.43429777	2	103.85860019		
C	1	1.53310988	3	112.98011932	2	114.34107247

H	1	1.07674130	3	114.09535733	4	131.42117122
O	2	1.19882095	1	112.02813848	3	−121.72999280
H	3	1.07662430	1	119.43046357	4	−149.87910954
H	4	1.08520156	1	108.91886862	3	70.78540963
H	4	1.08245877	1	109.55310973	3	−172.37548612
O	2	1.22130955	1	111.92059528	3	61.11248446
C	3	1.37734136	1	120.06240162	4	41.89731453
C	4	1.53836284	1	111.11902816	3	−50.39224171
H	11	1.07348704	3	121.24918864	1	162.63569948
H	12	1.08938527	4	110.97433425	1	138.70972037
H	12	1.07982638	4	112.33923178	1	−101.62442097
C	11	1.37972181	3	115.50091104	1	−0.08682814
H	16	1.07560273	11	118.82831268	3	155.92509545

Decarboxylation product complex **2.10**

E = −419.4684830 ZPC: 0.132436 Imag. Freq.: N/A

0 1

C						
C	1	4.14964815				
C	1	1.32474771	2	57.08085409		
C	1	1.51116077	3	120.79982080	2	85.99921930
H	1	1.07657247	3	120.67252522	4	176.51604930
O	2	1.14327554	1	94.13219344	3	−32.10782897
H	3	1.07597839	1	121.02074210	4	−177.33610870
O	2	1.14346113	1	86.76901161	3	148.28005591
H	3	2.20202262	1	145.05203245	4	−7.65438371
H	4	2.15813478	1	138.69177468	3	−18.45722891
H	4	2.16086987	1	104.29269925	3	−58.53579457
H	3	3.42308204	1	101.64466009	4	7.10841913
C	3	1.47614391	1	120.56215924	4	2.08119706
C	4	1.53378794	1	111.92769870	3	−29.77756558
C	13	1.32505998	3	120.60305613	1	13.78733257
H	4	1.09035968	1	108.33879683	3	91.32296527
H	4	1.08525311	1	110.53282956	3	−152.51884138

Cyclohexadiene (**2.11**)

E = −231.8318977 ZPC: 0.120263 Imag. Freq.: N/A

0 1

C		
C	1	1.32420302

C	2	1.47526409	1	120.60625074		
C	1	1.51123451	2	120.71639169	3	−1.63461971
H	1	1.07652044	2	120.75015579	3	−178.54117892
H	2	1.07619386	1	120.92653322	4	177.61190383
H	3	1.07619367	2	118.46285300	1	166.59847893
H	3	2.09049634	2	146.86025622	1	−15.31768939
H	4	2.15982122	1	103.81865401	2	58.46942157
H	4	2.15859453	1	138.67500486	2	19.03447998
H	4	1.09044854	1	108.49718413	2	−91.24687184
H	4	1.08540466	1	110.53636228	2	152.48747426
C	3	1.32420330	2	120.60618357	1	−14.13696706
C	13	1.51123851	3	120.71608659	2	−1.63596774

Carbon dioxide

E = −187.6341762 ZPC: 0.011643 Imag. Freq.: N/A

0 1

O

C	1	1.14326600		
O	2	1.14326600	1	180.00000000

Table A.2. 2*H*-Pyran-2-one and 2-cholroacrylaldehyde model system at HF/6-31G(d)//HF/6-31G(d).

2-Chloroacrylaldehyde, *cisoid* conformation (**2.2**)

E = −649.6591039 ZPC: 0.052019 Imag. Freq.: N/A

0 1

C

C	1	1.31626342				
C	2	1.49481680	1	122.37890691		
Cl	2	1.74208140	1	122.54005972	3	179.99536010
O	3	1.18638984	2	122.68248007	1	−0.00531596
H	1	1.07271238	2	122.48503913	3	−179.99509348
H	1	1.07350909	2	118.74765472	3	0.00000000
H	3	1.08999936	2	115.42885862	1	179.99293449

2-Chloroacrylaldehyde, conformational change transition state

E = −649.646626 ZPC: 0.051432 Imag. Freq.: −165.3957

0 1

C

C	1	1.31197530

C	2	1.50707755	1	123.91682049		
Cl	2	1.73988319	1	122.48394994	3	−179.27222679
O	3	1.18335493	2	123.07282318	1	97.86266681
H	1	1.07325221	2	122.13574534	3	−179.62116658
H	1	1.07535936	2	120.10996239	3	−0.28152507
H	3	1.09141944	2	115.45171765	1	−82.34309160

2-Chloroacrylaldehyde, *transoid* conformation

E = −649.6587433 ZPC: 0.052158 Imag. Freq.: N/A

0 1

C

C	1	1.31835358				
C	2	1.48827226	1	120.78986859		
Cl	2	1.73031975	1	122.42462446	3	180.00000000
O	3	1.18349660	2	125.03741981	1	179.98819350
H	1	1.07286119	2	122.49249000	3	−180.00000000
H	1	1.07540485	2	119.95179577	3	0.00000000
H	3	1.09296528	2	113.26174738	1	0.00450271

Prereaction complex **2.12a**

E = −991.0434339 ZPC: 0.132351 Imag. Freq.: N/A

0 1

C

C	1	1.45810136				
C	1	1.33523395	2	120.50897406		
H	1	1.07180546	3	123.39545672	2	179.39922787
O	2	1.18867340	1	125.77039875	3	179.35863308
H	3	1.07501224	1	120.40897081	2	−179.62593561
H	3	2.20693860	1	144.55027577	2	−0.36314268
H	2	3.26529079	1	99.60495908	3	−0.28146646
Cl	5	6.00914417	2	102.22783401	1	−112.68563537
O	2	3.29375159	1	97.40208406	3	77.36083728
H	5	2.37719237	2	109.17410504	1	−119.19606163
H	10	3.93967173	2	82.40785154	1	144.15773179
H	10	1.98750425	2	168.07801838	1	147.62362741
O	2	1.35624042	1	115.77978424	3	−1.55851327
C	3	1.44513544	1	120.19289417	2	0.19287592
C	15	1.32693420	3	117.39199355	1	0.32589763
C	10	2.36359257	2	108.42150725	1	144.71453964
C	17	1.31750526	10	98.34184208	2	−1.41659205

C	10	1.18822453	2	140.15509993	1	145.27197914

Diels–Alder transition state **2.13a**

E = −990.9651745 ZPC: 0.133714 Imag. Freq.: −780.3568

0 1

C						
C	1	1.46615304				
C	1	1.38369042	2	118.89651853		
H	1	1.07307463	3	121.96495491	2	−155.25998658
O	2	1.18319579	1	125.62675908	3	−149.72745445
H	3	1.07307741	1	120.91961129	2	159.79819226
H	3	2.15116335	1	140.84653223	2	−38.64645430
H	2	3.23622772	1	95.79697714	3	30.26340101
Cl	2	3.12226090	1	83.85631106	3	122.49931168
O	3	3.06816550	1	90.39173999	2	−121.33131439
H	10	2.49702702	3	73.84132568	1	92.31712703
H	2	3.42707192	1	93.43565524	3	72.73389152
H	10	1.99655081	3	91.71263083	1	−17.03371516
O	2	1.34714218	1	114.05864078	3	29.30861101
C	3	1.37436246	1	116.82070936	2	−30.32478155
C	14	1.36353416	2	119.31418187	1	3.30872862
C	10	2.34471348	3	64.85946621	1	38.01624555
C	17	1.39502084	10	94.64994438	3	82.25005089
C	10	1.19344606	3	78.02184575	1	7.12585569

Diels–Alder transition state **2.13b**

E = −990.9906919 ZPC: 0.133394 Imag. Freq.: −454.9804

0 1

C						
C	1	1.46591819				
C	1	1.38622458	2	118.61705332		
H	1	1.07300600	3	121.48340835	2	−154.11338692
O	2	1.18265322	1	125.74934821	3	−148.86203942
H	3	1.07329303	1	120.74237963	2	158.36194424
H	3	2.15483106	1	140.80472750	2	−39.39289621
H	2	3.23657192	1	95.52845893	3	31.69186665
H	3	3.51738975	1	90.05340096	2	−75.19582272
H	2	3.23248430	1	93.72262161	3	76.88462435
O	2	1.34699384	1	113.71028503	3	30.51251018
C	3	1.37442593	1	116.85689945	2	−31.39460152

C	11	1.36134321	2	119.46216875	1	2.60111998
C	1	2.42187302	3	94.27653164	12	61.79749108
C	14	1.39098472	1	103.16488330	3	−59.55639649
Cl	14	1.75401144	1	97.67546421	3	61.17093876
C	14	1.48665707	1	94.49293748	3	176.56220614
H	17	1.09014352	14	114.90539629	1	−83.30658600
O	17	1.18755909	14	122.98150217	1	96.84082775

Diels–Alder transition state **2.13c**

E = −990.9684765 ZPC: 0.133696 Imag. Freq.: −741.8642

0 1

C						
C	1	1.46830982				
C	2	2.33365308	1	83.27120885		
C	1	1.40536782	2	116.89304538	3	33.03337650
C	1	2.04294173	4	102.40133605	3	69.10123937
O	2	1.18170179	1	126.90471297	4	−147.84794166
Cl	5	2.72505313	1	117.23526704	4	−93.17837409
O	5	2.83151804	1	105.69158863	4	2.80566387
H	1	1.07370270	4	120.00361114	3	−177.54529583
H	3	1.07094663	2	140.95439466	1	165.20882366
H	4	1.07380791	1	120.41556676	2	156.42862575
H	3	2.13519441	2	119.72148692	1	−30.72441833
H	5	1.07206204	1	94.41765132	4	64.17730735
H	5	1.07447920	1	96.19738976	4	−179.63769741
H	8	1.99501679	5	88.16458895	1	−118.19384887
O	3	1.34054503	2	30.12122315	1	176.41680866
C	4	1.37031818	1	117.17904209	2	−34.17862674
C	5	1.40025683	1	111.27500189	4	−55.82536588
C	8	1.19508287	5	60.52605226	1	−114.78019227

Diels–Alder transition state **2.13d**

E = −990.9659718 ZPC: 0.133566 Imag. Freq.: −747.2801

0 1

C						
C	1	1.46892959				
C	2	2.33280277	1	83.28487764		
C	1	1.40237334	2	116.90583393	3	33.21658475
C	1	2.08018520	4	102.71810187	3	67.41268516
O	2	1.18093812	1	126.71129024	4	−146.69353201

H	1	1.07359513	4	120.28096461	3	−178.34611707
H	3	1.07138652	2	141.31904628	1	167.44765520
H	4	1.07432084	1	120.47605439	2	155.60372767
H	3	2.13593344	2	119.55611178	1	−31.30125088
H	5	1.07163124	1	94.12266287	4	74.89860107
H	5	1.07483008	1	95.79307744	4	−168.89896139
O	3	1.33992081	2	30.13765834	1	176.00724621
C	4	1.37114132	1	117.12799685	2	−34.26896584
C	5	1.39521311	1	110.46827740	4	−48.09621753
Cl	15	1.76347245	5	117.56031292	1	101.68822355
C	15	1.47771718	5	120.14787685	1	−110.84579811
H	17	1.09171655	15	114.81502446	5	−162.32953080
O	17	1.18990618	15	123.49648047	5	18.50559836

Adduct **2.14a**

E = −991.0661151 ZPC: 0.138255 Imag. Freq.: N/A

0 1

C						
C	1	1.52302382				
C	1	1.52113137	2	105.82663597		
C	1	1.55676015	3	106.92409929	2	114.27592875
H	1	1.07854556	3	114.47709170	2	−120.90902485
O	2	1.17912124	1	125.64211119	3	−122.44562679
Cl	4	1.81071610	1	109.20149477	3	179.36595082
H	3	1.07349837	1	121.40612576	2	125.65434579
O	4	2.39972080	1	119.18399588	3	41.73084091
H	3	2.12670420	1	137.32917233	2	−54.90933177
H	4	2.16444356	1	121.48547710	3	−31.20613661
H	4	2.17266456	1	118.90676767	3	−87.01998636
H	9	1.98712394	4	59.61760565	1	71.44596182
H	2	3.19985420	1	90.98247355	3	54.06813316
O	2	1.33334966	1	111.64946268	3	56.60303630
C	3	1.31741383	1	113.00753893	2	−54.25996077
C	4	1.54292109	1	108.60831022	3	−58.77488488
C	9	1.18293466	4	31.76058256	1	71.57423352
C	15	1.43161453	2	114.63614094	1	−3.05357164

Adduct **2.14b**

E = −991.0653464 ZPC: 0.138268 Imag. Freq.: N/A

0 1

C						
C	1	1.52634432				
C	1	1.51795140	2	106.16895132		
C	1	1.55616942	3	108.55748626	2	113.22823126
H	1	1.07885734	3	114.20800641	2	−120.93968874
O	2	1.18051956	1	125.19753911	3	−124.94475112
H	3	1.07273300	1	121.12912519	2	126.41407952
H	3	2.12685971	1	137.36240655	2	−54.18130448
H	4	2.17877925	1	119.94625797	3	−28.94415501
H	4	2.15674490	1	119.82339754	3	−84.64412129
H	2	3.19535135	1	90.96672827	3	53.83788334
O	2	1.32981476	1	111.86433254	3	55.65416966
C	3	1.31675745	1	113.06462366	2	−53.62903031
C	4	1.54281945	1	108.21097647	3	−56.35969625
C	12	1.43346001	2	114.36325246	1	−1.92147605
Cl	4	1.81036648	1	108.90155238	3	65.78871029
C	4	1.53082032	1	109.89512856	3	179.17641491
H	17	1.09067027	4	114.22467629	1	−63.03384041
O	17	1.18232172	4	123.86462654	1	116.45002398

Adduct **2.14c**

E = −991.0650939 ZPC: 0.138266 Imag. Freq.: N/A

0 1

C						
C	1	1.31799004				
C	1	1.51635374	2	113.25146792		
O	3	2.41442320	1	118.29657959	2	−75.32088767
Cl	3	3.86967847	1	106.31476291	2	21.56188895
O	2	3.47562327	1	90.87789428	3	−75.34685777
H	1	1.07368826	2	125.08204362	3	−179.96762054
H	2	1.07347139	1	125.75375925	3	−179.15196518
H	3	1.07845773	1	114.14807333	2	−174.90774849
H	3	2.17267978	1	95.05982210	2	84.86660897
H	3	2.17527283	1	135.99921244	2	57.07206833
H	2	2.18729346	1	138.94892485	3	5.07863952
H	6	1.98564695	2	71.49771061	1	158.26061411
C	3	1.55230816	1	108.28978772	2	59.77286446
C	4	1.17940561	3	30.26823938	1	63.36563109
C	2	1.51356847	1	112.49220114	3	0.41393776
C	14	1.54293379	3	108.28761196	1	−55.07068576

O	15	1.34086324	4	121.89191244	3	178.58911476
C	6	1.18288713	2	54.72748332	1	132.99856422

Adduct **2.14d**

E = −991.0668679 ZPC: 0.138301 Imag. Freq.: N/A

0 1

C						
C	1	1.31712486				
C	1	1.51674782	2	113.27439735		
O	3	2.41644912	1	117.82860112	2	−76.24080149
H	1	1.07378821	2	125.11401461	3	179.46761965
H	2	1.07256355	1	125.89812381	3	−178.36424220
H	3	1.07848016	1	114.12520991	2	−175.65794589
H	3	2.16558372	1	93.41504320	2	83.79947396
H	3	2.18488441	1	135.54107474	2	58.73879195
H	2	2.18249166	1	139.08053282	3	6.43534100
C	3	1.55416071	1	107.99623848	2	59.31435774
C	4	1.17843711	3	30.08286407	1	63.99642723
C	2	1.51013427	1	112.56245036	3	1.27030928
C	11	1.54118801	3	108.16024034	1	−59.20100176
O	12	1.34517155	4	121.72757843	3	179.02288123
Cl	14	1.80556000	11	112.91942655	3	123.90602229
C	14	1.53039415	11	113.38871764	3	−117.38976621
H	17	1.09140265	14	114.14840269	11	177.99791574
O	17	1.18187773	14	124.04100521	11	−2.46713144

Decarboxylation transition state **2.15a**

E = −990.9888662 ZPC: 0.133444 Imag. Freq.: −566.5810

0 1

C						
C	1	1.74650756				
C	1	1.43978844	2	101.95195752		
C	1	1.53123614	3	112.25003841	2	114.88502114
H	1	1.07669318	3	114.94949120	4	131.25481712
O	2	1.19124298	1	111.49134806	3	−116.28395794
H	3	1.07587519	1	118.77722250	4	−149.23925765
Cl	4	1.80340585	1	110.30817107	3	−174.44047311
O	2	1.21841296	1	110.69884962	3	64.28691497
H	3	2.13780734	1	143.64886286	4	55.70098991
H	4	2.15606657	1	130.11880288	3	−26.71797842

H	4	2.17588462	1	114.28180036	3	−81.01198588
H	9	2.69341358	2	132.16122869	1	−14.42725790
O	4	2.39671518	1	116.27550819	3	46.94208549
H	14	1.98986324	4	59.76830275	1	74.79877027
C	14	1.18454904	4	32.05445585	1	75.66497767
C	3	1.37027243	1	120.00340936	4	43.33900818
C	4	1.53506883	1	111.10990263	3	−51.45852082
C	17	1.38537605	3	114.89633654	1	−0.18764580

Decarboxylation transition state **2.15b**

E = −990.9906919 ZPC: 0.133394 Imag. Freq.: −454.9804

0 1

C						
C	1	1.72305562				
C	1	1.44225657	2	104.84143005		
C	1	1.52453765	3	112.88412356	2	113.42130604
H	1	1.07643176	3	114.18914311	4	130.63136684
O	2	1.19649933	1	111.15900576	3	−126.90601698
H	3	1.07564406	1	118.88970996	4	−148.77952983
O	2	1.21898604	1	111.86267405	3	56.06055819
H	3	2.13843712	1	143.80283620	4	54.33057110
H	4	2.16984481	1	130.68740937	3	−27.89156337
H	4	2.15443035	1	113.56910861	3	−81.22537454
H	8	2.76589030	2	130.82688792	1	−1.32085599
C	3	1.36892474	1	120.03123234	4	42.65229457
C	4	1.53002957	1	110.90371860	3	−51.02574938
C	13	1.38454051	3	115.11743634	1	−0.60607400
Cl	4	1.83275900	1	108.73080198	3	70.11019044
C	4	1.52960395	1	111.45702864	3	−176.99291474
H	17	1.08930674	4	114.52733426	1	−51.26881552
O	17	1.18207770	4	123.08139730	1	129.82259673

Decarboxylation transition state **2.15c**

E = −990.9782293 ZPC: 0.133566 Imag. Freq.: −736.8840

0 1

C						
C	1	1.76838112				
C	1	1.41855317	2	101.24739282		
C	1	1.52753340	3	116.19108195	2	110.77011585
H	1	1.07575249	3	115.64211677	2	−112.54940638

O	2	1.19054570	1	111.44209114	3	−116.84813911
H	3	1.07574196	1	119.66745443	4	−151.63401210
H	4	1.07940003	1	109.74071126	3	−160.69405583
O	2	1.21661773	1	110.25282042	3	66.50046532
H	4	1.08095219	1	109.35086508	3	81.04794629
H	3	2.14656823	1	142.01110338	4	56.72914492
Cl	4	2.78519633	1	128.08749069	3	−76.61275417
H	9	2.58899310	2	133.95159435	1	−18.28540694
O	4	2.81969423	1	121.27410516	3	27.08837172
H	14	1.98705139	4	92.88256775	1	−104.97289585
C	3	1.38371994	1	119.09418691	4	42.29939292
C	4	1.54039069	1	111.78073875	3	−38.44311377
C	14	1.18096946	4	65.23859001	1	−102.73221111
C	16	1.37572267	3	115.18606126	1	−2.02365790

Decarboxylation transition state **2.15d**

E = −990.9864241 ZPC: 0.133671 Imag. Freq.: −513.9895

0 1

C						
C	1	1.71553739				
C	1	1.43048864	2	102.29625597		
C	1	1.53307081	3	113.59372608	2	114.19798195
H	1	1.07654481	3	114.35879257	2	−113.77840404
O	2	1.19248860	1	112.69218895	3	−114.11729885
H	3	1.07611650	1	119.61557770	4	−150.09176144
H	4	1.07979221	1	110.81636684	3	−172.01638575
O	2	1.22682327	1	111.07220182	3	67.77111178
H	4	1.08151488	1	109.03835997	3	69.45733770
H	3	2.14645747	1	143.54802319	4	53.12359649
H	9	2.77084904	2	129.94248466	1	−19.56985890
C	3	1.38133988	1	119.75610509	4	41.62542113
C	4	1.53041257	1	110.36960532	3	−51.14942101
C	13	1.37303305	3	115.71213751	1	0.43353780
Cl	14	1.82882884	4	111.33159696	1	136.61099766
C	14	1.53507913	4	113.69106120	1	−106.70390060
H	17	1.08927573	14	115.10334129	4	155.00234505
O	17	1.17941712	14	122.29220055	4	−28.48443017

Decarboxylation product complex **2.16a**

E = −991.0905738 ZPC: 0.132799 Imag. Freq.: N/A

0 1

C						
C	1	3.65276539				
C	1	1.32541562	2	94.39282461		
C	1	1.51252803	3	119.77382240	2	103.48920989
H	1	1.07399117	3	122.02620641	4	175.63942610
O	2	1.14319263	1	83.76382829	3	−103.75416085
H	3	1.07575026	1	119.74410899	4	−176.32242670
Cl	4	1.81972282	1	109.26233152	3	−152.03556231
O	2	1.14349302	1	96.68342439	3	75.93422070
H	3	2.19979836	1	146.32050946	4	−5.19073924
H	4	2.14210646	1	139.42110351	3	−17.91805652
H	4	2.14350693	1	104.86017006	3	−59.23660313
H	3	3.41310246	1	102.16478172	4	8.15443791
O	4	2.39602362	1	120.42051283	3	71.69725972
H	14	1.98954902	4	59.82394873	1	64.64288351
C	14	1.18394938	4	32.04506233	1	65.18727150
C	3	1.47257259	1	121.65750465	4	3.49470730
C	4	1.52839365	1	112.60840306	3	−30.06459831
C	17	1.32266293	3	119.97886204	1	12.13509145

Decarboxylated intermediate, axial aldehyde (**2.17ax**)

E = −803.4544550 ZPC: 0.120767 Imag. Freq.: N/A

0 1

C						
C	1	1.32256827				
C	2	1.47292574	1	120.03548366		
C	1	1.50989041	2	121.46795096	3	1.56070117
Cl	4	2.73895901	1	147.49721810	2	−7.48728945
O	4	2.79907968	1	94.59747175	2	−86.23725381
H	1	1.07517490	2	121.02023569	3	178.35511061
H	2	1.07476327	1	121.35022871	4	−177.52577058
H	3	1.07561519	2	118.56165540	1	−167.64307103
H	3	2.10201289	2	147.23717836	1	12.62686533
H	4	1.08107677	1	110.84241484	2	−150.06744765
H	4	1.08645372	1	108.53040398	2	92.09078029
H	6	1.98937682	4	92.86255763	1	112.42638039
C	3	1.32437814	2	121.59617803	1	12.23075829
C	14	1.51267269	3	119.80637614	2	3.58740723
C	6	1.18412555	4	65.06743563	1	112.83467115

Decarboxylated intermediate, conformational transition state (**2.17ts**)

E = −803.4519290 ZPC: 0.120696 Imag. Freq.: −83.5572

0 1

C						
C	1	1.32071248				
C	2	1.46854419	1	120.35006399		
C	1	1.50445074	2	123.68666375	3	−0.61858317
Cl	4	2.77598439	1	132.53974215	2	39.53458174
O	4	2.82406058	1	123.61502214	2	−70.20078419
H	1	1.07616632	2	120.60197629	3	178.76180447
H	2	1.07468154	1	121.12330288	4	−179.86439948
H	3	1.07553649	2	118.35257958	1	−178.45953541
H	3	2.09246988	2	148.33746955	1	0.23175306
H	4	1.08339790	1	109.00089690	2	−124.10794772
H	4	1.08299218	1	108.40955208	2	120.58597296
H	6	1.98675538	4	92.56572424	1	106.59833469
C	3	1.32284747	2	122.26807624	1	0.97114815
C	14	1.50533996	3	122.48058677	2	2.22938593
C	6	1.18353122	4	64.71998653	1	105.31982249

Decarboxylated intermediate, equatorial aldehyde (**2.17eq**)

E = −803.4554987 ZPC: 0.120682 Imag. Freq.: N/A

0 1

C						
C	1	1.32339920				
C	2	1.46870543	1	119.96866877		
C	1	1.50394205	2	121.19510481	3	−3.06683483
Cl	4	2.76792489	1	104.67702972	2	67.29971377
O	4	2.79648565	1	159.21614694	2	−36.17249070
H	1	1.07531129	2	121.03021045	3	−179.46857248
H	2	1.07477454	1	121.42544119	4	176.88849690
H	3	1.07554718	2	118.51069979	1	169.69056138
H	3	2.09677726	2	147.64863329	1	−14.59045348
H	4	1.08745962	1	108.64027621	2	−91.40694037
H	4	1.08157426	1	111.51115722	2	151.69906877
H	6	1.98770486	4	92.56893746	1	78.93884130
C	3	1.32522788	2	121.72993043	1	−11.87797818
C	14	1.50265075	3	120.84215462	2	−0.17621617
C	6	1.18364397	4	64.74662182	1	77.36555011

Ammonia-catalysed dehydrohalogenation transition state **2.18am**

E = −859.5905238 ZPC: 0.152623 Imag. Freq.: −1664.6614

0 1

C						
C	1	1.36194181				
C	2	1.40786571	1	118.67216504		
C	1	1.42824569	2	121.02176834	3	−4.62261584
Cl	4	3.29412835	1	117.38308231	2	72.99217341
O	4	2.85729790	1	166.12383693	2	−45.46351001
H	1	1.07535321	2	120.31072050	3	177.86247084
H	2	1.07361141	1	121.27468964	4	177.23252662
H	3	1.07566779	2	118.80778335	1	−179.99730982
H	3	2.13018619	2	147.95178328	1	−3.24702279
H	4	1.35724921	1	103.67257798	2	−97.07662312
H	4	1.07889316	1	117.99992828	2	158.21330606
H	6	1.99886703	4	88.71823518	1	79.86844507
C	3	1.37437496	2	122.25205303	1	−0.65195083
C	14	1.39370799	3	119.43117321	2	−0.40798478
C	6	1.19679104	4	61.69969207	1	77.74242215
N	4	2.74977303	1	109.53704035	2	−100.48602602
H	17	1.00427175	4	113.05816119	1	−67.10102132
H	17	1.00433129	4	119.73952485	1	63.43290611
H	17	1.00733757	4	95.06167405	1	179.14510265

Pyridine-catalysed dehydrohalogenation transition state **2.18py**

E = −1050.1008691 ZPC: 0.203820 Imag. Freq.: −1763.6794

0 1

C						
C	1	1.35914234				
C	2	1.41311806	1	118.73222373		
C	1	1.43373073	2	120.92104924	3	−4.68725535
Cl	4	3.30311465	1	113.21379042	2	71.24425755
O	4	2.84155871	1	169.67151713	2	−34.89683252
H	1	1.07544564	2	120.46312230	3	178.54347946
H	2	1.07390148	1	121.31706330	4	177.17667612
H	3	1.07567639	2	118.77413612	1	179.40022798
H	3	2.12651011	2	147.85038598	1	−5.06675167
H	4	1.34581045	1	101.29341879	2	−93.61220691
H	4	1.07789370	1	118.01282700	2	160.42251498

H	6	1.99753654	4	89.25668029	1	65.50010885
C	3	1.36898933	2	122.18375742	1	−1.74012345
C	14	1.39936932	3	119.42711363	2	−0.23508817
C	6	1.19327114	4	62.18764310	1	63.82066021
N	4	2.75931770	1	101.27219613	2	−97.25276705
C	17	1.32516900	4	120.46967560	1	11.42173074
H	18	1.07439451	17	116.18491867	4	5.78705490
C	18	1.37820253	17	122.10325654	4	−174.19968525
H	20	1.07318268	18	120.34569783	17	−179.89432091
C	20	1.38737817	18	118.11082687	17	0.16792218
H	22	1.07474205	20	120.23284489	18	179.92445820
C	22	1.38350773	20	119.43295920	18	−0.07649394
H	24	1.07309160	22	121.48362649	20	−179.94037901
C	17	1.32526611	4	118.98936188	1	−162.74404417
H	26	1.07225762	17	115.98032423	4	−6.46071815

Ammonia-catalysed dehydrohalogenation transition state **2.20am**

E = −1047.170584 ZPC: 0.169772 Imag. Freq.: −1788.0295

0 1

C						
C	1	1.52666616				
C	1	1.53659787	2	103.76656374		
C	1	1.52063351	2	108.31393952	3	−111.05457451
H	1	1.07629713	4	113.89702403	3	−126.77443807
O	2	1.17726612	1	125.95290109	4	130.66898770
Cl	4	2.44555620	1	97.29739306	2	−70.34534381
H	3	1.07281099	1	120.97251217	4	−124.52780933
O	4	2.35550510	1	139.31255405	2	−177.57652070
H	3	2.12843851	1	136.82016276	4	58.51709747
H	4	2.10711124	1	133.49192628	2	71.29618726
H	4	2.26273081	1	116.19034381	2	7.01205749
H	9	1.99513766	4	60.37036540	1	43.56782838
H	2	3.20500016	1	90.41201287	4	−54.59342339
O	2	1.33943555	1	111.70367291	4	−51.98233065
C	3	1.31672875	1	112.59723949	4	57.69976863
C	4	1.39842154	1	113.37817889	2	48.67431487
C	9	1.18490246	4	33.24905706	1	45.47745594
C	15	1.43974891	2	113.70937956	1	−3.71318693
N	17	2.70805813	4	105.12054196	1	−100.72693443
H	20	1.00426294	17	116.27500566	4	−142.59912922

H	20	1.00914137	17	104.35231458	4	−20.22715432
H	20	1.00559293	17	106.43834002	4	94.50247026

Pyridine-catalysed dehydrohalogenation transition state **2.20py**

E = −1237.6769346 ZPC: 0.221257 Imag. Freq.: −1140.0115

0 1

C						
C	1	1.52403170				
C	1	1.53145736	2	104.51309191		
C	1	1.53268740	2	107.72348349	3	−111.93970313
H	1	1.07673702	2	109.92993694	3	123.79554954
O	2	1.18090053	1	126.23015379	3	−120.77812646
Cl	4	2.23484460	1	99.98454846	2	−71.62244275
H	3	1.07318278	1	121.22082013	2	122.78928213
O	4	2.37157105	1	135.07773914	2	174.38664942
H	3	2.12812762	1	136.76298242	2	−55.51683058
H	4	2.10858827	1	131.15945032	2	73.92457396
H	4	2.42461991	1	116.73301364	2	7.13513446
H	9	1.99086249	4	60.01460764	1	47.14005410
H	2	3.20359974	1	90.33679808	3	56.04843409
O	2	1.33620012	1	111.86875542	3	57.32226914
C	3	1.31725500	1	112.47014578	2	−55.73603464
C	4	1.41701726	1	112.46271539	2	49.53018694
C	9	1.18573003	4	32.46151304	1	48.17973763
C	15	1.44633634	2	113.50283038	1	−1.02786599
N	17	2.74110518	4	108.19780101	1	−105.37284993
C	20	1.32430189	17	117.42860430	4	−93.64265428
H	21	1.07291518	20	115.96182708	17	−0.47427904
C	21	1.37610802	20	121.02561498	17	178.93517387
H	23	1.07259767	21	120.24467344	20	−179.94973674
C	23	1.38727141	21	118.16937237	20	−0.66203247
H	25	1.07457858	23	120.04329286	21	−179.58532936
C	25	1.38513418	23	119.86685540	21	−0.04118245
H	27	1.07255745	25	121.55609240	23	−179.21261234
C	20	1.32498664	17	120.69359427	4	83.97572675
H	29	1.07204113	20	116.21294715	17	0.75073532

Dehydrohalogenated adduct (**2.21**)

E = −530.9725322 ZPC: 0.124083 Imag. Freq.: N/A

0 1

C						
C	1	1.53064139				
C	2	2.32399657	1	76.83634169		
C	1	1.52864486	2	104.02920832	3	56.92174478
C	1	1.52895375	4	108.75926539	3	54.40556210
O	2	1.18066955	1	125.92536554	4	−122.72347955
O	5	2.35739771	1	147.96682378	4	125.08267539
H	1	1.07885149	4	114.41375510	3	−176.10462645
H	3	1.07585851	2	137.51344229	1	179.84942745
H	4	1.07309821	1	121.26749430	5	−128.84208898
H	4	2.13355291	1	136.72444267	5	53.53797359
H	5	2.12539292	1	136.96900087	4	−53.02169566
H	7	1.98485328	5	59.87642113	1	6.25327556
O	2	1.33495982	1	111.36603682	4	57.47937417
C	4	1.31613814	1	112.79035997	5	53.33379623
C	5	1.32109713	1	112.50814516	4	−53.12425798
C	7	1.18922646	5	31.64760006	1	6.38037765

Decarboxylation transition state **2.22**

E = −530.9232305 ZPC: 0.120503 Imag. Freq.: −742.6251

0 1

C						
C	1	1.75402316				
C	1	2.57531885	2	74.32020169		
C	1	1.46295239	2	100.31944206	3	58.66259392
C	1	1.46837949	4	114.39321016	3	40.09854531
O	2	1.19042027	1	112.48610267	4	−120.79336648
O	5	2.35761673	1	146.00048205	4	143.30048604
H	1	1.07640561	4	115.83981495	3	179.22692443
H	3	1.07280008	1	161.80964821	4	−110.90047254
H	4	1.07396069	1	120.01121792	5	−149.23543083
H	4	2.13687651	1	140.25706324	5	47.58834246
H	5	2.12780810	1	140.34234314	4	−47.24539047
H	7	1.98756179	5	60.05329766	1	10.05812088
O	2	1.22998454	1	111.59249676	4	59.64650246
C	4	1.33892559	1	116.40699396	5	40.51616340
C	5	1.33710566	1	116.03802753	4	−40.86653298
C	7	1.18751943	5	32.09027444	1	10.29991598

Benzaldehyde (**2.19**)

E = −343.4335093 ZPC: 0.108025 Imag. Freq.: N/A

0 1

C						
C	1	1.38107477				
C	2	1.38950440	1	119.93540589		
C	1	1.39183609	2	119.89002741	3	0.00494880
O	4	2.37072515	1	95.85786550	2	180.00000000
H	1	1.07395958	2	121.09407925	3	180.00000000
H	2	1.07506418	1	120.06963327	4	−179.99618703
H	3	1.07553599	2	119.79598442	1	180.00000000
H	3	2.13817842	2	146.17197218	1	−0.00272287
H	4	2.13838124	1	145.83194555	2	−0.00887003
H	5	1.98381971	4	59.43131431	1	180.00000000
C	3	1.38492426	2	120.42041777	1	−0.00316258
C	12	1.38536720	3	119.59221720	2	0.00000000
C	5	1.19044627	4	31.01017818	1	−180.00000000

Hydrogen chloride

E = −460.0599763 ZPC: 0.006630 Imag. Freq.: N/A

0 1

H						
Cl	1	1.26622600				

Ammonia

E = −56.1843563 ZPC: 0.033806 Imag. Freq.: N/A

0 1

N						
H	1	1.00244109				
H	1	1.00244095	2	107.18211305		
H	1	1.00244095	3	107.18218232	2	−114.78820861

Ammonium

E = −56.5307714 ZPC: 0.048672 Imag. Freq.: N/A

1 1

N						
H	1	1.01344025				
H	1	1.01344025	2	109.47122063		
H	1	1.01344025	2	109.47122063	3	120.00000000
H	1	1.01344025	2	109.47122063	3	−120.00000000

Pyridine

E = −246.6958197 ZPC: 0.087184 Imag. Freq.: N/A

0 1

C						
C	1	1.38530093				
C	2	1.38375630	1	118.22553121		
C	3	1.38375738	2	118.61841867	1	−0.00422486
C	4	1.38530136	3	118.22547450	2	0.00326730
N	1	1.32088829	2	123.62240024	3	0.00000000
H	3	1.07555600	2	120.69067276	1	−179.99735118
H	1	1.07613621	6	116.10360862	5	−180.00000000
H	2	1.07443944	1	120.35522563	6	−180.00000000
H	4	1.07443902	3	121.41958738	2	−179.99527111
H	5	1.07613699	4	120.27404658	3	180.00000000

Pyridinium

E = −247.0708561 ZPC: 0.100901 Imag. Freq.: N/A

1 1

C						
C	1	1.37093070				
C	2	1.39049634	1	118.59313539		
C	3	1.39049476	2	120.32914816	1	−0.00655356
C	4	1.37093182	3	118.59303353	2	0.00514203
N	1	1.33772677	2	119.66541629	3	0.00324373
H	3	1.07418301	2	119.83532314	1	−179.99519544
H	1	1.07209870	6	116.72477530	5	−180.00000000
H	2	1.07229519	1	119.80490322	6	−180.00000000
H	4	1.07229551	3	121.60234052	2	−179.99456250
H	5	1.07209880	4	123.60976513	3	179.99669501
H	6	1.00206500	1	118.42309626	2	180.00000000

Table A.3. HF/6-31G(d) optimised geometries for the full Narasimhan Diels–Alder system.

1-Methylpyrano[3,4-*b*]indol-3(9*H*)-one (**2.1**)

E = −663.8387201 ZPC: 0.180983 Imag. Freq.: N/A

0 1

C						
C	1	1.38100215				

C	1	1.38807904	2	118.90456515		
H	1	1.07513897	2	120.57119677	3	179.51530953
H	2	1.07426861	1	120.19357238	3	−179.83933051
H	2	2.13673692	1	146.09645972	3	−0.07301054
H	3	3.14593552	1	148.30651910	2	16.00299831
H	3	3.40094432	1	99.98244782	2	−0.45774824
H	3	2.96502087	1	89.73052804	2	178.81421402
O	3	4.90515574	1	116.62734759	2	177.64088153
H	10	4.60486989	3	70.83712245	1	169.34269326
H	3	4.87323281	1	175.10410497	2	−12.93209026
H	10	4.71663850	3	69.30046118	1	−167.69367956
C	2	1.39507870	1	120.03001835	3	0.04411167
C	3	1.39539483	1	120.48549662	2	−0.73343874
C	3	1.46110801	1	132.43927119	2	177.95880494
C	14	1.38294163	2	121.79089205	1	0.50537603
N	15	1.39475286	3	111.21675924	1	−177.86834061
C	18	1.41110056	15	107.02152837	3	−4.90429382
C	16	1.33997283	3	134.14825690	1	0.87518482
C	10	1.18737194	3	23.36012999	1	−179.86442950
C	19	1.32702522	18	130.95090655	15	−178.56215993
O	22	1.35223249	19	119.03203225	18	−178.27926440
C	22	1.49213786	19	128.44267290	18	2.19885521

Diels–Alder transition state **2.23a**

E = −1313.4332826 ZPC: 0.234780 Imag. Freq.: −665.4825

0 1

C						
C	1	1.38087635				
C	1	1.38754710	2	118.70703461		
H	1	1.07495755	2	120.53767646	3	179.99664337
C	2	1.39558329	1	120.58821556	3	0.28035783
H	2	1.07436916	1	119.89473104	3	−179.70452086
C	3	1.39474733	1	119.86614897	2	−0.19245246
C	3	1.45806436	1	133.89044104	2	−178.56236683
H	5	1.07499667	2	119.29410864	1	179.96919433
C	5	1.38218925	2	121.54164254	1	−0.01076138
N	7	1.39318097	3	108.91280098	1	−179.48819764
C	11	1.35305389	7	109.41898645	3	1.54569098
C	8	1.35936574	3	135.83134932	1	−11.52882133
H	11	0.99333102	7	124.72185886	3	175.33772477

H	10	1.07497415	5	121.16779331	2	−179.92555160
H	13	1.07262294	8	123.53425456	3	3.55174222
C	13	1.46742120	8	119.31192222	3	168.25313874
C	12	1.40460011	11	130.10428706	7	−168.29321632
O	17	1.18516553	13	124.23128767	8	−158.17470280
O	17	1.34628164	13	115.67966114	8	18.52437474
C	18	1.50829904	12	121.11112309	11	−27.92425490
H	21	1.08151922	18	109.90527987	12	174.91720759
H	21	1.08493021	18	110.66304527	12	−65.79309747
H	21	1.08467269	18	110.77946608	12	55.10726047
Cl	17	3.21854391	13	93.64956587	8	111.85245966
C	13	2.76161939	8	93.47974455	3	−112.95188245
C	26	1.39720329	13	97.73586317	8	−46.58701959
C	26	1.45098142	13	84.31835004	8	73.06048988
O	28	1.20171878	26	123.02038461	13	−84.74365096
H	27	1.07577948	26	115.32851314	13	100.50159601
H	27	1.07524486	26	116.28917425	13	−120.45722001
H	28	1.09136016	26	115.74689500	13	95.08401058

Diels–Alder transition state **2.23b**

E = −1313.4369946 ZPC: 0.234591 Imag. Freq.: −539.7608

0 1

C						
C	1	1.37029543				
C	1	1.40073440	2	118.61328887		
H	1	1.07516968	2	120.78244616	3	−179.95280285
C	2	1.40701926	1	120.29329857	3	0.01046333
H	2	1.07416212	1	120.30087156	3	−179.90831459
C	3	1.40120253	1	120.40784790	2	−0.59997322
C	3	1.43039769	1	133.40309063	2	177.68414805
H	5	1.07519475	2	118.82192360	1	−179.71735434
C	5	1.37426593	2	122.12965341	1	0.55843848
N	7	1.37888397	3	110.51714560	1	−178.26321248
C	8	1.39178979	3	106.82669387	1	179.88107861
C	8	1.42122390	3	134.01314369	1	−15.85684643
H	11	0.99660647	7	118.90440491	3	−142.75195535
H	10	1.07432957	5	121.29062477	2	179.71080400
H	13	1.07553899	8	118.83298553	3	26.29418159
C	13	1.47396000	8	114.22603062	3	162.39155074
C	12	1.36637800	8	119.08985946	3	175.96280231

O	17	1.17901964	13	126.86598477	8	−149.19179460
O	18	1.33687183	12	119.31596224	8	18.48141887
C	18	1.48973926	12	127.10867526	8	−175.57268977
H	21	1.08110541	18	111.57683552	12	18.99773667
H	21	1.08247977	18	109.42131082	12	140.51359819
H	21	1.08580684	18	109.07608080	12	−101.48799904
C	13	1.87433277	8	103.37580718	3	−87.97643734
H	25	1.07622733	13	97.97239371	8	56.62066303
H	25	1.07737006	13	97.96798827	8	171.68840894
C	25	1.41809473	13	115.57933115	8	−64.48774592
Cl	28	1.75945876	25	118.63351346	13	−97.58114438
C	28	1.42672599	25	122.49804846	13	98.07367429
O	30	1.21166489	28	124.72763810	25	−15.33802299
H	30	1.09352717	28	115.02946790	25	166.09838796

Diels–Alder transition state **2.23c**

E = −1313.4297894 ZPC: 0.234622 Imag. Freq.: −710.5124

0 1

C						
C	1	1.37989512				
C	1	1.38954078	2	118.77907900		
H	1	1.07497545	2	120.56271297	3	−179.82006628
C	2	1.39695385	1	120.56525806	3	0.26688752
H	2	1.07441319	1	119.92281724	3	−179.88847166
C	3	1.39622630	1	119.84908849	2	0.07592063
C	3	1.45757439	1	133.89449096	2	−178.05746110
H	5	1.07506147	2	119.27411406	1	179.81534699
C	5	1.38112406	2	121.54795442	1	−0.22990437
N	7	1.39113449	3	109.10524293	1	179.43764233
C	11	1.36511754	7	108.79122765	3	3.47772783
C	8	1.36928582	3	135.72981904	1	−13.67442417
H	11	0.99375658	7	123.95023960	3	165.88325328
H	10	1.07508180	5	121.14809056	2	−179.80413252
H	13	1.07246510	8	123.22342588	3	5.29381669
C	13	1.46634779	8	118.42991509	3	166.04293161
C	12	1.40096433	11	130.04625008	7	−167.80080473
O	17	1.18443107	13	124.73969131	8	−153.90319110
O	17	1.34677700	13	115.03257481	8	24.08478124
C	18	1.50560402	12	122.20896864	11	−26.04384967
H	21	1.08423767	18	110.77597193	12	50.36405480

H	21	1.08153140	18	110.09559880	12	170.51224564
H	21	1.08510829	18	110.36625441	12	−70.35774442
Cl	13	3.24210428	8	79.39587341	3	−77.20991473
C	13	2.57916135	8	93.38860304	3	−106.85602240
C	26	1.39201880	13	100.27549575	8	−55.55217753
C	26	1.47174600	13	97.08377953	8	−179.57965962
O	28	1.19225162	26	123.49821080	13	95.38492315
H	27	1.07505231	26	118.35391507	13	111.39517715
H	27	1.07534860	26	114.04311711	13	−106.99813836
H	28	1.09113163	26	114.92666322	13	−84.68199975

Diels–Alder transition state **2.23d**

E = −1313.4335869 ZPC: 0.234552 Imag. Freq.: −629.4011

0 1

C						
C	1	1.37212622				
C	1	1.39895549	2	118.82950740		
H	1	1.07522413	2	120.66646539	3	−179.39073944
C	2	1.40551768	1	120.34961329	3	0.10167151
H	2	1.07422152	1	120.22560295	3	179.87304544
C	3	1.40287473	1	120.06686540	2	0.77740390
C	3	1.43750065	1	133.59631423	2	−178.17904806
H	5	1.07522188	2	118.93084869	1	179.75603601
C	5	1.37478494	2	122.01048015	1	−0.41512868
N	7	1.37230167	3	109.65940197	1	178.22390899
C	11	1.38897543	7	107.67912885	3	4.01584515
C	8	1.41321661	3	135.02101342	1	−15.37629758
H	11	0.99336682	7	123.45782862	3	161.00151570
H	10	1.07479378	5	121.21287737	2	−179.42233190
H	13	1.07455850	8	119.86557448	3	21.82694870
C	13	1.47025707	8	114.38015525	3	160.85375137
C	12	1.37518878	11	130.73385154	7	−172.95912154
O	17	1.17975837	13	127.03102297	8	−146.57384637
O	18	1.33678703	12	118.11464767	11	−166.64215707
C	18	1.49285210	12	126.01054255	11	−6.62410242
C	13	1.95582400	8	105.11702104	3	−93.16095007
H	21	1.08240272	18	110.74821776	12	38.49847475
H	21	1.08081064	18	109.74173587	12	159.90528145
H	21	1.08708202	18	109.56733057	12	−81.83871804
H	22	1.07446705	13	95.59202813	8	74.92988229

H	22	1.07657557	13	97.27837842	8	−169.58531628
C	22	1.40396634	13	114.02626908	8	−48.38378673
Cl	28	1.76129817	22	118.18122486	13	98.01830400
C	28	1.44991060	22	121.53848753	13	−106.65219372
O	30	1.19906109	28	124.21919541	22	18.49858770
H	30	1.09306111	28	114.88551099	22	−162.61756928

Diels–Alder adduct **2.24a**

E = −1313.5333771 ZPC: 0.239709 Imag. Freq.: N/A

0 1

C						
C	1	1.37405141				
C	1	1.39832442	2	118.91226388		
H	1	1.07554977	2	120.48502896	3	−179.74987695
C	2	1.40370112	1	120.99008350	3	0.07062208
H	2	1.07489752	1	119.77911309	3	179.96087081
C	3	1.40537945	1	119.26678648	2	−0.07996997
C	3	1.43926561	1	135.42629574	2	−179.89940894
H	5	1.07502929	2	119.27263451	1	179.94967457
C	5	1.37487555	2	121.30973269	1	−0.00388396
N	7	1.38057902	3	108.56761407	1	−179.88272067
C	8	1.34217093	3	107.46142129	1	179.58173533
C	8	1.50873654	3	140.05012147	1	−1.73788670
H	11	0.99296119	7	125.52141659	3	177.67886544
H	10	1.07552843	5	121.14315275	2	179.97345592
H	13	1.07854807	8	115.90979613	3	6.22998144
C	13	1.55507705	8	105.90756021	3	−119.06741841
C	13	1.52465102	8	105.25397044	3	127.68971429
C	12	1.50609944	8	115.36857472	3	179.48589757
O	18	1.17879331	13	125.77444871	8	−123.44570586
Cl	17	1.81494451	13	109.38763389	8	178.43949460
C	19	1.54048916	12	107.12994922	8	−59.44881673
O	18	1.34087669	13	112.40353135	8	55.74535787
C	19	1.51362044	12	116.26253745	8	172.12831009
C	17	1.52735126	13	109.59795482	8	65.23815905
O	25	1.18279744	17	124.20627497	13	−125.81517841
H	22	1.08040288	19	110.74914453	12	−67.10680318
H	22	1.08074002	19	108.58206726	12	173.68912957
H	24	1.08251505	19	110.02188257	12	−177.41074167
H	24	1.08359961	19	110.31643888	12	−58.02474367

H	24	1.08498991	19	110.38997659	12	62.77829203
H	25	1.09144138	17	114.06050767	13	54.90965024

Diels–Alder adduct **2.24b**

E = −1313.5269369 ZPC: 0.239793 Imag. Freq.: N/A

0 1

C						
C	1	1.37325185				
C	1	1.39884817	2	118.90876177		
H	1	1.07535941	2	120.56636237	3	−179.80592748
C	2	1.40469819	1	120.91916188	3	−0.00430507
H	2	1.07487088	1	119.85114776	3	179.93354538
C	3	1.40528061	1	119.35506807	2	0.28978179
C	3	1.43816431	1	135.17724716	2	−179.48037057
H	5	1.07513174	2	119.21507102	1	179.92409372
C	5	1.37414686	2	121.40994991	1	−0.15263093
N	7	1.37854294	3	108.70676109	1	179.51015906
C	8	1.33880093	3	107.31922336	1	179.54899529
C	8	1.50611125	3	140.15221621	1	−3.11354755
H	11	0.99288718	7	125.16069558	3	171.38427513
H	10	1.07551705	5	121.15636988	2	−179.81429036
H	13	1.07870366	8	115.56397842	3	7.76002094
C	13	1.54972757	8	107.67951948	3	−118.30398734
C	13	1.51757605	8	105.68821316	3	129.22780127
C	12	1.50546638	8	115.83896964	3	179.04379345
O	18	1.17922735	13	126.91164919	8	−125.44633011
H	17	1.07941411	13	109.44659746	8	64.94266594
H	17	1.08079261	13	110.42095009	8	−175.75423061
C	17	1.55206894	13	109.50988294	8	−54.70392718
O	18	1.34816857	13	112.07069661	8	56.26009880
C	19	1.51709619	12	114.95782467	8	169.66754352
Cl	23	1.81351569	17	110.19774912	13	−123.88596702
H	25	1.08458794	19	111.35213787	12	61.10812276
H	25	1.07964077	19	110.79351507	12	−177.46564423
H	25	1.08312617	19	108.60559121	12	−58.57087621
C	23	1.53062738	17	112.95279375	13	120.56727640
O	30	1.18266980	23	123.99758460	17	−9.05606557
H	30	1.09028676	23	114.68087102	17	170.18885578

Diels–Alder adduct **2.24c**

E = −1313.5312346 ZPC: 0.239670 Imag. Freq.: N/A

0 1

C						
C	1	1.37409792				
C	1	1.39801562	2	118.91988600		
H	1	1.07528844	2	120.54083672	3	−179.99323424
C	2	1.40371983	1	120.98622182	3	−0.02238389
H	2	1.07494684	1	119.78434305	3	179.96179757
C	3	1.40533279	1	119.27531996	2	0.24116282
C	3	1.43856381	1	135.40154701	2	−179.67815308
H	5	1.07512133	2	119.27839203	1	179.91603279
C	5	1.37492192	2	121.30596231	1	−0.13592933
N	7	1.38070726	3	108.60698597	1	179.58383593
C	8	1.34024306	3	107.49205958	1	179.77396932
C	8	1.50511104	3	139.92500430	1	−1.26357936
H	11	0.99289026	7	125.44560746	3	174.61542305
H	10	1.07562422	5	121.14246279	2	−179.88462248
H	13	1.07903064	8	115.64182270	3	6.83057954
C	13	1.55896716	8	108.41759595	3	−120.15199742
C	13	1.52866003	8	105.32761211	3	128.04183331
C	12	1.50424777	8	115.29932507	3	178.93759527
O	18	1.18016918	13	125.33793777	8	−125.47418661
Cl	17	1.80762147	13	109.05000463	8	67.21560527
C	19	1.54355926	12	107.15468090	8	−58.78767833
O	18	1.33703082	13	112.57744716	8	55.48535510
C	19	1.51350425	12	116.41899805	8	172.85832441
C	17	1.53079041	13	109.89384679	8	−179.45867074
O	25	1.18292134	17	124.05912999	13	117.01387070
H	22	1.08009738	19	109.99573609	12	−65.25333968
H	22	1.08118109	19	109.03521683	12	175.68675405
H	24	1.08503397	19	110.35838618	12	62.90189079
H	24	1.08242620	19	110.04252534	12	−177.23973630
H	24	1.08364461	19	110.31421537	12	−57.79638554
H	25	1.09078330	17	114.13371178	13	−62.45327486

Diels–Alder adduct **2.24d**

E = −1313.5282178 ZPC: 0.239858 Imag. Freq.: N/A

0 1

C

C	1	1.37335827				
C	1	1.39902471	2	118.94434662		
H	1	1.07545461	2	120.54008748	3	−179.89196995
C	2	1.40473762	1	120.92809884	3	0.09318876
H	2	1.07492576	1	119.84177071	3	180.00000000
C	3	1.40589333	1	119.30441285	2	−0.17003164
C	3	1.43798264	1	135.24473431	2	179.85722273
H	5	1.07515639	2	119.22738776	1	179.96946234
C	5	1.37414456	2	121.38532849	1	0.04524576
N	7	1.37732558	3	108.62845922	1	−179.67123008
C	8	1.33923743	3	107.29851674	1	179.84198987
C	8	1.50593778	3	140.14015567	1	−2.39440709
H	11	0.99260014	7	125.59298374	3	−178.07379637
H	10	1.07556322	5	121.14993504	2	179.90408404
H	13	1.07874937	8	115.53586195	3	6.57907104
C	13	1.55166689	8	107.67106588	3	−119.34894430
C	13	1.51666019	8	105.54607117	3	127.95545863
C	12	1.50226008	8	115.87443293	3	−179.92717926
O	18	1.17813808	13	127.25290250	8	−124.46336436
H	17	1.07909133	13	109.06116872	8	63.06921744
H	17	1.08065999	13	110.57391066	8	−177.68511103
C	17	1.55088046	13	109.60284078	8	−57.62573136
O	18	1.35160890	13	111.81540904	8	56.84007893
C	19	1.51824239	12	115.16662960	8	168.79840766
Cl	23	1.80916980	17	111.44308062	13	122.60939684
H	25	1.08248748	19	111.20859681	12	66.28898569
H	25	1.08159533	19	111.02057711	12	−172.05164197

Decarboxylation transition state **2.25a**

E = −1313.4732013 ZPC: 0.236371 Imag. Freq.: −202.4635

0 1

C						
C	1	1.36391003				
C	1	1.40887937	2	118.53249043		
H	1	1.07435148	2	121.09864559	3	179.92328159
H	2	1.07390435	1	120.37469233	3	−179.81082527
H	2	2.14848775	1	146.54262624	3	0.31457905
H	3	3.18548763	1	149.10653966	2	4.01335176
H	2	3.41790835	1	101.04962840	3	0.88988312
H	3	2.91483190	1	88.73873897	2	179.92578635

O	3	4.00579015	1	94.72578994	2	−142.88844447
Cl	10	3.68677558	3	87.81868269	1	−117.15036257
O	3	4.46382902	1	122.08435998	2	129.95711357
H	12	2.35396407	3	85.03376097	1	150.31951667
H	12	3.73394165	3	76.01395827	1	130.94107054
H	12	4.69466293	3	73.12385296	1	170.09882198
H	10	4.82941655	3	71.92763819	1	171.37916677
H	3	4.62736611	1	163.56524494	2	−74.13199881
H	12	1.98835007	3	71.91479391	1	35.43572421
C	2	1.41544300	1	120.47460079	3	0.37430102
C	3	1.40572034	1	120.15308032	2	−2.26732319
C	3	1.41923385	1	133.39036176	2	177.70056625
C	19	1.36832070	2	122.41987920	1	0.68100851
N	20	1.36103793	3	109.41520903	1	−176.12917490
C	21	1.38442074	3	107.14385110	1	179.56570452
C	21	1.47612390	3	132.71415685	1	15.95277732
C	25	1.53774454	21	107.78704593	3	−151.87768324
C	10	1.20287356	3	54.10653803	1	−168.24442913
C	24	1.38614007	21	117.92052870	3	−164.19339728
C	28	1.50176970	24	118.34238985	21	−40.25594750
O	27	1.23930764	10	132.83695583	3	−127.47954595
C	28	1.49029970	24	123.36187480	21	151.77098848
C	12	1.18506011	3	61.84023613	1	63.75406605

Decarboxylation transition state **2.25b**

E = −1313.4576099 ZPC: 0.236161 Imag. Freq.: −125.0707

0 1

C						
C	1	1.36407334				
C	1	1.40880673	2	118.49791974		
H	1	1.07408357	2	121.24296348	3	179.81400468
H	2	1.07373305	1	120.48493320	3	−179.75309696
H	2	2.14728095	1	146.41436520	3	0.45668355
H	3	3.18176371	1	149.14014287	2	4.67929168
H	2	3.41982188	1	100.98205380	3	1.04312255
H	3	2.89640984	1	88.35401495	2	−179.38023299
O	3	3.94404509	1	93.44470716	2	−141.57023534
H	3	4.01423348	1	115.90251987	2	154.00636662
H	10	3.38149162	3	79.45671756	1	−123.82915726
Cl	10	4.78642606	3	83.53047995	1	−156.21381271

H	3	5.51442752	1	170.71985992	2	−153.21386707
H	10	4.82228711	3	70.77778233	1	170.06930094
H	3	4.58902401	1	164.30510244	2	−69.51143050
O	3	4.98160954	1	133.71203437	2	129.55378643
H	17	1.98373416	3	104.23228503	1	163.77246044
C	2	1.41483877	1	120.31116773	3	0.48527594
C	3	1.40540863	1	120.32093066	2	−2.37859656
C	3	1.41708584	1	132.85218323	2	177.95299839
C	19	1.36975551	2	122.60730213	1	0.67581007
N	20	1.36234630	3	109.63900059	1	−175.80977291
C	23	1.40171417	20	107.69664748	3	−6.22740906
C	21	1.45617316	3	132.79803987	1	17.11273624
C	25	1.52876416	21	110.59685330	3	−154.67080784
C	10	1.20555966	3	55.41487466	1	−168.39655813
C	24	1.36922605	23	128.84605132	20	164.93687328
C	28	1.52195752	24	115.72918226	23	161.19792029
O	27	1.23237096	10	133.51240355	3	−129.65054736
C	28	1.49205158	24	122.62923480	23	−7.01891778
C	17	1.18120565	3	82.61964214	1	145.98677180

Decarboxylated 3,3-substituted intermediate, axial aldehyde (**2.26a**)

E = −1125.9144658 ZPC: 0.222317 Imag. Freq.: N/A

0 1

C						
C	1	1.38565061				
C	2	1.39048204	1	119.96643090		
C	1	1.38350007	2	119.08726474	3	−0.20611075
H	4	3.16685232	1	148.17289668	2	−13.21736241
Cl	4	5.23707253	1	110.78212454	2	−173.38961666
O	4	5.21054102	1	131.16337067	2	145.97673169
H	1	1.07552881	4	120.58893442	2	179.31652844
H	2	1.07445160	1	120.12226983	4	179.65848383
H	3	1.07549565	2	119.33830167	1	179.91683784
H	3	2.14735428	2	147.04959404	1	−0.90715138
H	7	2.50549253	4	76.64799030	1	130.79752742
H	7	3.81648161	4	58.35886057	1	118.51669169
H	4	2.90724383	1	88.81882336	2	176.68690573
H	7	4.77064342	4	66.21579198	1	159.82948023
H	7	3.64076477	4	75.27965446	1	176.90387634
H	7	4.78717205	4	57.59679596	1	−178.16817055

H	7	1.98945829	4	66.83739389	1	13.27920873
C	3	1.38658495	2	121.61902053	1	−0.33014885
C	19	1.38366700	3	117.84244752	2	0.37432813
N	20	1.39356179	19	127.97781281	3	−178.39284674
C	4	1.46812960	1	132.58999573	2	−179.35891719
C	21	1.40815307	20	108.73777293	19	−174.38865995
C	23	1.32293596	21	130.34853871	20	170.17702083
C	24	1.51862437	23	117.69660054	21	−175.39676283
C	25	1.52943028	24	113.64791558	23	−29.13287265
C	22	1.32608680	4	132.52897452	1	−5.86940406
C	24	1.50206518	23	125.38120556	21	−0.03708489
C	7	1.18445800	4	51.41884563	1	40.48114588

Decarboxylated 3,3-substituted intermediate, equatorial aldehyde (**2.26a'**)

E = −1125.9150436 ZPC: 0.221936 Imag. Freq.: N/A

0 1

C						
C	1	1.38485523				
C	2	1.39117816	1	119.96104984		
C	1	1.38424803	2	119.11245684	3	0.22645801
H	4	3.16684460	1	148.44548324	2	−13.58424861
Cl	4	4.75050479	1	119.05312734	2	−146.96497962
O	4	5.81558266	1	115.92834735	2	169.86885600
H	1	1.07549574	4	120.58333548	2	179.63597025
H	2	1.07443542	1	120.14190867	4	−179.98705841
H	3	1.07549821	2	119.31659392	1	179.73867952
H	3	2.14689938	2	147.06655897	1	−1.18285088
H	7	2.45100001	4	49.42331066	1	−159.19320544
H	7	2.96880678	4	63.71427051	1	161.07580634
H	4	2.89063243	1	88.31403853	2	−173.35625060
H	4	5.48067687	1	169.65502909	2	−130.29424144
H	7	5.09950845	4	60.44177795	1	−169.56116319
H	4	4.80959351	1	171.79813041	2	28.15394815
H	7	1.98739609	4	64.49240115	1	45.66972349
C	3	1.38588277	2	121.63731372	1	−0.59374524
C	19	1.38429878	3	117.84327828	2	0.25832838
N	20	1.39149686	19	128.00932235	3	−177.99039310
C	4	1.46722382	1	132.51381634	2	−176.71117251
C	21	1.40888037	20	108.86072269	19	−177.75151895
C	23	1.32368672	21	129.87729318	20	−177.75622096

C	24	1.51166208	23	117.74314031	21	172.11455447
C	25	1.52608701	24	115.47189284	23	25.47288276
C	22	1.32795093	4	132.20212990	1	5.36696323
C	24	1.50235259	23	124.98227826	21	−1.90706963
C	7	1.18390323	4	42.34833136	1	67.19150080

Decarboxylated 4,4-substituted intermediate, axial aldehyde (**2.26b**)

E = −1125.911901 ZPC: 0.222280 Imag. Freq.: N/A

0 1

C						
C	1	1.38950912				
C	2	1.38686458	1	120.13258000		
C	1	1.38009297	2	119.09047034	3	0.14589471
H	4	3.19522588	1	148.44196127	2	9.33495958
Cl	4	5.95479483	1	145.34144040	2	−179.25954739
O	4	4.94096198	1	120.44879061	2	142.94153369
H	1	1.07550922	4	120.64140143	2	−179.38231600
H	2	1.07457828	1	119.95889323	4	−179.67208707
H	3	1.07540237	2	119.49578622	1	−179.89214164
H	3	2.15026835	2	146.83503915	1	0.59336225
H	7	2.50257625	4	68.89618985	1	90.09142618
H	7	3.80968938	4	57.49577046	1	110.77134746
H	4	2.90979551	1	89.83033817	2	−175.61423622
H	4	4.76855154	1	169.56420893	2	30.35353121
H	7	5.10661652	4	66.15241732	1	171.24214572
H	7	4.19125377	4	74.38662825	1	−171.17529712
H	7	1.98572745	4	92.82786457	1	−160.61844711
C	3	1.38997343	2	121.42679467	1	0.21250330
C	19	1.37977018	3	117.70215790	2	−0.30662508
N	20	1.39562305	19	128.32118420	3	178.76687129
C	4	1.47079439	1	133.01040690	2	179.91796027
C	21	1.39147113	20	110.08739548	19	174.98622641
C	23	1.33251801	21	129.20222656	20	−170.73612585
C	24	1.52514506	23	115.53396262	21	174.32636099
C	25	1.53169256	24	114.33436514	23	30.79592612
C	22	1.32130823	4	133.61878733	1	6.98111020
C	24	1.50816369	23	123.91992254	21	−0.34783071
C	7	1.18524083	4	76.08298378	1	176.78309233

Decarboxylated 4,4-substituted intermediate, equatorial aldehyde (**2.26b'**)

E = −1125.9146002 ZPC: 0.222236 Imag. Freq.: N/A

0 1

C						
C	1	1.38902342				
C	2	1.38734715	1	120.16040106		
C	1	1.38054078	2	119.06632381	3	−0.18873557
H	4	3.19297185	1	148.49236262	2	−9.43975665
Cl	4	5.00764277	1	132.68976155	2	−141.60885175
O	4	6.23338038	1	139.84415681	2	166.08278622
H	1	1.07552182	4	120.66995245	2	179.42819786
H	2	1.07458351	1	119.95388265	4	179.66263845
H	3	1.07537447	2	119.48893149	1	179.90804668
H	3	2.15000566	2	146.82825464	1	−0.64505825
H	7	2.41050014	4	29.64622330	1	−19.81985469
H	7	2.95486308	4	45.67889551	1	35.42835330
H	4	2.91307704	1	89.89919172	2	176.70031438
H	4	4.76821961	1	169.95795333	2	−25.57039965
H	7	4.12959194	4	59.55987511	1	155.43317410
H	7	3.43404412	4	62.60409458	1	−176.48196112
H	7	1.98341984	4	84.88446483	1	137.88624433
C	3	1.38952607	2	121.42247278	1	−0.24328013
C	19	1.37996264	3	117.67253376	2	0.33858341
N	20	1.39580875	19	128.33715671	3	−178.78941479
C	4	1.47015880	1	133.08896645	2	−179.89644145
C	21	1.38861942	20	110.10643087	19	−175.46544252
C	23	1.33433596	21	129.07108987	20	170.63095745
C	24	1.50726054	23	116.63763512	21	−175.55514032
C	25	1.52788648	24	114.50049016	23	−26.43440623
C	22	1.32236978	4	133.73179774	1	−5.51503653
C	24	1.50881838	23	123.92706723	21	−2.13186355
C	7	1.18479151	4	57.86439542	1	130.21875380

3-Substituted product, conformation **2.4a**

E = −665.9027428 ZPC: 0.209566 Imag. Freq.: N/A

0 1

C						
C	1	1.37937149				
C	1	1.39161419	2	119.07049521		
H	1	1.07566009	2	120.31064849	3	−180.00000000

H	2	1.07483402	1	119.92569381	3	180.00000000
C	2	1.39797875	1	120.58263698	3	0.00000000
C	3	1.39870649	1	119.49539661	2	0.00000000
C	3	1.45424740	1	134.13287645	2	−180.00000000
H	6	1.07531274	2	119.33057821	1	180.00000000
C	6	1.37973319	2	121.38547731	1	0.00000000
N	7	1.38077829	3	108.69717871	1	179.99546705
C	11	1.37149132	7	109.57242209	3	0.00865103
C	8	1.38859853	3	134.16143556	1	0.00000000
H	11	0.99247715	7	125.06280537	3	179.94899642
H	10	1.07547040	6	121.09560757	2	−180.00000000
H	13	1.07663300	8	120.71475237	3	0.00000000
C	12	1.40174840	11	128.28346337	7	179.99463561
C	13	1.38155260	8	118.98104774	3	180.00000000
C	17	1.37411445	12	116.07667173	11	179.99566273
C	17	1.50816870	12	121.09064239	11	−0.00348554
C	18	1.47564195	13	119.65772615	8	−180.00000000
O	21	1.19250813	18	125.03238934	13	180.00000000
H	19	1.07442480	17	120.02264253	12	180.00000000
H	20	1.08263945	17	110.86307156	12	180.00000000
H	20	1.08732489	17	111.42052979	12	60.11072129
H	20	1.08732826	17	111.42142161	12	−60.11571439
H	21	1.09545211	18	114.78188609	13	0.00000000

3-Substituted product, conformation **2.4b**

E = −665.9022448 ZPC: 0.209446 Imag. Freq.: N/A

0 1

C						
C	1	1.37987583				
C	1	1.39092789	2	119.02426187		
H	1	1.07547452	2	120.40851429	3	180.00000000
H	2	1.07479497	1	119.92496786	3	−180.00000000
H	2	2.14038125	1	146.54726191	3	0.00000000
H	3	3.21373265	1	149.15717283	2	0.01364468
H	2	3.40074150	1	100.40980921	3	0.00000000
H	3	2.96449773	1	90.54378914	2	179.99579564
O	3	5.40915430	1	102.23017309	2	179.99545339
H	10	3.85828496	3	66.72339235	1	180.00000000
H	3	5.71684606	1	169.40094950	2	−179.91018598
H	3	4.97820747	1	169.33992273	2	72.53573648

H	3	4.97665628	1	169.34834048	2	−72.34635692
H	10	1.98325086	3	96.56438099	1	180.00000000
C	2	1.39745527	1	120.56820774	3	0.00000000
C	3	1.39819886	1	119.56672997	2	0.00000000
C	3	1.45539462	1	133.97451214	2	179.99686824
C	16	1.38027474	2	121.41766157	1	0.00000000
N	17	1.38184993	3	108.73642899	1	−179.99658867
C	20	1.37179197	17	109.60815006	3	−0.00534806
C	18	1.38363227	3	133.92720930	1	−0.00262409
C	21	1.39681812	20	128.38430132	17	−179.99723126
C	22	1.38597143	18	118.70550274	3	−180.00000000
C	23	1.37888613	21	115.78665583	20	180.00000000
C	23	1.50828815	21	121.30662406	20	0.00596347
C	10	1.19256444	3	68.02149703	1	180.00000000

2-Substituted product, conformation **2.3a**

E = −665.8939596 ZPC: 0.209241 Imag. Freq.: N/A

0 1

C						
C	1	1.37749713				
C	1	1.39340829	2	119.07252365		
H	1	1.07554114	2	120.39978099	3	179.99133382
H	2	1.07473414	1	120.04280523	3	−179.99528198
C	2	1.40017379	1	120.45912624	3	0.00000000
C	3	1.39950741	1	119.65426072	2	−0.01776347
C	3	1.45087560	1	133.85545673	2	179.96235104
H	6	1.07543839	2	119.21819136	1	−179.99588202
C	6	1.37804882	2	121.57365024	1	0.00952568
N	7	1.37477109	3	108.86352924	1	−179.95743172
C	11	1.38239131	7	109.28911920	3	−0.08872860
C	8	1.39457992	3	133.85927392	1	0.00574168
H	11	0.99176661	7	124.95887216	3	−179.47790176
H	10	1.07543693	6	121.10661390	2	179.98697292
H	13	1.07504174	8	120.90953717	3	0.01801190
C	12	1.39577245	11	128.04109969	7	−179.96280997
C	13	1.37044422	8	118.46845795	3	−179.96583642
H	18	1.07252192	13	120.67428437	8	179.97586054
C	17	1.39339264	12	115.96021511	11	−179.98912179
C	17	1.51358053	12	117.80371403	11	0.02481684
H	21	1.07824803	17	113.92490155	12	−179.22580801

H	21	1.08687950	17	110.36761922	12	60.10303168
H	21	1.08679931	17	110.31594679	12	−58.65344002
C	20	1.48659969	17	122.37136462	12	−179.91321474
O	25	1.19262414	20	123.87146889	17	−179.91560038
H	25	1.08884069	20	117.00239930	17	0.11756290

2-Substituted product, conformation **2.3b**

E = −665.8957975 ZPC: 0.209446 Imag. Freq.: N/A

0 1

C						
C	1	1.37739756				
C	1	1.39326285	2	119.06217310		
H	1	1.07560872	2	120.38301189	3	180.00000000
C	2	1.40033250	1	120.39336773	3	0.00000000
H	2	1.07470176	1	120.08231503	3	−180.00000000
C	3	1.39849338	1	119.75246153	2	0.00000000
C	3	1.45065650	1	133.80164057	2	179.99397208
H	5	1.07545714	2	119.19366689	1	−180.00000000
C	5	1.37790543	2	121.62619678	1	0.00000000
N	7	1.37295565	3	108.98994638	1	−179.99376739
C	11	1.38394685	7	109.61269865	3	−0.01508206
C	8	1.38875986	3	133.26910335	1	0.00000000
H	11	0.99113641	7	124.67407334	3	−179.91022660
H	10	1.07535498	5	121.11819357	2	180.00000000
H	13	1.07483252	8	121.08765292	3	0.00577355
C	12	1.39187034	11	128.79058069	7	−179.99201284
C	13	1.37467707	8	118.07180758	3	−179.99459150
H	18	1.07581292	13	119.50259221	8	180.00000000
C	17	1.39937057	12	115.67407407	11	−179.99525393
C	17	1.51192854	12	121.11101260	11	0.00000000
H	21	1.08195134	17	111.24138794	12	−120.54391913
H	21	1.08196073	17	111.24291991	12	120.47233146
H	21	1.08314235	17	111.22397628	12	−0.03844371
C	20	1.48188664	17	122.72705959	12	−179.99621375
O	25	1.19248564	20	126.62826670	17	0.00629136
H	25	1.09458197	20	113.75797899	17	−179.99466627

A.2 Ring-opening reaction of protonated oxirane and methylpropene

Table A.4. MP2(Full)/6-31G(d) optimised geometries for the reaction of protonated oxirane and methylpropene.

Protonated oxirane (**3.4**)

E = −153.6164971 ZPC: 0.069405 Imag. Freq.: N/A

1 1

C						
C	1	1.45823000				
O	2	1.52522583	1	61.44278067		
H	1	1.08466432	2	120.04218011	3	−101.41986274
H	1	1.08321277	2	120.11392045	3	96.11624105
H	2	1.08466431	1	120.04217518	3	101.41989635
H	2	1.08321358	1	120.11395628	3	−96.11633299

Methylpropene (**3.5**)

E = −156.646397 ZPC: 0.106767 Imag. Freq.: N/A

0 1

C						
C	1	1.33928000				
H	1	1.08569748	2	121.65950898		
H	1	1.08569611	2	121.65957732	3	−180.00000000
C	2	1.50239114	1	122.10322030	4	0.00000000
C	2	1.50239061	1	122.10327356	5	−180.00000000
H	5	1.09577601	2	110.78365917	1	120.77530431
H	5	1.09577439	2	110.78419921	1	−120.79232049
H	5	1.09263307	2	111.59577202	1	−0.00822913
H	6	1.09577588	2	110.78366930	1	120.77561459
H	6	1.09263307	2	111.59580435	1	−0.00789075
H	6	1.09577456	2	110.78420249	1	−120.79200575

Prereaction complex **3.6**

E = −310.2783001 ZPC: 0.176704 Imag. Freq.: N/A

1 1

C						
C	1	1.44933087				
O	2	1.51944797	1	64.78401015		

H	1	1.08233463	2	120.56967958	3	−97.66364158
H	1	1.08095332	2	120.24988229	3	92.42177456
H	2	1.08496632	1	119.91502501	3	103.37907868
H	2	1.08337002	1	119.91975256	3	−98.10174351
H	3	0.98828775	2	110.89717830	1	101.76632832
H	1	3.12577875	2	88.10530769	3	−158.52551814
C	1	2.80824800	2	91.46469307	3	−178.46070353
H	10	1.08730728	1	99.23396126	2	−38.11924287
C	10	1.34771921	1	81.61159117	2	−158.64285612
C	12	1.50227290	10	121.94793411	1	93.04768864
C	12	1.50230919	10	121.92793053	1	−89.67455777
H	13	1.09480593	12	109.86878683	10	115.69420130
H	13	1.09660966	12	111.53904507	10	−126.86516787
H	13	1.09269420	12	112.11079757	10	−4.31308568
H	14	1.09640960	12	111.42581790	10	125.64715957
H	14	1.09306621	12	112.08968998	10	3.13482969
H	14	1.09475362	12	109.97216879	10	−116.79087019

Transition state **3.7**

E = −310.2870224 ZPC: 0.176252 Imag. Freq.: −247.8222

1 1

C

C	1	1.44976869				
O	2	1.50029885	1	69.40166925		
H	1	1.08172437	2	120.76492210	3	−92.01369416
H	1	1.08038858	2	120.03307228	3	86.70496506
H	2	1.08575546	1	119.49297008	3	106.18154840
H	2	1.08402756	1	119.38616192	3	−100.90648932
H	3	0.98690984	2	110.31754616	1	100.84997065
H	1	2.93067525	2	90.96526311	3	−156.99046656
C	1	2.59934075	2	94.68375042	3	−178.32278254
H	10	1.08729816	1	99.44667752	2	−37.95602290
C	10	1.35184179	1	82.93451503	2	−158.43894159
C	12	1.50084661	10	121.86424062	1	93.09317135
C	12	1.50073794	10	121.84263210	1	−89.17607491
H	13	1.09488135	12	109.63556229	10	115.55467824
H	13	1.09634579	12	111.46984288	10	−127.14587133
H	13	1.09251447	12	112.21078038	10	−4.42331091
H	14	1.09624297	12	111.31598063	10	125.20203117
H	14	1.09290039	12	112.19347300	10	2.57350747

H	14	1.09480561	12	109.79841892	10	−117.36492048

Carbocationic product **3.8**

E = −310.3326020 ZPC: 0.178441 Imag. Freq.: N/A

1 1

C						
C	1	1.52520237				
H	1	1.09107477	2	112.73479763		
H	1	1.10133676	2	105.95770839	3	115.59409727
C	1	1.60945724	2	109.54058251	4	124.93791023
H	2	1.09795257	1	109.26693554	5	−63.23428687
H	2	1.09971474	1	109.97811298	5	55.46420778
H	5	1.08805951	1	109.70365585	2	110.28190820
H	5	1.08944171	1	110.21612928	2	−14.98160907
O	2	1.41004815	1	103.88276217	5	175.89044716
C	5	1.42519772	1	88.45011505	2	−131.88510553
H	10	0.97364607	2	109.29294008	1	169.51580746
C	11	1.47748116	5	120.36753913	1	93.53956044
C	11	1.47614542	5	120.40693074	1	−89.01654926
H	13	1.10208362	11	104.96704538	5	98.80639231
H	13	1.09140865	11	112.77971282	5	−144.93233169
H	13	1.09067033	11	112.93247263	5	−17.86344040
H	14	1.09195347	11	112.51434295	5	141.58670141
H	14	1.09041668	11	113.05867287	5	14.63618574
H	14	1.10220511	11	105.16874308	5	−102.52583617

Product bond-rotation transition state **3.9**

E = −310.3324811 ZPC: 0.178083 Imag. Freq.: −32.4873

1 1

C						
C	1	1.52867524				
H	1	1.09059564	2	110.68084421		
H	1	1.09683478	2	106.92526996	3	117.03335020
C	1	1.60256062	2	108.50112783	4	123.76392469
H	2	1.09826142	1	109.48810418	5	−58.74728976
H	2	1.09868585	1	109.96173306	5	60.34097405
H	5	1.08962277	1	108.52493655	2	91.34695517
H	5	1.09049211	1	109.86229724	2	−32.42617820
O	2	1.41048894	1	103.55154983	5	−179.32876426
C	5	1.42945590	1	93.04636030	2	−150.11835010

H	10	0.97371756	2	109.15712253	1	174.17864858
C	11	1.47271619	5	120.25357167	1	94.82724844
C	11	1.47146185	5	120.60136765	1	−85.29849406
H	13	1.10367807	11	104.61634310	5	97.07022459
H	13	1.09137893	11	113.08243275	5	−146.78910148
H	13	1.09081040	11	112.93606045	5	−19.02213991
H	14	1.09403135	11	111.66016858	5	132.51722377
H	14	1.08941001	11	113.42118333	5	5.97420618
H	14	1.10248627	11	105.86230025	5	−112.75011620

Product conformational isomer **3.10**

E = −310.3326058 ZPC: 0.177805 Imag. Freq.: N/A

1 1

C						
C	1	1.52904880				
H	1	1.09161898	2	108.85575125		
H	1	1.09339514	2	108.07690605	3	117.89121331
C	1	1.59046535	2	108.56184650	4	121.87860533
H	2	1.09832079	1	109.84104145	5	−58.20279087
H	2	1.09818563	1	110.00825814	5	61.18008180
H	5	1.09147906	1	108.02648867	2	69.93200081
H	5	1.09167978	1	108.98359787	2	−52.38429308
O	2	1.41184140	1	103.44318851	5	−178.53723359
C	5	1.43677316	1	98.30940356	2	−171.29747971
H	10	0.97359799	2	109.04698064	1	179.32261020
C	11	1.46735260	5	120.12524930	1	94.52030512
C	11	1.46789382	5	120.75469725	1	−83.97583481
H	13	1.10556691	11	104.21398469	5	92.64042406
H	13	1.09116677	11	113.48165129	5	−151.08349388
H	13	1.09140270	11	112.85959034	5	−22.54282926
H	14	1.09763365	11	109.86500910	5	121.57466452
H	14	1.08881887	11	113.68061926	5	−3.12488250
H	14	1.10080579	11	107.52221239	5	−124.72644422

Table A.5. Reaction of protonated oxirane and methylpropene at HF/6-31G(d)//HF/6-31G(d).

Protonated oxirane (**3.11**)

E = −153.1771010 ZPC: 0.069327 Imag. Freq.: N/A

1 1

C						
C	1	1.44657603				
O	2	1.49816325	1	61.13379415		
H	1	1.07313770	2	119.85781298	3	−101.00935998
H	1	1.07171211	2	120.46417011	3	96.33311655
H	2	1.07313860	1	119.85817343	3	101.01043799
H	2	1.07171189	1	120.46418540	3	−96.33362669
H	3	0.96088175	2	115.93151323	1	105.54869203

Methylpropene (**3.12**)

E = −156.1106669 ZPC: 0.105662 Imag. Freq.: N/A

0 1

C						
C	1	1.32098701				
C	2	1.50805229	1	122.25423141		
H	1	1.07617541	2	121.77579457	3	−179.98843659
H	1	1.07617491	2	121.77557103	3	0.01101244
H	3	1.08758538	2	110.76909139	1	120.71951922
H	3	1.08757683	2	110.77184526	1	−120.83577922
H	3	1.08351019	2	111.76483070	1	−0.05642780
H	2	2.14945656	1	132.42367445	3	−146.58080507
H	2	2.15869693	1	94.46752027	3	179.96931471
H	2	2.14953744	1	132.46612528	3	146.57381148
C	2	1.50806496	1	122.25219476	3	179.98966387

Prereaction complex **3.13**

E = −309.2975497 ZPC: 0.175651 Imag. Freq.: N/A

1 1

C						
C	1	1.44163707				
O	2	1.49470443	1	62.55596411		
H	1	1.07103317	2	120.05410204	3	−99.73710426
H	1	1.06968502	2	120.48930809	3	95.05508115
H	2	1.07303551	1	119.83452124	3	101.82352275
H	2	1.07150881	1	120.41362589	3	−97.24071902
H	3	0.95965801	2	115.32884673	1	105.41915452
H	1	3.37737944	2	86.54216712	3	−163.55665343
C	1	3.13717445	2	94.53054008	3	179.66752176
H	10	1.07736032	1	92.12399500	2	−52.04010947
C	10	1.32785364	1	90.23297429	2	−173.58490298

C	12	1.50860217	10	122.19599923	1	90.45962505
C	12	1.50860246	10	122.18496410	1	−91.97421347
H	13	1.08575423	12	110.04671720	10	116.98859617
H	13	1.08747620	12	111.21845160	10	−125.21329668
H	13	1.08337269	12	112.10175401	10	−3.18135558
H	14	1.08747001	12	111.20269582	10	125.04118509
H	14	1.08348026	12	112.10017816	10	3.00020936
H	14	1.08574236	12	110.06027752	10	−117.15311732

Transition state **3.14**

E = −309.2943227 ZPC: 0.174949 Imag. Freq.: −392.9589

1 1

C						
C	1	1.44916347				
O	2	1.44583497	1	74.01353540		
H	1	1.06957013	2	120.19644684	3	−88.50244424
H	1	1.06867745	2	119.87828737	3	83.17219502
H	2	1.07494600	1	118.33525300	3	108.87611363
H	2	1.07308667	1	118.72786009	3	−104.62964553
H	3	0.95625344	2	113.47341709	1	105.94877219
H	1	2.96817382	2	88.98319174	3	−162.63779175
H	1	2.96204778	2	85.69316253	3	161.43630722
H	1	4.68429248	2	131.34243200	3	151.73647727
H	1	3.62214937	2	144.44931306	3	130.35986764
H	1	3.71226538	2	116.79333014	3	134.73671707
H	1	3.62305132	2	151.52253941	3	−144.42870924
H	1	3.72688050	2	123.82201863	3	−141.20077908
H	1	4.68869841	2	135.51304052	3	−162.79024584
C	1	2.67163375	2	98.55834049	3	178.39377068
C	17	1.33568253	1	89.06818639	2	−174.64554516
C	18	1.50711724	17	122.07907303	1	91.02951569
C	18	1.50712689	17	122.08099823	1	−91.38006334

Carbocationic product **3.15**

E = −309.3628031 ZPC: 0.176464 Imag. Freq.: N/A

1 1

C						
C	1	1.52711638				
H	1	1.08319819	2	108.44008110		
H	1	1.08321657	2	108.43839134	3	116.94004717

O	2	1.39035795	1	105.21405267	3	−58.45537055
H	2	1.08722287	1	110.01930634	5	120.51287975
H	2	1.08720676	1	110.02174852	5	−120.50682970
H	5	0.94835011	2	110.84954319	1	−179.98191720
H	1	2.18102750	2	95.43509864	5	−155.78844493
C	1	1.56870244	2	110.57982742	5	−179.99029172
H	10	1.08304145	1	109.33946939	2	−60.44425073
C	10	1.46748796	1	105.50662413	2	−179.99722879
C	12	1.47503242	10	119.99544070	1	91.29869004
C	12	1.47493905	10	120.08270740	1	−90.45974196
H	13	1.09489160	12	104.57566081	10	92.63430166
H	13	1.08103880	12	113.02618884	10	−150.77056700
H	13	1.08143812	12	112.49174289	10	−23.24781089
H	14	1.08144611	12	112.79927268	10	148.26453144
H	14	1.08104398	12	112.66784373	10	20.78746076
H	14	1.09487569	12	104.62876720	10	−95.50719499

A.3 Cyclisation of monocyclic oxidosqualene models

Table A.6. Monocyclic dimethyloxirane oxidosqualene model at HF/6-31G(d)//HF/6-31G(d); also given are B3LYP/6-31+G(d) single point energies.

Reactant **4.2**

E (HF) = −464.3148730 ZPC: 0.266446 Imag. Freq.: N/A

E (B3LYP) = −467.4325942

1 1

C						
C	1	1.54318743				
C	1	1.51931340	2	114.18999514		
H	1	1.08533114	3	110.18009841	2	−123.02988585
H	1	1.08499308	3	109.81288786	2	120.20546195
C	2	1.50426599	1	110.08414483	3	−64.58299668
H	2	1.08483071	1	109.56901020	3	177.62504702
H	2	1.08036004	1	111.53157057	3	59.07553154
C	3	1.32797837	1	119.87962910	2	104.90714774
C	3	1.51161612	1	114.82926190	2	−78.07282484
H	6	1.07611458	2	114.14409055	1	−57.02717167
H	9	1.08086086	3	117.29327659	1	1.13765315
H	10	1.08010359	3	113.15209808	1	171.44725379

H	10	1.08649608	3	109.77024593	1	−68.26593300
H	10	1.08669966	3	111.72721788	1	49.72641050
C	6	1.45599491	2	127.79006159	1	101.35462920
O	6	1.51121261	2	114.03709072	1	176.29769800
C	9	1.50485230	3	128.87211639	1	177.67534688
H	17	0.95758200	6	114.32084033	2	133.02547994
H	18	1.08088248	9	113.51066562	3	7.68209494
H	18	1.08675670	9	110.68982956	3	129.37008434
H	18	1.08594651	9	109.92189052	3	−113.08900303
C	16	1.50156060	6	122.77606110	2	6.33174830
C	16	1.50442628	6	118.94611453	2	−158.20749651
H	23	1.07851291	16	112.53603422	6	27.66182101
H	23	1.08192079	16	110.04635519	6	149.41445562
H	23	1.08403347	16	107.64381352	6	−92.38640788
H	24	1.08341696	16	112.61732369	6	−19.78422539
H	24	1.08443311	16	107.58880421	6	98.95044147
H	24	1.08247765	16	110.85181845	6	−143.03848600

Six-membered transition state **4.3**

E (HF) = −464.3130416 ZPC: 0.264922 Imag. Freq.: −151.0941

E (B3LYP) = −467.4312572

1 1

C						
C	1	1.53986362				
C	1	1.51957150	2	114.16523994		
H	1	1.08541907	3	110.02268950	2	−122.84205207
H	1	1.08497767	3	109.53988796	2	120.65264571
C	2	1.51102522	1	111.34833931	3	−64.52609941
H	2	1.08491159	1	109.67346963	3	177.81965267
H	2	1.08186920	1	111.70847712	3	59.90638510
C	3	1.32946962	1	120.07315747	2	103.43800881
C	3	1.51184533	1	114.79632349	2	−79.69423428
H	6	1.07910943	2	111.58592818	1	−53.82273971
H	9	1.08093120	3	117.23594962	1	1.56632086
H	10	1.08050604	3	113.33172089	1	169.65346461
H	10	1.08637817	3	109.59403595	1	−70.16628100
H	10	1.08651999	3	111.66445738	1	47.58900014
C	6	1.47412675	2	124.12092605	1	86.37583530
O	6	1.44433934	2	113.74978440	1	179.68878452
C	9	1.50565396	3	128.78820714	1	177.14478177

H	17	0.95347147	6	112.68679662	2	128.87311413
H	18	1.08105183	9	113.53229201	3	9.59560018
H	18	1.08705597	9	110.89459473	3	131.45288967
H	18	1.08591645	9	109.88465346	3	−111.06823672
C	16	1.48696980	6	122.28924903	2	27.50119490
C	16	1.48830452	6	119.37193213	2	−154.13965388
H	23	1.07777827	16	112.74146149	6	17.92315956
H	23	1.08112594	16	110.98411977	6	141.92833326
H	23	1.08746439	16	105.91097327	6	−100.79567304
H	24	1.08087257	16	113.07555821	6	−8.58216360
H	24	1.08854340	16	105.67094145	6	109.38981771
H	24	1.08183276	16	111.52672002	6	−134.00222142

Five-membered transition state **4.4**

E (HF) = −464.2999997 ZPC: 0.265712 Imag. Freq.: −125.0314

E (B3LYP) = −467.4236017

1 1

C						
C	1	1.53104578				
C	1	1.52240967	2	101.66481181		
C	2	1.51018164	1	102.86630640	3	−37.21258686
H	4	1.07363429	2	114.89965344	1	−71.36332657
H	4	2.68928756	2	116.31191011	1	−167.57246884
H	1	1.08155315	3	112.61951773	2	120.06456032
H	1	1.08311982	3	111.15666790	2	−118.50056211
H	2	1.07886109	1	111.51440995	3	81.72851715
H	2	1.08445402	1	114.49467816	3	−155.18000684
H	3	2.07778198	1	92.20376986	2	94.45090630
H	3	2.17610069	1	141.66182469	2	−80.12549020
H	3	2.15624168	1	94.08805181	2	−73.00415965
H	3	2.10696598	1	105.72531653	2	−120.66542920
H	3	2.79952635	1	163.77718901	2	47.93336340
H	3	3.37450432	1	134.95226059	2	75.30201626
H	3	3.08573423	1	144.53313383	2	121.79449419
H	4	2.93548853	2	102.18783321	1	95.17743334
H	4	2.82031260	2	78.33078495	1	121.88952565
H	4	3.47883186	2	107.94502834	1	126.02131298
H	4	2.93435401	2	154.01941077	1	79.15773998
H	4	3.44800407	2	148.08621352	1	143.95474168
H	4	2.71139342	2	167.58118603	1	−143.67262233

C	3	1.35078871	1	119.10497931	2	88.55326613
C	3	1.50516588	1	115.93214172	2	−91.00994578
C	4	1.51798973	2	125.17465635	1	138.59294465
C	24	1.50463570	3	127.48996578	1	−178.26548803
C	26	1.51820089	4	116.58412218	2	−43.65393075
C	26	1.52189843	4	113.33290784	2	−175.94915368
O	26	1.41878041	4	92.72215490	2	68.85594443

Six-membered product **4.5**

E (HF) = −464.3440382 ZPC: 0.268205 Imag. Freq.: N/A

E (B3LYP) = −467.4572192

1 1

C						
C	1	1.55791985				
C	1	1.47708344	2	106.04689973		
H	1	1.08544463	3	109.06035124	2	−117.06281143
H	1	1.08089613	3	112.34425185	2	121.64426800
C	2	1.53057149	1	111.81197938	3	−52.60730074
H	2	1.08328436	1	107.23956355	3	−173.84195116
H	2	1.08263801	1	110.50133980	3	70.02943341
C	3	1.47637909	1	116.49140280	2	63.75934318
C	3	1.47144773	1	119.78237031	2	−113.48450412
H	6	1.08889179	2	108.64588976	1	−65.45973391
H	9	1.08700006	3	106.23402887	1	43.28587496
H	10	1.07858647	3	113.99696493	1	156.12015117
H	10	1.09590539	3	104.01563410	1	−86.93319951
H	10	1.08232669	3	112.01762692	1	27.93790956
C	6	1.55010710	2	113.30212745	1	53.82207048
O	6	1.39452807	2	109.73019609	1	173.88017662
C	9	1.53225583	3	115.62776388	1	164.00173001
H	17	0.94800668	6	111.17533945	2	79.21469991
H	18	1.08164633	9	113.08252500	3	70.62449985
H	18	1.08044044	9	109.49108078	3	−169.04719297
H	18	1.08449922	9	110.91059542	3	−51.22413320
C	16	1.53754295	6	111.24242157	2	67.79001079
C	16	1.53462253	6	108.81285761	2	−171.98520246
H	23	1.08074185	16	109.21631664	6	60.10525915
H	23	1.08289401	16	111.10977893	6	178.75401399
H	23	1.08605591	16	113.69009725	6	−59.49677517
H	24	1.08553043	16	111.73367077	6	63.40417408

H	24	1.08225983	16	111.73659548	6	−174.92358812
H	24	1.08172317	16	108.78492662	6	−56.03444180

Five-membered product **4.6**

E (HF) = −464.3412849 ZPC: 0.266211 Imag. Freq.: N/A

E (B3LYP) = −467.4545797

1 1

C						
C	1	1.53722071				
C	1	1.47490552	2	105.88256252		
H	1	1.09126662	3	105.78664392	2	120.45547760
H	1	1.08743853	3	110.44038834	2	−126.32304633
C	2	1.54767614	1	105.66769171	3	20.42244390
H	2	1.07770268	1	112.40001410	3	142.93333579
H	2	1.08418338	1	109.32194584	3	−97.66411749
C	3	1.46747723	1	110.58280972	2	−0.46063786
C	3	1.47327344	1	123.90727771	2	178.04647649
H	6	1.08340118	2	109.19163046	1	−144.65478844
H	9	1.10966811	3	95.04444459	1	85.59795847
H	10	1.09121368	3	106.61418551	1	108.13342265
H	10	1.08007629	3	112.82096228	1	−11.63643634
H	10	1.08450300	3	110.98006932	1	−136.68675220
C	6	1.56142545	2	113.42096839	1	97.46044965
C	9	1.52931816	3	118.54139585	1	−162.21036550
H	17	1.08185902	9	112.16121705	3	64.77618617
H	17	1.08101273	9	109.68482214	3	−174.91522597
H	17	1.08323859	9	111.04079078	3	−56.41128954
C	16	1.52835594	6	113.93409362	2	−65.37538027
C	16	1.53143543	6	112.21672302	2	168.22948285
O	16	1.40925529	6	106.29134151	2	49.57083897
H	23	0.94857035	16	111.07379981	6	84.58134077
H	21	1.08711710	16	112.41297085	6	−58.51295035
H	21	1.08315264	16	111.09457899	6	64.47085732
H	21	1.08210315	16	109.38177297	6	−177.80397329
H	22	1.08077569	16	113.12468501	6	72.04737619
H	22	1.08348724	16	108.72300806	6	−168.44848976
H	22	1.08694736	16	111.18545728	6	−49.64916950

Table A.7. Monocyclic *trans*-monomethyloxirane oxidosqualene model at HF/6-31G(d)//HF/6-31G(d); also given are B3LYP/6-31+G(d) single point energies.

Reactant **4.10**

E (HF) = −425.2707946 ZPC: 0.239486 Imag. Freq.: N/A

E (B3LYP) = −428.1071882

1 1

C						
C	1	1.54424348				
C	1	1.51978951	2	114.14120607		
H	1	1.08502764	3	110.18748844	2	−123.08631975
H	1	1.08503416	3	109.93795501	2	120.00665118
H	2	1.08392496	1	109.92433523	3	178.71012648
H	2	1.08276600	1	111.51427466	3	59.47913103
H	2	2.20759746	1	97.80325338	3	−85.52121723
H	3	2.06073197	1	91.95024572	2	108.68494270
H	3	2.17452827	1	142.06816737	2	−71.04112653
H	3	2.14057765	1	100.68069786	2	−100.59897174
H	3	2.16719055	1	97.10977099	2	−52.42132875
H	2	3.28670674	1	139.34164820	3	−67.30089284
H	3	2.77594884	1	169.69335368	2	102.05289450
H	3	3.29611426	1	137.88156396	2	88.95665884
H	3	3.20191486	1	138.82362855	2	136.45201671
H	2	2.79284718	1	108.71290601	3	−8.97415341
H	2	4.23520848	1	103.74999005	3	−57.66159468
H	3	3.97967908	1	103.71657860	2	43.65109834
H	2	4.73114918	1	111.67155194	3	−36.17614534
C	2	1.50090082	1	109.84063981	3	−62.01642967
C	3	1.32813149	1	119.73013095	2	108.27862865
C	3	1.51183822	1	115.01200941	2	−74.59579401
C	21	1.44669444	2	124.22879864	1	95.87789929
O	24	1.52677600	21	61.89066121	2	99.64487429
C	22	1.50472881	3	128.93178372	1	177.53070264
C	24	1.49775682	21	123.84804762	2	−156.98066820

Six-membered transition state **4.11**

E (HF) = −425.2645817 ZPC: 0.238018 Imag. Freq.: −267.8538

E (B3LYP) = −428.1054224

1 1

C

C	1	1.53905573				
C	1	1.52052447	2	112.91004219		
H	1	1.08509308	3	110.08496039	2	−122.50371314
H	1	1.08453345	3	109.69234408	2	120.60743336
H	2	1.08354460	1	110.55804338	3	179.68450443
H	2	1.08413849	1	111.54483536	3	60.68504565
H	2	2.18228983	1	98.80501148	3	−85.40493089
H	3	2.06481299	1	92.26327383	2	104.86145702
H	3	2.17832716	1	141.56445515	2	−71.50240368
H	3	2.13402850	1	103.14335235	2	−106.93767878
H	3	2.16389990	1	95.07057655	2	−59.16732450
H	2	3.20019598	1	138.64509714	3	−64.02979345
H	3	2.78547604	1	169.35193482	2	88.40719233
H	3	3.33692100	1	137.62243725	2	88.23450822
H	3	3.15675380	1	140.04989040	2	135.86383320
H	2	2.75170563	1	97.95876527	3	−8.47460274
H	2	4.18898133	1	95.72702200	3	−56.36629380
H	3	3.72657340	1	110.99022046	2	48.70822569
H	2	4.61504444	1	105.08977586	3	−35.31831210
C	2	1.50882858	1	110.19292828	3	−60.19439048
C	3	1.33421395	1	120.00022777	2	103.74217045
C	3	1.51166500	1	115.12397698	2	−79.23458923
C	21	1.46474388	2	118.68928136	1	70.34738248
O	21	1.44003931	2	113.15349485	1	162.14932076
C	22	1.50575176	3	128.53625638	1	176.10102805
C	24	1.48080839	21	125.29329825	2	−158.16182779

Five-membered transtion state **4.12**

E (HF) = −425.2612666 ZPC: 0.238031 Imag. Freq.: −126.3106

E (B3LYP) = −428.1021867

1 1

C

C	1	1.53942861				
C	1	1.52561148	2	105.71542446		
H	1	1.08243340	3	112.15163112	2	120.25396771
H	1	1.08285087	3	110.72791433	2	−119.39828773
H	2	1.08094746	1	112.15598290	3	81.20938273
H	2	1.08457882	1	113.06389621	3	−155.73290173
H	2	2.21316963	1	93.94075770	3	−61.24526508
H	3	2.07056451	1	91.74472938	2	98.44409130

H	3	2.17684528	1	141.50951733	2	−75.49208695
H	3	2.16057370	1	94.35336896	2	−66.48998816
H	3	2.12490118	1	104.69084556	2	−114.06309663
H	3	2.78198348	1	167.36968598	2	67.27425424
H	3	3.33203503	1	135.80887141	2	77.58181539
H	3	3.15941388	1	141.07431971	2	124.44615352
H	2	2.80204341	1	117.30449166	3	13.33464905
H	2	3.63796713	1	141.07684809	3	−43.82116326
H	3	3.67869277	1	121.31728925	2	19.13527101
H	2	4.75434579	1	116.75797395	3	−14.26197444
H	2	4.26861361	1	107.01667161	3	−35.19796798
C	2	1.49548908	1	103.61864045	3	−37.42436932
C	3	1.34078900	1	119.18715807	2	95.08522739
C	3	1.50915094	1	115.49554315	2	−85.37293765
C	21	1.49015538	2	123.74317728	1	128.13550449
C	22	1.50337389	3	128.40163637	1	−179.29728017
C	24	1.51193256	21	117.98377929	2	−162.86970154
O	24	1.41811251	21	89.52320319	2	79.20795669

Six-membered product **4.13**

E (HF) = −425.3135883 ZPC: 0.240857 Imag. Freq.: N/A

E (B3LYP) = −428.1458831

1 1

C

C	1	1.56341161				
C	1	1.47218743	2	103.21177211		
H	1	1.08356861	3	110.81558045	2	−116.75793007
H	1	1.08082664	3	112.62827158	2	119.60978508
H	2	1.08316747	1	107.28244747	3	−178.41608576
H	2	1.08474356	1	110.55781913	3	65.09704368
H	2	2.15312834	1	98.46675227	3	−82.49436841
H	3	2.08063294	1	93.58162994	2	89.00667292
H	3	2.14665959	1	142.02481978	2	−82.32122819
H	3	2.03937664	1	117.01140180	2	−139.99496370
H	3	2.13279973	1	93.60967151	2	−94.18349545
H	2	2.74110567	1	151.01519090	3	−83.91082774
H	3	2.93660349	1	159.87022262	2	41.84297818
H	3	3.44679105	1	136.30500987	2	81.49274477
H	3	2.77164820	1	148.33154647	2	127.97439863
H	3	2.61335865	1	106.96166710	2	8.17358288

H	3	4.09161733	1	98.67894166	2	56.95982026
H	3	4.14598024	1	119.31927515	2	42.59233566
H	2	4.14734288	1	112.34810647	3	−40.68518733
C	2	1.53051032	1	111.61787466	3	−56.24195782
C	3	1.47507919	1	116.73279911	2	69.34926234
C	3	1.47254325	1	119.88836371	2	−104.31150002
C	21	1.53777283	2	111.89248263	1	53.80180194
O	21	1.39390272	2	109.64811270	1	171.66036024
C	22	1.53144154	3	115.91266945	1	165.97980542
C	24	1.53017200	21	111.48796534	2	−176.67363107

Five-membered product **4.14**

E (HF) = −425.3079052 ZPC: 0.238960 Imag. Freq.: N/A

E (B3LYP) = −428.1399281

1 1

C

C	1	1.53452508				
C	1	1.47394162	2	105.09855324		
H	1	1.09685876	3	104.12271169	2	116.12431675
H	1	1.08465395	3	112.71535236	2	−129.33560380
H	2	1.07623048	1	111.91409943	3	152.12489916
H	2	1.08507547	1	109.84142339	3	−87.37663371
H	2	2.17122901	1	128.05002020	3	15.72777267
H	3	1.95152126	1	106.75658452	2	28.32479454
H	3	2.06249174	1	125.89157818	2	−149.81847896
H	3	2.13782084	1	97.47712406	2	165.40705791
H	3	2.12136829	1	143.39895572	2	142.51793954
H	3	2.93135859	1	131.81977147	2	−55.91562057
H	3	3.47507107	1	128.67682341	2	−16.12239914
H	3	2.85216762	1	158.57750823	2	−11.78527224
H	3	2.87646434	1	83.52928365	2	−66.52291282
H	2	3.23271766	1	114.91158443	3	96.69477136
H	2	4.31042146	1	104.66045940	3	41.41442590
H	2	4.68338971	1	104.04452189	3	64.12949320
H	2	4.01312107	1	124.49355608	3	56.29073948
C	2	1.53829371	1	103.24122157	3	29.93591196
C	3	1.47606807	1	110.18601935	2	−7.63203275
C	3	1.47194773	1	124.41077960	2	172.59700007
C	21	1.55964055	2	113.43637938	1	80.86495331
C	22	1.52986443	3	118.42707507	1	−155.09880832

C	24	1.52420722	21	112.46911328	2	150.19083659
O	24	1.40042351	21	111.36860198	2	24.85277631

Table A.8. Monocyclic *cis*-monomethyloxirane oxidosqualene model at HF/6-31G(d)//HF/6-31G(d); also given are B3LYP/6-31+G(d) single point energies.

Reactant **4.15**

E (HF) = −425.2682698 ZPC: 0.239730 Imag. Freq.: N/A

E (B3LYP) = −428.1046976

1 1

C						
C	1	1.54447199				
C	1	1.51941848	2	114.03605148		
H	1	1.08521385	3	110.25561923	2	−122.94534894
H	1	1.08487031	3	109.99918781	2	120.08354613
H	2	1.08450901	1	109.66510431	3	178.48520431
H	2	1.08060641	1	111.57871539	3	59.53786454
H	2	2.18960391	1	94.51883901	3	−85.74011032
H	3	2.06120079	1	92.03404120	2	105.00631800
H	3	2.17557061	1	141.59309540	2	−72.16247854
H	3	2.13955856	1	101.97166033	2	−105.29074231
H	3	2.16410322	1	95.67757778	2	−57.32679609
H	2	3.28599241	1	137.98940181	3	−76.48142649
H	3	2.77227121	1	169.88522899	2	99.52198418
H	3	3.28714257	1	138.08593888	2	84.08803564
H	3	3.21086251	1	138.80943134	2	131.73812286
H	2	3.54239276	1	107.70824965	3	−46.03480146
H	2	2.94966066	1	118.33174059	3	13.97804614
H	2	4.21124568	1	120.12553626	3	−9.00156807
H	3	3.38012096	1	106.97083224	2	5.57983116
C	2	1.50242417	1	109.63095649	3	−63.56519347
C	3	1.32785980	1	119.80158692	2	104.41551510
C	3	1.51153846	1	114.84165225	2	−78.34050349
C	21	1.45194197	2	127.23401698	1	104.12861370
O	24	1.52454032	21	61.97121201	2	99.31089915
C	22	1.50445260	3	128.91153376	1	178.08115171
C	24	1.49631759	21	126.34714043	2	0.27766555

Six-membered transition state **4.16**

E (HF) = −425.2601252 ZPC: 0.238080 Imag. Freq.: −308.9176

E (B3LYP) = −428.1005474

1 1

C						
C	1	1.54135657				
C	1	1.52122842	2	113.03051480		
H	1	1.08508907	3	110.03062778	2	−122.04289849
H	1	1.08416358	3	109.83437322	2	121.02668799
H	2	1.08400608	1	110.25326785	3	−177.56062940
H	2	1.08266284	1	111.93391086	3	63.57892497
H	2	2.15520926	1	93.30026584	3	−82.42240719
H	3	2.06591255	1	92.49192348	2	99.35221126
H	3	2.17992161	1	140.87783111	2	−75.25633674
H	3	2.13237325	1	104.03509395	2	−113.10586745
H	3	2.16038414	1	93.88907547	2	−65.67075830
H	2	3.18940575	1	135.72342992	3	−72.62455687
H	3	2.77927624	1	169.85656013	2	84.15656400
H	3	3.32456142	1	138.01830667	2	80.58199831
H	3	3.17540850	1	140.06956113	2	128.55688948
H	2	3.49954175	1	97.06818424	3	−40.85037367
H	2	2.90680908	1	107.72279374	3	16.33598440
H	2	4.08482162	1	113.92896575	3	−6.47225976
H	3	3.20800433	1	116.56894699	2	2.77613566
C	2	1.50812478	1	109.06922872	3	−59.09239643
C	3	1.33410897	1	120.18476441	2	97.84698693
C	3	1.51085228	1	114.85414070	2	−84.77400386
C	21	1.46993913	2	121.21847542	1	77.73974037
O	21	1.43685045	2	115.66430307	1	173.55081914
C	22	1.50640889	3	128.55537051	1	177.02232652
C	24	1.47845348	21	127.05295199	2	36.27553652

Five-membered transition state **4.17**

E (HF) = −425.2593694 ZPC: 0.238194 Imag. Freq.: −105.7360

E (B3LYP) = −428.1003173

1 1

C						
C	1	1.54025171				
C	1	1.52536005	2	105.59953228		
H	1	1.08231830	3	112.19620429	2	120.05996243

H	1	1.08333804	3	110.92388459	2	−119.46648620
H	2	1.07905449	1	111.89131253	3	77.83563293
H	2	1.08569947	1	112.99209640	3	−159.35190755
H	2	2.19088232	1	91.42361118	3	−65.41329502
H	3	2.07168485	1	92.10561429	2	96.88945866
H	3	2.17657718	1	141.25898981	2	−77.44681160
H	3	2.15979540	1	94.06428584	2	−68.52246546
H	3	2.12041465	1	104.52964433	2	−116.12188727
H	3	2.77834388	1	166.77353957	2	58.79338628
H	3	3.32784002	1	135.56417860	2	74.05295278
H	3	3.16541233	1	142.12132082	2	120.99001383
H	2	3.53746819	1	110.60694522	3	−27.72273078
H	2	3.68691229	1	138.39186341	3	−54.64701523
H	3	3.40845032	1	108.63051045	2	−15.89948600
H	2	2.98212142	1	126.87184921	3	33.48970344
H	2	4.23197509	1	125.67778227	3	8.83160520
C	2	1.49396425	1	103.57489861	3	−42.05512613
C	3	1.34045716	1	119.39098713	2	92.65177927
C	3	1.50812406	1	115.26159358	2	−87.29086252
C	21	1.49390770	2	127.10102625	1	133.76191782
C	22	1.50403198	3	128.29162725	1	−177.29031447
C	24	1.50977066	21	120.04326686	2	−34.09156131
O	24	1.42023148	21	89.30924109	2	80.42496893

Six-membered product **4.18**

E (HF) = −425.3101963 ZPC: 0.240755 Imag. Freq.: N/A

E (B3LYP) = −428.1417824

1 1

C

C	1	1.55882278				
C	1	1.48078836	2	107.34907396		
H	1	1.08630567	3	108.44355105	2	−117.31316871
H	1	1.08075363	3	112.04710427	2	122.33063805
H	2	1.08320672	1	107.27775939	3	−173.95570591
H	2	1.08303697	1	110.42293596	3	69.83518122
H	2	2.14456821	1	97.39940640	3	−78.43814951
H	3	2.06318920	1	93.80703057	2	83.12587689
H	3	2.14689524	1	143.52308588	2	−96.78814138
H	3	2.03316145	1	114.62732300	2	−151.20595208
H	3	2.13024197	1	94.39793537	2	−103.98390010

H	2	2.73141567	1	150.17527789	3	−82.03948396
H	3	2.90667009	1	160.89087160	2	33.73265797
H	3	3.46272270	1	135.83040205	2	69.06261904
H	3	2.85123212	1	146.42988660	2	115.24001314
H	3	3.33792777	1	100.93330240	2	37.78612767
H	2	3.52791517	1	116.94244869	3	0.84453653
H	3	3.49690225	1	124.22923132	2	−0.48880752
H	3	2.80026912	1	102.29302798	2	−22.66729503
C	2	1.53112331	1	111.37779015	3	−52.41848254
C	3	1.47939926	1	116.29667848	2	61.67520734
C	3	1.46999376	1	120.00808328	2	−116.03923408
C	21	1.53821846	2	111.88276172	1	54.10154945
O	21	1.39227284	2	110.87662438	1	173.73277052
C	22	1.52952119	3	117.05780338	1	167.47712696
C	24	1.53263850	21	113.28082910	2	70.99801043

Five-membered product **4.19**

E (HF) = −425.3095434 ZPC: 0.239047 Imag. Freq.: N/A

E (B3LYP) = −428.1405713

1 1

C						
C	1	1.53941244				
C	1	1.47682092	2	106.09680567		
H	1	1.09231107	3	105.24159514	2	120.11817388
H	1	1.08704057	3	110.75051560	2	−126.79718759
H	2	1.07927824	1	112.52379230	3	142.35490713
H	2	1.08350651	1	109.52194412	3	−98.36138754
H	2	2.16582087	1	127.26523358	3	0.29026785
H	3	1.92724287	1	106.40000844	2	35.27680690
H	3	2.06552651	1	126.35054535	2	−144.95212434
H	3	2.13866412	1	96.95426853	2	171.06430557
H	3	2.12056339	1	142.42411509	2	147.16524703
H	3	2.93556636	1	133.23879175	2	−49.15602208
H	3	3.47560123	1	128.68135271	2	−9.19140645
H	3	2.87210695	1	158.44431922	2	−1.47195057
H	2	3.49690129	1	106.30194763	3	41.84033103
H	2	3.82629258	1	125.68915103	3	75.92801441
H	3	2.91390050	1	89.95867181	2	−76.70086850
H	2	2.89842652	1	77.76665335	3	90.56499185
H	2	4.15210273	1	88.98541761	3	73.69709921

C	2	1.54340859	1	105.24229256	3	19.79028677
C	3	1.46886536	1	110.62339624	2	−1.34980745
C	3	1.47288742	1	124.01073343	2	177.63708852
C	21	1.53780542	2	114.47409574	1	96.29015519
C	22	1.52985038	3	119.35453033	1	−156.80272966
C	24	1.52817751	21	116.41870054	2	−57.56203517
O	24	1.40019312	21	103.92808999	2	64.14358482

Table A.9. Monocyclic oxidosqualene model with no terminal methyl groups at HF/6-31G(d)//HF/6-31G(d); also given are B3LYP/6-31+G(d) single point energies.

Reactant **4.20**

E (HF) = −386.2212562 ZPC: 0.212453 Imag. Freq.: N/A

E (B3LYP) = −388.776331

1 1

C						
C	1	1.54620150				
C	1	1.51993896	2	113.95521886		
H	1	1.08497946	3	110.29524660	2	−123.04594316
H	1	1.08487251	3	110.12119154	2	119.84487303
H	2	1.08359100	1	110.02813067	3	179.03297157
H	2	1.08266955	1	111.49374404	3	59.40815612
H	2	2.21260700	1	97.99135344	3	−85.34747986
H	3	2.06094201	1	91.91396506	2	107.56144820
H	3	2.17422447	1	142.01831371	2	−71.64145035
H	3	2.16715304	1	96.93102606	2	−53.49968634
H	3	2.14078279	1	100.83540473	2	−101.65364496
H	2	2.83612028	1	107.51283409	3	−9.25884869
H	2	3.53886013	1	104.92343091	3	−41.29128266
H	3	2.77458233	1	169.69343688	2	101.44729157
H	3	3.28924411	1	137.87661307	2	87.03408088
H	3	3.20810227	1	138.72400468	2	134.53056037
H	2	3.31243301	1	139.09894555	3	−65.19907586
C	2	1.49901649	1	109.24859319	3	−61.74323417
C	3	1.32807576	1	119.69149895	2	107.04375821
C	3	1.51177192	1	114.98224957	2	−75.54037629
C	19	1.44402524	2	123.94555283	1	96.64077533
C	20	1.50432602	3	128.96171240	1	177.98011653
O	22	1.49187439	19	63.79315113	2	98.74254642

Six-membered transition state **4.21**

E (HF) = −386.2113486 ZPC: 0.211412 Imag. Freq.: −453.5909

E (B3LYP) = −388.7747979

1 1

C						
C	1	1.54527000				
C	1	1.52271368	2	112.53305044		
H	1	1.08485335	3	110.10050710	2	−122.08835204
H	1	1.08384961	3	109.85076760	2	120.76576732
H	2	1.08253174	1	110.68864818	3	−177.53895764
H	2	1.08408562	1	111.62036733	3	62.59880881
H	2	2.18743319	1	97.92551131	3	−82.53902894
H	3	2.06826296	1	92.54615784	2	101.33399471
H	3	2.17842043	1	141.28680125	2	−73.96137822
H	3	2.16110450	1	94.48934960	2	−62.89732666
H	3	2.13074146	1	103.54298926	2	−110.57033388
H	3	2.70162065	1	97.40117585	2	6.20297852
H	3	3.37715753	1	96.60609641	2	39.38339756
H	2	3.25235385	1	134.14718253	3	−56.06657987
H	3	2.78917336	1	169.24203238	2	80.44303850
H	3	3.34349494	1	137.63247002	2	84.25614846
H	3	3.15160049	1	140.66784133	2	132.16029522
C	2	1.50484681	1	107.41199974	3	−57.04955630
C	3	1.33901827	1	120.22283818	2	99.50058857
C	3	1.51067268	1	115.02433979	2	−82.51029823
C	19	1.44997252	2	117.27154713	1	67.69333935
O	19	1.45063481	2	116.16407257	1	155.21829798
C	20	1.50686498	3	128.43682191	1	176.43062646

Five-membered transition state **4.22**

E (HF) = −386.216997 ZPC: 0.210776 Imag. Freq.: −171.8925

E (B3LYP) = −388.7747237

1 1

C						
C	1	1.54881501				
C	1	1.52489006	2	109.04684129		
H	1	1.08313187	3	110.56643943	2	−120.35783179
H	1	1.08316068	3	111.76544128	2	120.04662093
H	2	1.08425807	1	111.53204571	3	−161.00886308

H	2	1.08085793	1	112.21640674	3	76.56082117
H	2	2.20878658	1	93.12430194	3	−66.03977735
H	3	2.06663591	1	91.75293656	2	101.24073753
H	3	2.17562009	1	141.60176139	2	−73.92399725
H	3	2.16345114	1	94.99518736	2	−61.98178111
H	3	2.13136798	1	103.28009784	2	−109.77026543
H	2	2.84322708	1	116.61830243	3	7.74419796
H	2	3.52845529	1	109.00630604	3	−24.11602232
H	3	2.77447433	1	168.40106152	2	76.27577253
H	3	3.30740897	1	136.36562044	2	79.15715312
H	3	3.18761685	1	140.29108476	2	126.29876483
H	2	3.59986598	1	138.89080451	3	−50.13808307
C	2	1.48630291	1	104.26445610	3	−42.92592006
C	3	1.33438141	1	119.33353318	2	98.72586868
C	3	1.51022700	1	115.16878480	2	−81.93287712
C	19	1.46944609	2	124.72685662	1	123.91183360
C	20	1.50372967	3	128.61258086	1	−179.17840193
O	22	1.42254963	19	84.56208202	2	85.27255415

Six-membered product **4.23**

E (HF) = −386.2780418 ZPC: 0.213113 Imag. Freq.: N/A

E (B3LYP) = −388.8288391

1 1

C						
C	1	1.56385331				
C	1	1.47587047	2	104.94709790		
H	1	1.08436717	3	110.20481305	2	−117.11682275
H	1	1.08078191	3	112.25431406	2	120.30889397
H	2	1.08141792	1	107.87389423	3	−177.69633724
H	2	1.08485183	1	110.55158897	3	65.35515775
H	2	2.14399375	1	98.35944203	3	−82.41785302
H	3	2.07965232	1	94.02707025	2	88.33447804
H	3	2.14624019	1	142.39041303	2	−84.89792620
H	3	2.13281706	1	93.91201837	2	−96.67289615
H	3	2.03408339	1	117.14977757	2	−142.73645578
H	3	2.64843114	1	105.59019388	2	7.97816933
H	3	3.31450672	1	102.29659702	2	40.34016874
H	2	3.16718157	1	138.86599161	3	−59.69765425
H	3	2.92002203	1	158.84633981	2	35.61741297
H	3	3.46384177	1	135.81759358	2	74.77084683

H	3	2.84714249	1	148.79246889	2	120.70243812
C	2	1.52621707	1	111.32431272	3	−55.87660701
C	3	1.47900612	1	116.38468975	2	67.55914547
C	3	1.47086168	1	120.16001585	2	−106.80183369
C	19	1.53292886	2	110.61096857	1	53.05607124
O	19	1.39166921	2	106.21503312	1	173.14148134
C	20	1.52868054	3	117.39743979	1	169.59923718

Five-membered product **4.24**

E (HF) = −386.2717783 ZPC: 0.211408 Imag. Freq.: N/A

E (B3LYP) = −388.8225811

1 1

C						
C	1	1.53737100				
C	1	1.47545841	2	105.69896122		
H	1	1.08519963	3	112.15383366	2	−128.49333720
H	1	1.09580978	3	104.19247852	2	118.01608484
H	2	1.08440818	1	109.65849646	3	−92.52652624
H	2	1.07888335	1	112.41749713	3	147.32114815
H	2	2.17487602	1	127.74384452	3	9.46829071
H	3	1.95098222	1	108.09912577	2	30.28867114
H	3	2.12184277	1	143.69863341	2	144.94444732
H	3	2.06185110	1	125.25066142	2	−148.07096577
H	3	2.13803335	1	97.44550603	2	166.86631104
H	2	2.84026356	1	78.95793531	3	68.34899199
H	2	3.49101342	1	102.10764390	3	49.51376763
H	3	2.90916751	1	130.81525072	2	−55.72018244
H	3	3.47533417	1	128.06768836	2	−16.41267674
H	3	2.87563739	1	158.09358907	2	−13.52945247
H	2	3.52209617	1	128.03053307	3	78.33139409
C	2	1.53907774	1	104.01239092	3	25.64352834
C	3	1.47419285	1	110.50726798	2	−5.95665867
C	3	1.47195589	1	124.27602325	2	174.47497485
C	19	1.53616977	2	112.31059043	1	86.70060574
C	20	1.53112928	3	118.45094595	1	−152.54513766
O	22	1.39284352	19	110.97479613	2	54.14191753

A.4 Cyclisations of bicyclic oxidosqualene model

Table A.10. Reaction path A of bicyclic oxidosqualene model at HF/6-31G(d)//HF/6-31G(d).

Prereaction conformer **5.1a**

E = −658.3000375 ZPC: 0.382536 Imag. Freq.: N/A

1 1

C						
C	1	1.54325310				
C	1	1.51989093	2	114.11478178		
H	1	1.08505084	3	109.91108329	2	120.23020699
H	1	1.08529782	3	110.15012010	2	−122.92960340
H	2	1.08042304	1	111.52728818	3	59.09809735
H	2	1.08487497	1	109.65757197	3	177.73549701
C	2	1.50401729	1	109.95336156	3	−64.46067528
C	3	1.32870834	1	119.74083212	2	103.59879184
C	9	3.64906271	3	137.95427514	1	66.31540454
C	3	1.51202893	1	114.59331041	2	−78.97955123
C	8	1.45555814	2	127.74788528	1	100.98020445
H	8	1.07607156	2	114.14690630	1	−57.27460306
H	9	1.07984145	3	117.23430795	1	1.37327137
H	10	1.07940748	9	78.55255587	3	20.39721196
H	11	1.08700371	3	111.63253317	1	50.56042521
H	11	1.07994210	3	113.22333302	1	172.13543853
H	11	1.08659329	3	109.86041954	1	−67.34693846
C	9	1.50720035	3	128.94966767	1	177.72147099
O	8	1.51186920	2	114.09155215	1	176.00170897
C	10	1.50463393	9	137.63398040	3	−92.38894197
C	10	1.32648325	9	57.38793883	3	153.33798646
H	20	0.95746057	8	114.28832027	2	133.11129467
H	19	1.08832475	9	109.20257711	3	118.50332587
H	19	1.08216076	9	111.19070437	3	1.63405855
H	21	1.08125185	10	113.64499548	9	−78.51835785
H	21	1.08715498	10	110.37248573	9	42.74355827
H	21	1.08645426	10	110.21831586	9	160.34204786
C	22	1.51801870	10	120.09335881	9	−54.00065651
C	22	1.51196619	10	124.79121339	9	128.15861742
H	29	1.08754715	22	108.89098780	10	−127.15426550
H	29	1.08434742	22	109.80332566	10	−10.69223556
H	30	1.08008847	22	113.01755343	10	2.83225416

H	30	1.08672089	22	110.21708417	10	123.32126057
H	30	1.08787361	22	111.56482914	10	−118.35653331
C	12	1.50145715	8	122.78086622	2	6.43234566
H	36	1.08398979	12	107.60912930	8	−92.21436925
H	36	1.07851464	12	112.52384670	8	27.78850512
H	36	1.08192311	12	110.05784877	8	149.55351774
C	12	1.50433750	8	118.93507642	2	−158.10964876
H	40	1.08340227	12	112.60940309	8	−19.85509620
H	40	1.08438985	12	107.55986817	8	98.83040588
H	40	1.08247203	12	110.86164552	8	−143.12878570

A-ring cyclisation transition state **5.2a**

E = −658.2983611 ZPC: 0.381080 Imag. Freq.: −162.4211

1 1

C						
C	1	1.54001559				
C	1	1.52015779	2	114.11153693		
H	1	1.08505150	3	109.63857244	2	120.65655807
H	1	1.08539155	3	109.99944922	2	−122.76238969
H	2	1.08184935	1	111.70559232	3	59.83416396
H	2	1.08497237	1	109.75413152	3	177.85462124
C	2	1.51038852	1	111.16331320	3	−64.46660944
C	3	1.33016571	1	119.93351162	2	102.33343070
C	9	3.63902332	3	137.62266220	1	66.04536640
C	3	1.51229006	1	114.54984357	2	−80.40936132
C	8	1.47222118	2	124.29978548	1	86.43657245
H	8	1.07891491	2	111.68082516	1	−54.41488521
H	9	1.07991604	3	117.18402432	1	1.68219615
H	10	1.07941272	9	77.88248553	3	19.38562629
H	11	1.08681485	3	111.55667472	1	48.50586618
H	11	1.08027392	3	113.39534496	1	170.37237205
H	11	1.08647895	3	109.71044489	1	−69.17299471
C	9	1.50790228	3	128.88494219	1	177.14278561
O	8	1.44687560	2	113.86044495	1	178.98462009
C	10	1.50457878	9	137.83052930	3	−92.69914068
C	10	1.32652786	9	57.92390074	3	152.55150803
H	20	0.95357428	8	112.69209466	2	129.30630079
H	19	1.08885959	9	109.45067573	3	119.25645520
H	19	1.08221476	9	111.18238453	3	2.26537294
H	21	1.08122330	10	113.65758631	9	−79.61560441

H	21	1.08710460	10	110.37835538	9	41.69123506
H	21	1.08640049	10	110.18352746	9	159.27473200
C	22	1.51808571	10	120.09075290	9	−53.52107382
C	22	1.51192761	10	124.80401495	9	128.78640291
H	29	1.08745546	22	108.92547191	10	−127.99406170
H	29	1.08426410	22	109.84056170	10	−11.48215151
H	30	1.08004088	22	113.04125597	10	1.23669827
H	30	1.08672749	22	110.21367048	10	121.75831513
H	30	1.08797687	22	111.58975823	10	−119.95886512
C	12	1.48765951	8	122.39767601	2	26.85015178
H	36	1.08717716	12	105.96404977	8	−101.33325059
H	36	1.07768951	12	112.76402171	8	17.47173897
H	36	1.08118570	12	110.89323790	8	141.36062964
C	12	1.48906547	8	119.33731737	2	−154.32463453
H	40	1.08096120	12	113.03401893	8	−9.19358096
H	40	1.08822819	12	105.70891688	8	108.70225663
H	40	1.08178027	12	111.53119901	8	−134.55112653

Monocyclic intermediate **5.3a**

E = −658.330188 ZPC: 0.384625 Imag. Freq.: N/A

1 1

C						
C	1	1.55905037				
C	1	1.47627369	2	104.80440222		
H	1	1.08132352	3	112.44199436	2	120.46451002
H	1	1.08383822	3	109.68483409	2	−117.36840093
H	2	1.08296723	1	110.47574368	3	69.64998488
H	2	1.08339957	1	107.28902723	3	−174.24840816
C	2	1.53082289	1	111.98437866	3	−52.92742137
C	3	1.47369409	1	116.22220228	2	66.46774059
C	3	3.67326960	1	99.77318920	2	148.44934971
C	3	1.47518460	1	118.55946359	2	−106.76561082
C	8	1.55153375	2	113.52883619	1	53.27256076
H	8	1.08864739	2	108.57319299	1	−65.95567712
H	9	1.08377370	3	106.39422025	1	39.32258125
H	10	1.08107959	3	69.27336342	1	97.68905582
H	11	1.08472764	3	110.33275827	1	36.91120464
H	11	1.07740157	3	114.32081462	1	163.11389902
H	11	1.09148964	3	105.45977428	1	−77.18100418
C	9	1.53721092	3	116.92061102	1	160.66704316

O	8	1.39528074	2	109.67292699	1	173.49066046
C	10	1.50486480	3	129.39257558	1	−6.33738511
C	10	1.32822259	3	73.60186041	1	−133.84138820
H	20	0.94794736	8	111.10567924	2	78.73220420
H	19	1.08075616	9	106.90299031	3	−177.87347545
H	19	1.08379913	9	111.31094300	3	66.81693993
H	21	1.08070469	10	113.48511934	3	−93.61159399
H	21	1.08672408	10	110.49337847	3	27.60111947
H	21	1.08608555	10	110.13783137	3	145.28188180
C	22	1.51732773	10	119.92819050	3	−53.94236318
C	22	1.51129341	10	124.90828555	3	128.37235772
H	29	1.08652053	22	109.33696611	10	−122.36728309
H	29	1.08445263	22	109.35630193	10	−7.07052458
H	30	1.07946771	22	112.98360516	10	2.62360808
H	30	1.08635520	22	109.91242484	10	122.90218022
H	30	1.08764326	22	111.81833288	10	−118.84739770
C	12	1.53710868	8	111.40403043	2	69.12465457
H	36	1.08311079	12	110.97689433	8	−179.19944341
H	36	1.08512662	12	113.81270958	8	−57.35649290
H	36	1.08077391	12	109.17531030	8	62.14905425
C	12	1.53570694	8	108.40153776	2	−171.17622789
H	40	1.08549021	12	111.80539084	8	65.12025411
H	40	1.08190804	12	111.84948960	8	−172.97766569
H	40	1.08187762	12	108.59511192	8	−54.20744047

B-ring cyclisation transition state **5.4a**

E = −658.3218391 ZPC: 0.387685 Imag. Freq.: −189.2534

1 1

C

C	1	1.54249844				
C	1	1.51212762	2	108.22996331		
H	1	1.08113837	3	111.64738209	2	120.94658557
H	1	1.08398445	3	110.30550917	2	−118.91631767
H	2	1.08318438	1	110.97040233	3	66.71893241
H	2	1.08553521	1	107.77665535	3	−177.34784301
C	2	1.52994638	1	112.61979534	3	−56.75077793
C	3	1.53621485	1	111.13377433	2	58.37106030
C	3	1.51746789	1	114.75935512	2	−78.82234008
C	3	2.11075165	1	103.02308078	2	179.70982413
C	8	1.54860931	2	113.72442639	1	56.13695782

H	8	1.09043580	2	107.97599769	1	−62.67741787
H	9	1.08384208	3	105.06152772	1	50.57196614
H	10	1.08129389	3	111.48021586	1	−51.85388123
H	10	1.08056487	3	112.98792363	1	−175.32391191
H	10	1.08052924	3	108.30650941	1	65.91029312
C	9	1.53442603	3	112.50022935	1	166.21639419
O	8	1.39747245	2	110.45856684	1	177.21091990
C	11	1.37175933	3	84.45127791	1	−117.54105240
H	11	1.07278834	3	94.92240968	1	127.56925821
C	11	1.51010292	3	113.80078478	1	8.90365817
H	19	0.94773131	8	110.77806324	2	71.06324987
H	18	1.08003937	9	109.23978166	3	−164.59192708
H	18	1.08123868	9	111.97648768	3	77.40273389
C	20	1.50133613	11	119.75068265	3	−73.64827953
C	12	1.54041917	8	111.03451908	2	75.29377614
C	12	1.54155454	8	107.90585723	2	−167.39939332
C	20	1.49830855	11	123.07024631	3	104.47658668
H	22	1.08035722	11	113.91320086	3	−61.22162765
H	22	1.08251133	11	110.73139344	3	61.29416818
H	22	1.08601538	11	108.67678770	3	178.51130520
H	26	1.08299949	20	109.66106639	11	−145.31546564
H	26	1.08145008	20	110.03920528	11	−27.35706251
H	27	1.08069542	12	113.96164963	8	−45.50302229
H	27	1.08064446	12	108.92335837	8	72.93508482
H	27	1.08395707	12	111.53922791	8	−168.49444486
H	28	1.08661397	12	111.96088894	8	67.22922460
H	28	1.08373700	12	111.66236210	8	−171.23750045
H	28	1.08154652	12	109.28658092	8	−52.32728281
H	29	1.08056493	20	113.46720576	11	−28.67144594
H	29	1.08181666	20	112.00343679	11	−153.50789026
H	29	1.08905766	20	106.70833504	11	89.35838021

Bicyclic product conformational isomer **5.5a**

E = −658.3321674 ZPC: 0.388083 Imag. Freq.: N/A

1 1

C

C	1	1.52876643				
C	1	1.54258221	2	112.68085210		
H	1	1.08454706	2	109.81300275	3	−122.92740755
H	1	1.08388202	2	107.33413372	3	121.31548589

H	2	1.08287321	1	112.24269342	3	64.79132028
H	2	1.08667548	1	108.24248752	3	−178.43420985
C	2	1.52392293	1	110.99780991	3	−58.79900738
C	3	1.56628188	1	108.74656827	2	51.60791363
C	3	1.54123165	1	108.72807504	2	−74.10593930
C	3	1.62674956	1	109.52498361	2	168.83012573
C	8	1.54566248	2	113.09374876	1	59.85145028
H	8	1.09141893	2	107.88198375	1	−58.54042937
H	9	1.09364467	3	103.69484071	1	64.64834191
H	10	1.08486551	3	109.79916084	1	−65.35476895
H	10	1.08333818	3	113.33112022	1	174.25160291
H	10	1.07748370	3	111.82916035	1	53.13567130
C	9	1.54219388	3	112.24062795	1	178.82219484
O	8	1.39946147	2	111.29153558	1	−178.61699996
C	11	1.48283504	3	108.96342534	1	−138.17959640
H	11	1.09093007	3	105.11759335	1	113.21303162
C	11	1.53358853	3	118.13907089	1	−5.76070250
H	19	0.94759427	8	110.35662849	2	66.31705262
H	18	1.07973054	9	109.77259977	3	−157.04092533
H	18	1.07886611	9	111.98411892	3	83.69120924
C	20	1.46604163	11	116.49604542	3	−46.96873700
C	12	1.54143876	8	110.47664211	2	73.72887031
C	12	1.54300749	8	107.60459973	2	−169.62737164
C	20	1.47409475	11	124.03820507	3	131.63308841
H	22	1.08234918	11	113.23320972	3	−63.42785830
H	22	1.08016694	11	110.09484331	3	57.32700832
H	22	1.08452539	11	110.40612613	3	175.14394922
H	26	1.08028326	20	112.71718417	11	−167.21906040
H	26	1.08091872	20	109.75229392	11	−45.13412853
H	27	1.08004183	12	113.97512694	8	−58.05213298
H	27	1.08042812	12	108.82799169	8	61.32713361
H	27	1.08374985	12	111.59724169	8	179.43146730
H	28	1.08708128	12	111.74949570	8	66.23855749
H	28	1.08436131	12	112.00171368	8	−172.23761972
H	28	1.08115498	12	109.56131016	8	−53.18010714
H	29	1.07907891	20	113.80926359	11	−28.43855127
H	29	1.08167906	20	111.86196976	11	−156.07435334
H	29	1.09505619	20	104.61317345	11	88.43806843

Table A.11. Reaction path B of bicyclic oxidosqualene model at HF/6-31G(d)//HF/6-31G(d).

Prereaction conformer **5.1b**

E = −658.2979045 ZPC: 0.382514 Imag. Freq.: N/A

1 1

C						
C	1	1.54330185				
C	1	1.51959153	2	114.04528496		
H	1	1.08495501	3	109.91870727	2	120.20993842
H	1	1.08546930	3	110.21136582	2	−122.88463527
H	2	1.08036638	1	111.50949933	3	59.34505604
H	2	1.08485719	1	109.63425065	3	177.95065858
C	2	1.50420810	1	109.99306653	3	−64.24230458
C	3	1.32861919	1	119.85906300	2	104.43884922
C	9	4.04873673	3	97.98923932	1	135.94174678
C	3	1.51149089	1	114.73491025	2	−78.31022317
C	8	1.45574963	2	127.77986186	1	101.12770092
H	8	1.07609024	2	114.12709289	1	−57.11200149
H	9	1.08209717	3	117.16027767	1	1.73135011
H	10	1.08082606	9	94.88948433	3	107.98041467
H	11	1.08716035	3	111.78478061	1	52.54099127
H	11	1.07938779	3	113.08883223	1	174.62963813
H	11	1.08619783	3	109.59847692	1	−65.47680848
C	9	1.50724597	3	129.15925893	1	179.04670828
O	8	1.51129050	2	114.08970173	1	176.19170757
C	10	1.50427591	9	135.31516523	3	−23.39208204
C	10	1.32534015	9	40.87136431	3	−125.20393588
H	20	0.95748580	8	114.30125913	2	133.05085333
H	19	1.08966792	9	108.11362539	3	128.41764903
H	19	1.08188388	9	111.41396239	3	11.59966406
H	21	1.08123251	10	113.45428427	9	−53.14373544
H	21	1.08703021	10	110.44204968	9	68.09919461
H	21	1.08654934	10	110.26850299	9	−174.13326773
C	22	1.52299566	10	119.43042617	9	−62.78304524
C	12	1.50141612	8	122.80232791	2	6.49813634
C	12	1.50431229	8	118.93690544	2	−158.10427511
C	22	1.51029655	10	125.12716571	9	119.00581115
H	29	1.08713897	22	109.77378577	10	−155.52978925
H	29	1.08472352	22	109.56370850	10	−39.25176589
H	30	1.07849826	12	112.53461850	8	27.60647693

H	30	1.08192197	12	110.04251400	8	149.37221282
H	30	1.08400186	12	107.61810984	8	−92.41973132
H	31	1.08341279	12	112.61494471	8	−19.82782110
H	31	1.08444086	12	107.55374242	8	98.88191360
H	31	1.08246432	12	110.86292558	8	−143.09461930
H	32	1.08047704	22	113.17177604	10	−6.12256221
H	32	1.08745528	22	110.04432551	10	114.38527072
H	32	1.08641093	22	111.00829851	10	−127.52979706

A-ring cyclisation transition state **5.2b**

E = −658.2962266 ZPC: 0.381066 Imag. Freq.: −161.5312

1 1

C						
C	1	1.54010490				
C	1	1.51985527	2	114.03060188		
H	1	1.08495888	3	109.65011912	2	120.63645084
H	1	1.08555622	3	110.06310462	2	−122.71341679
H	2	1.08178080	1	111.68100130	3	60.14857072
H	2	1.08494407	1	109.73816692	3	178.14163508
C	2	1.51056744	1	111.19794893	3	−64.16656459
C	3	1.33005414	1	120.03604270	2	103.07146789
C	9	4.04212560	3	97.30200983	1	135.75734721
C	3	1.51170964	1	114.68883485	2	−79.87341095
C	8	1.47243246	2	124.31275349	1	86.56419830
H	8	1.07894326	2	111.67534846	1	−54.27641115
H	9	1.08217546	3	117.09117630	1	2.01474608
H	10	1.08086043	9	94.79261556	3	108.26301613
H	11	1.08695002	3	111.68921627	1	49.77180366
H	11	1.07976219	3	113.27908385	1	172.14200185
H	11	1.08603124	3	109.44333514	1	−68.02062216
C	9	1.50787518	3	129.11804469	1	178.39926840
O	8	1.44660850	2	113.84642096	1	179.14743949
C	10	1.50424540	9	135.30042010	3	−22.95370390
C	10	1.32536073	9	41.04940107	3	−124.90952770
H	20	0.95358891	8	112.70717809	2	129.24761450
H	19	1.09019171	9	108.33977580	3	129.48531373
H	19	1.08202965	9	111.43729426	3	12.50278026
H	21	1.08120072	10	113.45344621	9	−53.29252154
H	21	1.08701070	10	110.44271930	9	67.96395485
H	21	1.08650985	10	110.25611918	9	−174.27727977

C	22	1.52303787	10	119.41137599	9	−62.80903650
C	12	1.48757580	8	122.39654035	2	26.87274721
C	12	1.48902242	8	119.35674516	2	−154.30641378
C	22	1.51030783	10	125.14934980	9	119.05783038
H	29	1.08702803	22	109.78803540	10	−155.82803802
H	29	1.08470645	22	109.59709433	10	−39.50410557
H	30	1.07768149	12	112.77421101	8	17.47448554
H	30	1.08118373	12	110.88929194	8	141.37495533
H	30	1.08722401	12	105.96845331	8	−101.34095796
H	31	1.08097225	12	113.04496649	8	−9.07881493
H	31	1.08830115	12	105.70701974	8	108.87277322
H	31	1.08179517	12	111.52260131	8	−134.41877249
H	32	1.08043838	22	113.16344567	10	−6.25796896
H	32	1.08742530	22	110.04242213	10	114.23552320
H	32	1.08643281	22	111.03349269	10	−127.67610389

Monocyclic intermediate **5.3b**

E = −658.3257651 ZPC: 0.384602 Imag. Freq.: N/A

1 1

C						
C	1	1.56262426				
C	1	1.47387706	2	102.73882066		
H	1	1.08114189	3	112.71706379	2	119.11163037
H	1	1.08258725	3	111.14480725	2	−117.04885014
H	2	1.08322630	1	110.60242436	3	67.55313416
H	2	1.08346304	1	107.19057604	3	−176.34091965
C	2	1.53107066	1	111.89412766	3	−55.19548439
C	3	1.47441377	1	116.05521642	2	70.03057278
C	3	3.59081304	1	120.22183757	2	169.61990623
C	3	1.47841140	1	117.66872478	2	−100.36266194
C	8	1.55300088	2	114.01301277	1	53.53918565
H	8	1.08865796	2	108.30833666	1	−65.64502718
H	9	1.08386423	3	106.95803072	1	36.52540966
H	10	1.08116465	3	90.73036548	1	159.20117881
H	11	1.08381060	3	110.28349612	1	31.89595805
H	11	1.07693986	3	114.40054515	1	157.74175496
H	11	1.08914684	3	105.43481977	1	−82.92634838
C	9	1.54193954	3	116.57389289	1	158.27007459
O	8	1.39511506	2	109.71001625	1	173.90290518
C	10	1.50529006	3	114.46871528	1	42.56373232

C	10	1.32808693	3	68.00458270	1	−81.78362402
H	20	0.94797938	8	111.12829594	2	78.54312281
H	19	1.08035139	9	109.51864294	3	147.51484486
H	19	1.08181243	9	111.09698005	3	30.91665930
H	21	1.08093140	10	113.56536540	3	−72.17835211
H	21	1.08754720	10	110.83901078	3	49.55661503
H	21	1.08602203	10	109.96431829	3	166.94618742
C	22	1.52748415	10	119.87318092	3	−78.77191734
C	12	1.53541874	8	111.89396917	2	71.46823493
C	12	1.53699156	8	107.79023779	2	−168.72142784
C	22	1.51159107	10	124.77515067	3	105.82163793
H	29	1.08577711	22	109.19483459	10	−169.71343653
H	29	1.08480955	22	109.68347812	10	−54.05758219
H	30	1.08440440	12	113.72193085	8	−53.78756668
H	30	1.08074822	12	109.32809360	8	65.74891368
H	30	1.08423539	12	110.66396025	8	−175.53873508
H	31	1.08528143	12	111.85469259	8	66.76651602
H	31	1.08145606	12	112.21462581	8	−171.11556802
H	31	1.08205000	12	108.42173810	8	−52.54117419
H	32	1.08015005	22	113.42198056	10	−8.02969732
H	32	1.08656321	22	109.75276837	10	112.42019560
H	32	1.08824482	22	111.51115833	10	−130.13728582

B-ring cyclisation transition state **5.4b**

E = −658.3211824 ZPC: 0.387287 Imag. Freq.: −154.9992

1 1

C

C	1	1.55002944				
C	1	1.50375346	2	106.09959983		
H	1	1.08151228	3	112.17648570	2	120.01778071
H	1	1.08318926	3	110.88379254	2	−118.50314375
H	2	1.08291957	1	110.73164603	3	68.26497404
H	2	1.08517555	1	107.63677119	3	−176.03395103
C	2	1.53408406	1	113.45377842	3	−55.21246365
C	3	1.52394936	1	111.95332343	2	61.12503884
C	3	2.22101165	1	106.74732222	2	−179.09636796
C	3	1.51410031	1	114.57737887	2	−80.32320613
C	8	1.55205046	2	114.59954579	1	53.71776439
H	8	1.08993309	2	107.84248852	1	−65.14115468
H	9	1.08421061	3	105.57036067	1	45.09009646

H	10	1.07499513	3	94.35640609	1	146.14071044
H	11	1.08145047	3	107.59533047	1	59.84206632
H	11	1.07868032	3	113.62402607	1	178.97021691
H	11	1.08010990	3	111.50745920	1	−56.72600542
C	9	1.52914982	3	111.22200211	1	159.99393839
O	8	1.39709076	2	110.02846329	1	174.99625295
C	10	1.50832932	3	109.83628340	1	28.27358137
C	10	1.36184458	3	83.71940036	1	−98.63701745
H	20	0.94777064	8	110.89547984	2	72.38684781
H	19	1.07977415	9	111.09632284	3	174.31057172
H	19	1.08190997	9	111.46147334	3	55.68781844
H	21	1.08031483	10	113.68785395	3	−63.52528257
H	21	1.08342752	10	110.91210001	3	58.76537941
H	21	1.08581266	10	108.97997169	3	176.06929097
C	22	1.51559360	10	119.82812732	3	−79.62483880
C	12	1.53865441	8	111.93193353	2	76.31601674
C	12	1.54087398	8	107.65255979	2	−165.87275841
C	22	1.49963374	10	123.66558240	3	101.86712137
H	29	1.08238380	22	108.72967405	10	−169.26669674
H	29	1.08394354	22	109.54698663	10	−52.56702520
H	30	1.08052012	12	114.07304921	8	−45.59329961
H	30	1.08073040	12	109.12088743	8	73.17789978
H	30	1.08494938	12	110.97619974	8	−168.28823745
H	31	1.08638244	12	112.01506108	8	67.51874076
H	31	1.08338505	12	111.70830423	8	−170.87096680
H	31	1.08181831	12	109.17458317	8	−52.08386356
H	32	1.07889512	22	114.03449361	10	−11.98541220
H	32	1.08828785	22	107.07963751	10	107.15961280
H	32	1.08409152	22	111.57240134	10	−136.72375483

Bicyclic product conformational isomer **5.5b**

E = −658.3362616 ZPC: 0.387091 Imag. Freq.: N/A

1 1

C

C	1	1.53340356				
C	1	1.54274163	2	111.34620175		
H	1	1.08319735	2	108.92322787	3	−122.82232092
H	1	1.08857937	2	108.88850424	3	121.12355778
H	2	1.08292914	1	111.12264925	3	67.15778255
H	2	1.08682904	1	108.40449231	3	−176.83606715

C	2	1.52791721	1	113.14336004	3	−56.18992794
C	3	1.55767121	1	106.78967666	2	55.31473731
C	3	1.60587120	1	111.04557031	2	173.67736100
C	3	1.54209297	1	109.69372789	2	−70.98915891
C	8	1.54763199	2	114.24616709	1	53.98422435
H	8	1.09121709	2	107.75814365	1	−64.46553798
H	9	1.09422002	3	103.88730730	1	54.24810587
H	10	1.10188457	3	103.92867270	1	149.20480321
H	11	1.07586999	3	112.62080599	1	46.65389359
H	11	1.08376599	3	112.39250695	1	168.30970574
H	11	1.08494246	3	109.88063836	1	−72.09059144
C	9	1.53581389	3	109.96826825	1	165.97329309
O	8	1.39967550	2	110.75222557	1	175.73707472
C	10	1.53294687	3	115.57142722	1	32.00207673
C	10	1.47355723	3	114.83560423	1	−106.91078013
H	20	0.94766695	8	110.49672204	2	65.94437745
H	19	1.07940784	9	112.36933822	3	169.11398309
H	19	1.08304231	9	111.78998412	3	49.32746609
H	21	1.08040793	10	109.85160414	3	46.55319033
H	21	1.08264353	10	112.33377932	3	−73.27895519
H	21	1.08315375	10	111.57434653	3	164.68171314
C	22	1.48081847	10	118.57257171	3	−45.20013970
C	12	1.53973303	8	111.91529181	2	76.78632764
C	12	1.54307285	8	107.08684920	2	−166.10385628
C	22	1.47762219	10	123.01089564	3	138.76532580
H	29	1.08770232	22	107.56161898	10	143.69557497
H	29	1.09480934	22	104.50592688	10	−105.51495212
H	30	1.07930429	12	113.88289637	8	−47.00035573
H	30	1.08098602	12	109.33695368	8	72.26876207
H	30	1.08590286	12	110.88101932	8	−169.19860978
H	31	1.08732769	12	111.95733781	8	68.81440578
H	31	1.08409588	12	112.09702673	8	−169.41208457
H	31	1.08158634	12	109.34976557	8	−50.64359430
H	32	1.08243951	22	111.85491902	10	42.04219785
H	32	1.08011453	22	112.76877661	10	167.68227490
H	32	1.09220987	22	105.98602810	10	−73.16213097

Table A.12. Path interchange transition states of bicyclic oxidosqualene model at HF/6-31G(d)//HF/6-31G(d).

Reactant conformational change transition state **5.1ts**

E = −658.2901659 ZPC: 0.382399 Imag. Freq.: −107.6617

1 1

C						
C	1	1.54327417				
C	1	1.51877142	2	114.00831997		
H	1	1.08493965	3	109.92561921	2	120.26737738
H	1	1.08538585	3	110.15989816	2	−122.88013585
H	2	1.08043028	1	111.50626255	3	59.48751017
H	2	1.08485051	1	109.68878496	3	178.14293563
C	2	1.50406818	1	109.89953111	3	−64.01914125
C	3	1.32782495	1	120.05354827	2	104.38523297
C	9	3.69864410	3	89.11512240	1	114.49881496
C	3	1.51063474	1	114.96698369	2	−78.83923714
C	8	1.45550193	2	127.75401707	1	100.92572471
H	8	1.07607329	2	114.12664261	1	−57.22810933
H	9	1.08000712	3	117.04650125	1	1.56655622
H	10	1.07980066	9	95.60223716	3	70.46437695
H	11	1.08702287	3	111.96465036	1	50.06406490
H	11	1.08041834	3	112.97509292	1	172.14180207
H	11	1.08614294	3	109.49553914	1	−68.11879451
C	9	1.51036636	3	128.06618101	1	179.31757479
O	8	1.51157153	2	114.14972277	1	176.03334964
C	10	1.50443859	9	129.26146332	3	−56.70243719
C	10	1.32540603	9	46.66884318	3	−166.92884852
H	20	0.95745330	8	114.29123134	2	133.09871845
H	19	1.08613928	9	107.71187344	3	143.65421229
H	19	1.08298347	9	109.51281730	3	29.22100463
H	21	1.08130022	10	113.50855038	9	−58.30495041
H	21	1.08719419	10	110.51719391	9	63.07073094
H	21	1.08655554	10	110.22117369	9	−179.20530077
C	22	1.51744679	10	120.05578551	9	−71.22130056
C	22	1.51132766	10	124.84463261	9	112.67259448
H	29	1.08574503	22	108.46262336	10	−135.59328817
H	29	1.08286882	22	108.82084015	10	−20.77928042
H	30	1.08062019	22	113.28258851	10	−13.11120502
H	30	1.08741020	22	109.96627637	10	107.53545243

H	30	1.08625648	22	111.34587330	10	−134.58621918
C	12	1.50140177	8	122.79905671	2	6.61347695
H	36	1.08393775	12	107.60888246	8	−92.53142864
H	36	1.07849266	12	112.54022828	8	27.49148129
H	36	1.08192716	12	110.04060918	8	149.26387463
C	12	1.50424783	8	118.93063933	2	−157.95377482
H	40	1.08342190	12	112.60633353	8	−20.08582439
H	40	1.08446051	12	107.51419247	8	98.58422098
H	40	1.08243950	12	110.88799157	8	−143.36452318

Monocyclic intermediate conformational change transition state **5.3ts**

E = −658.3236364 ZPC: 0.385363 Imag. Freq.: −17.1902

1 1

C						
C	1	1.56024709				
C	1	1.47906694	2	103.79601616		
H	1	1.08095943	3	112.69560814	2	119.75864650
H	1	1.08271550	3	110.60564371	2	−117.32422203
H	2	1.08322671	1	110.52385562	3	68.27534479
H	2	1.08378844	1	107.22579976	3	−175.87426774
C	2	1.53247091	1	112.58686302	3	−54.73021337
C	3	1.48670017	1	115.14267905	2	66.54759833
C	3	1.48560768	1	117.46556465	2	−96.98788423
C	3	2.99613914	1	106.52041139	2	173.74071279
C	8	1.55277934	2	114.11656823	1	53.58473823
H	8	1.08892539	2	108.21366648	1	−65.52287369
H	9	1.08188706	3	106.15622029	1	39.23404725
H	10	1.08128743	3	110.27007886	1	−51.23691094
H	10	1.07627187	3	114.41456903	1	−176.66416823
H	10	1.08873607	3	106.17102748	1	63.46870663
C	9	1.53262484	3	114.91102013	1	158.97821025
O	8	1.39553432	2	109.69046722	1	174.22290666
C	11	1.33442194	3	73.49427160	1	−101.68634210
H	11	1.07902328	3	90.12017946	1	140.17012156
C	11	1.50468315	3	111.14608361	1	24.24337106
H	19	0.94790668	8	111.08075907	2	77.38545576
H	18	1.07975447	9	108.64181854	3	169.79445595
H	18	1.08207025	9	110.40862112	3	54.32696521
C	20	1.52299731	11	120.38499221	3	−79.83192838
C	12	1.53604662	8	111.81703393	2	72.81724309

C	12	1.53800551	8	107.89285565	2	−168.15588082
C	20	1.51209898	11	124.00695763	3	106.03040088
H	22	1.08092550	11	113.63095565	3	−72.81528691
H	22	1.08703454	11	110.86932587	3	49.22359742
H	22	1.08610785	11	109.71461586	3	166.50708068
H	26	1.08374754	20	108.14242051	11	−149.22800238
H	26	1.08307511	20	109.45786613	11	−34.13786428
H	27	1.08302894	12	113.93780914	8	−52.51647387
H	27	1.08069586	12	109.16535296	8	66.66196887
H	27	1.08387599	12	110.83340091	8	−174.70524867
H	28	1.08562104	12	111.90987728	8	67.24479844
H	28	1.08211295	12	111.91161723	8	−170.85217955
H	28	1.08194759	12	108.68840739	8	−52.19938660
H	29	1.08084122	20	113.58251239	11	−18.98122095
H	29	1.08567959	20	111.89693840	11	−141.95866847
H	29	1.08675068	20	109.03360349	11	100.92223565

Bicyclic product conformational change transition state **5.5ts**

E = −658.3314161 ZPC: 0.387843 Imag. Freq.: −62.9726

1 1

C						
C	1	1.52946960				
C	1	1.54052515	2	112.16913987		
H	1	1.08338823	2	109.54109900	3	−122.96115522
H	1	1.08609294	2	107.88516789	3	121.07191219
H	2	1.08295276	1	111.81803924	3	64.66141489
H	2	1.08669796	1	108.34662304	3	−178.75857756
C	2	1.52424531	1	111.52307062	3	−58.84194053
C	3	1.56565722	1	107.88004974	2	53.96668514
C	3	1.63553613	1	109.97337038	2	172.34804411
C	3	1.53879224	1	109.92534051	2	−72.27743398
C	8	1.54629165	2	113.51699098	1	57.85244585
H	8	1.09147689	2	107.80996974	1	−60.59571147
H	9	1.09496662	3	104.03178417	1	60.79303934
H	10	1.08656156	3	104.29599599	1	129.51443799
H	11	1.07691948	3	112.48328167	1	54.32195228
H	11	1.08462734	3	112.28425550	1	175.80667870
H	11	1.08517315	3	109.64904262	1	−64.70227043
C	9	1.53734636	3	112.11557149	1	174.79035667
O	8	1.39941927	2	111.13785902	1	179.38237658

C	10	1.53255498	3	117.56687721	1	11.29702976
C	10	1.47689022	3	108.00212679	1	−121.42408359
H	20	0.94763372	8	110.40730993	2	66.03864518
H	19	1.07846773	9	109.93205960	3	−170.10727230
H	19	1.07905201	9	111.76465291	3	70.80759820
H	21	1.08102903	10	113.66863389	3	−61.99844931
H	21	1.08133766	10	109.63949014	3	58.63511006
H	21	1.08488063	10	110.43132593	3	176.14242255
C	22	1.47648661	10	116.00268903	3	−58.91888596
C	12	1.54116650	8	110.87255534	2	75.23444981
C	12	1.54380073	8	107.23543876	2	−168.20170375
C	22	1.47243159	10	124.02793532	3	120.94647694
H	29	1.08031425	22	111.82147927	10	−172.36677218
H	29	1.08450339	22	108.07178830	10	−53.01162555
H	30	1.07976781	12	113.90881812	8	−52.21992603
H	30	1.08058534	12	108.95234836	8	66.92279568
H	30	1.08430133	12	111.43265254	8	−174.74396437
H	31	1.08721723	12	111.88139061	8	68.85450441
H	31	1.08400572	12	112.14192284	8	−169.35694699
H	31	1.08120205	12	109.34185744	8	−50.51840566
H	32	1.09544005	22	104.45581166	10	92.43082849
H	32	1.08195375	22	111.93791849	10	−152.33517524
H	32	1.07916260	22	113.77330809	10	−24.48037712

Table A.13. Bicyclic oxidosqualene model system at HF/3-21G//HF/3-21G.

Monocyclic intermediate **5.6**

E = −654.6976845 ZPC: 0.395805 Imag. Freq.: N/A

1 1

C						
C	1	1.57738178				
C	1	1.47582504	2	104.02054221		
H	1	1.07990248	3	112.81093797	2	119.37291711
H	1	1.08219159	3	110.51266127	2	−116.51854188
H	2	1.08034964	1	110.83447779	3	66.86516025
H	2	1.08242130	1	107.23792554	3	−175.65486883
C	2	1.53238452	1	110.62620622	3	−54.65156237
C	3	1.46690042	1	116.05210274	2	68.53028106
C	3	1.47656440	1	118.75078853	2	−103.23417227

C	8	1.54800846	2	113.20212568	1	54.97396489
H	8	1.08557477	2	109.33595152	1	−65.63362580
H	9	1.08225228	3	107.80784066	1	38.74233554
H	10	1.09213347	3	106.32750282	1	−79.05183383
H	10	1.07642918	3	113.78272460	1	161.40681071
H	10	1.08482893	3	110.62582228	1	35.69008015
C	9	1.53722796	3	116.75339872	1	161.95531553
O	8	1.43375284	2	109.38421258	1	172.38270486
H	18	0.96632922	8	112.71717533	2	79.85818747
H	17	1.08011752	9	107.19932810	3	−176.91584284
H	17	1.08228328	9	111.35440528	3	66.51284995
C	17	1.55729068	9	112.96035277	3	−57.05511174
C	11	1.53794119	8	110.75871168	2	68.26900579
C	11	1.54015843	8	107.82610055	2	−172.64592947
H	22	1.08509652	17	107.59201256	9	−164.20229292
H	22	1.08294394	17	110.01716066	9	79.99915578
H	23	1.08279551	11	113.46992303	8	−60.43329779
H	23	1.07950550	11	107.89295740	8	58.65960987
H	23	1.08205705	11	110.78290116	8	177.38604359
H	24	1.08473419	11	111.48547568	8	65.07172995
H	24	1.08093913	11	111.69335289	8	−172.64080431
H	24	1.08144196	11	107.29480321	8	−53.88160990
C	22	1.51998858	17	113.28130319	9	−43.12441197
C	33	1.32453505	22	120.30787947	17	115.38104118
C	33	1.51548602	22	114.50120167	17	−67.00567250
H	34	1.07875306	33	117.91598164	22	2.25025204
H	35	1.07885992	33	112.81211905	22	177.75518745
H	35	1.08612223	33	111.46334872	22	56.00860270
H	35	1.08599446	33	109.30156002	22	−62.24320479
C	34	1.51078703	33	128.22248433	22	178.15963831
H	40	1.07979157	34	112.98866949	33	10.81434030
H	40	1.08582074	34	110.56226597	33	132.14397135
H	40	1.08574880	34	109.90303591	33	−109.85277062

B-ring cyclisation transition state **5.7**

E = −654.6965723 ZPC: 0.396328 Imag. Freq.: −61.5530

1 1

C

C	1	1.57491382		
C	1	1.48117199	2	104.00089683

H	1	1.07969863	3	112.75201169	2	119.47538301
H	1	1.08129099	3	110.75931619	2	−116.68305418
H	2	1.08053401	1	110.93308154	3	66.21778373
H	2	1.08279833	1	107.29396286	3	−176.50750124
C	2	1.53394989	1	111.06750841	3	−55.65132836
C	3	1.47815295	1	115.40392716	2	66.63462299
C	3	1.48555441	1	118.03070911	2	−96.32624186
C	8	1.54830525	2	113.41980072	1	55.78937193
H	8	1.08594087	2	109.03629054	1	−64.57017276
H	9	1.08155307	3	106.94564004	1	40.69818505
H	10	1.08204939	3	110.37947934	1	−56.20526286
H	10	1.07543941	3	113.71685825	1	178.84656339
H	10	1.08891701	3	107.05466055	1	58.75984360
C	9	1.53753291	3	115.60190484	1	161.70058539
O	8	1.43351136	2	109.56571539	1	173.64806132
H	18	0.96626623	8	112.67422324	2	78.52952427
H	17	1.08029762	9	107.36038313	3	−169.87984698
H	17	1.08153075	9	111.44102709	3	73.22796032
C	17	1.56838421	9	111.98521405	3	−49.81153129
C	11	1.53741835	8	110.89736644	2	70.51933844
C	11	1.54202623	8	107.68841003	2	−170.97508541
H	22	1.08396794	17	108.46673902	9	−146.29789411
H	22	1.08191974	17	110.01815712	9	97.02937406
H	23	1.08105630	11	113.63731428	8	−58.33177259
H	23	1.07939752	11	107.86976504	8	60.43143756
H	23	1.08210844	11	110.82474049	8	179.17934906
H	24	1.08492584	11	111.45608501	8	64.85135614
H	24	1.08144053	11	111.55873471	8	−173.08911138
H	24	1.08133443	11	107.59008673	8	−54.19966679
C	22	1.51557586	17	111.85781261	9	−25.17176067
C	33	1.33054952	22	120.75094170	17	111.51888598
C	33	1.51603709	22	115.01933883	17	−71.43371394
H	34	1.07581805	33	117.93589060	22	4.65594326
H	35	1.08116921	33	113.06776190	22	153.83692119
H	35	1.08356275	33	111.45312064	22	31.15583613
H	35	1.08648076	33	108.82814290	22	−86.59149154
C	34	1.51061239	33	127.24549971	22	177.65051704
H	40	1.08056400	34	112.94697495	33	17.28953130
H	40	1.08533545	34	110.81652543	33	139.14193726
H	40	1.08607131	34	109.70866055	33	−102.92648515

Bicyclic product **5.8a**

E = −654.7082841 ZPC: 0.399351 Imag. Freq.: N/A

1 1

C						
C	1	1.53866939				
C	1	1.54305164	2	111.56442288		
H	1	1.08298083	2	110.02506181	3	−122.21742880
H	1	1.08224394	2	107.39822538	3	120.77880818
H	2	1.07997752	1	112.38715960	3	62.17387466
H	2	1.08569913	1	108.36967513	3	−179.77614878
C	2	1.52650795	1	109.77866115	3	−60.44165273
C	3	1.56539822	1	109.17744587	2	53.26383388
C	3	1.54330730	1	109.12345890	2	−73.26897539
C	8	1.54298705	2	112.87278589	1	61.70211104
H	8	1.08826288	2	108.43424357	1	−57.74953609
H	9	1.09098532	3	104.60455857	1	64.48104427
H	10	1.08410012	3	109.42621569	1	−64.15115095
H	10	1.08143830	3	112.83615891	1	175.31149225
H	10	1.07618210	3	111.25417775	1	54.21917500
C	9	1.54669012	3	111.69840848	1	−179.76793063
O	8	1.43692034	2	111.33361555	1	−179.14867067
H	18	0.96601667	8	111.99085858	2	67.24261835
H	17	1.07805403	9	110.11325542	3	−159.13474860
H	17	1.07723338	9	111.36769309	3	79.82675404
C	17	1.61117626	9	112.54890023	3	−39.26126846
C	11	1.54293937	8	110.16923067	2	72.71882174
C	11	1.54848125	8	106.81619164	2	−171.11779492
H	22	1.07847232	17	109.69950913	9	−144.57459320
H	22	1.07809042	17	108.56184401	9	94.17525188
H	23	1.07797970	11	113.52856796	8	−63.45387434
H	23	1.07894784	11	107.68253126	8	55.66326469
H	23	1.08300180	11	111.16983727	8	173.98027264
H	24	1.08613189	11	111.23918548	8	65.53910495
H	24	1.08317871	11	111.79579863	8	−172.60049383
H	24	1.08029541	11	108.25470802	8	−53.42092750
C	22	1.45911806	17	101.88536323	9	−23.94774719
C	33	1.47645521	22	116.72307174	17	76.91107711
C	33	1.47623747	22	119.51602027	17	−98.17820161
H	34	1.08683358	33	105.47581338	22	56.89178107

H	35	1.07971300	33	112.99644014	22	144.32104769
H	35	1.08079439	33	112.14593392	22	17.62389371
H	35	1.09557217	33	105.93956565	22	−99.15078915
C	34	1.53781918	33	114.42531495	22	175.87508192
H	40	1.08077090	34	112.79502949	33	64.82936636
H	40	1.08009110	34	109.83244478	33	−174.66029345
H	40	1.08440109	34	110.36077126	33	−56.74055084

Bicyclic product conformational isomer **5.8b**

E = −654.7087257 ZPC: 0.398354 Imag. Freq.: N/A

1 1

C						
C	1	1.54475854				
C	1	1.54160395	2	110.20220639		
H	1	1.08173495	3	110.89536375	2	121.04217325
H	1	1.08682873	3	109.98025493	2	−119.85188141
H	2	1.08004150	1	111.33980549	3	65.06557118
H	2	1.08580032	1	108.45799728	3	−177.69402459
C	2	1.53154074	1	112.08781197	3	−57.34203081
C	3	1.55691359	1	107.37121111	2	56.54445554
C	3	1.63714797	1	111.28906093	2	174.55278680
C	3	1.54409744	1	110.03535302	2	−70.70573732
C	8	1.54508498	2	114.06025951	1	55.95243588
H	8	1.08812459	2	108.28058726	1	−63.56378018
H	9	1.09414306	3	104.56506859	1	53.53409404
H	10	1.09146259	3	102.56746095	1	149.98006250
H	11	1.07445434	3	111.89642168	1	46.87618113
H	11	1.08209455	3	111.96973368	1	168.33675738
H	11	1.08403703	3	109.57281046	1	−71.67953629
C	9	1.54302668	3	109.47142141	1	165.81260446
O	8	1.43652288	2	110.72664177	1	175.28419031
C	10	1.53542181	3	114.40403752	1	31.98783662
C	10	1.46759598	3	110.04290876	1	−100.65363925
H	20	0.96608998	8	112.09740730	2	66.59154019
H	19	1.07850303	9	111.88328633	3	168.63347350
H	19	1.08019429	9	111.40002375	3	47.88904171
H	21	1.08082155	10	109.62092380	3	51.48336900
H	21	1.08120713	10	112.20423949	3	−68.42584796
H	21	1.08394841	10	110.99980944	3	169.57580166
C	22	1.48504524	10	117.09558105	3	−59.26897063

C	12	1.54047598	8	111.51522084	2	75.38630391
C	12	1.54827027	8	106.51186722	2	−167.95700048
C	22	1.47602577	10	123.04036027	3	120.91363315
H	29	1.08309768	22	109.80578084	10	155.68046715
H	29	1.09545075	22	105.36922023	10	−89.90710501
H	30	1.07687462	12	113.49920161	8	−51.47691234
H	30	1.07936634	12	108.34503433	8	67.37888061
H	30	1.08463969	12	110.51210308	8	−173.81904752
H	31	1.08621946	12	111.44120296	8	67.30655494
H	31	1.08299647	12	111.79404840	8	−170.66960373
H	31	1.08082513	12	108.12061188	8	−51.79148384
H	32	1.08304426	22	111.72916947	10	42.93856368
H	32	1.07934618	22	112.87795934	10	168.73707253
H	32	1.09483390	22	106.42201841	10	−72.34456762

Acknowledgements

I would like to thank Professor Jim Coxon for providing me with the opportunity to complete this project; his knowledge, advice and encouragement have been very much appreciated. A big thank you must go to Bryce Williamson, the Head of Department, and my research committee for giving me the impetus to begin writing this thesis.

I am very grateful to my family, Mum, Dad and Helen, for there support, encouragement and love, especially over the last few months of writing. Thank you very much, love you lots.

A large portion of this work was performed with the financial assistance of a Doctoral Scholarship from the University of Canterbury and a Bright Futures Top Achiever Doctoral Scholarship from FRST and I acknowledge their support.